



Experimental targets for dark photon dark matter

David Cyncynates¹,  and Zachary J. Weiner^{1,2}, 

¹*Department of Physics, University of Washington, Seattle, Washington, 98195, USA*

²*Perimeter Institute for Theoretical Physics, Waterloo, Ontario N2L 2Y5, Canada*


(Dated: June 3, 2025)

Ultralight dark photon dark matter features distinctive cosmological and astrophysical signatures and is also supported by a burgeoning direct-detection program searching for its kinetic mixing with the ordinary photon over a wide mass range. Dark photons, however, cannot necessarily constitute the dark matter in all of this parameter space. In minimal models where the dark photon mass arises from a dark Higgs mechanism, early-Universe dynamics can easily breach the regime of validity of the low-energy effective theory for a massive vector field. In the process, the dark sector can collapse into a cosmic string network, precluding dark photons as viable dark matter. We establish the general conditions under which dark photon production avoids significant backreaction on the dark Higgs and identify regions of parameter space that naturally circumvent these constraints. After surveying implications for known dark photon production mechanisms, we propose novel models that set well-motivated experimental targets across much of the accessible parameter space. We also discuss complementary cosmological and astrophysical signatures that can probe the dark sector physics responsible for dark photon production.

CONTENTS

I. Introduction	2
II. Backreaction, defect formation, and a survey of production scenarios	3
III. Clockworked couplings and backreaction	16
IV. Detectable dark photons from axions	20
V. Dark photon dark matter in scalar–Abelian-Higgs theories	25
VI. Discussion	46
VII. Conclusion	50
Acknowledgments	51
A. Scalar–Abelian-Higgs model	52
B. Quantum corrections	54
C. Axion to dark photon conversion at large coupling	60
D. Delayed axion oscillations	65
E. Plasma dynamics	67
References	69

 davidcyn@uw.edu

 zweiner@perimeterinstitute.ca

I. INTRODUCTION

The cosmological and astrophysical evidence for cold, nonbaryonic dark matter provides some of the most compelling motivation for physics beyond the Standard Model [1–3]. These observations, however, only evince dark matter through its gravitational effects, allowing a broad range of new particles to effectively reproduce the cold dark matter paradigm in its observed regimes. From a bottom-up perspective, dark matter candidates span dozens of orders of magnitude in mass and all possible spins; the only general requirement of their nongravitational interactions with Standard Model (SM) particles is that they are sufficiently weak to have evaded detection thus far.

Confronted with so vast a landscape of possibilities, top-down theoretical approaches can provide essential guidance by motivating concrete models and identifying consistent scenarios. The canonical example, a weakly interacting massive particle [1], sets specific experimental targets by determining the dark matter relic abundance via its interaction strength with SM particles through thermal freeze-out [4–6]. Dark matter as a thermal relic would be too warm at late times if its mass were below $\sim \text{keV}$ [7–14]; in this mass range, the dark matter must also be bosonic [15–27]. Axions and dark photons dominate theoretical and experimental efforts in this ultralight regime, since symmetries can protect their masses from large quantum corrections. Notably, the quantum chromodynamics (QCD) axion, initially proposed to resolve the strong CP problem [28–30], is an excellent dark matter candidate [31–34] and has inspired a broad experimental program targeting its couplings to SM particles in the Kim-Shifman-Vainshtein-Zakharov/Dine-Fischler-Srednicki-Zhitnisky range [35–38].

New, massive gauge bosons may not solve specific problems in the SM like the axion does, but they are well motivated (if not expected) in extensions of the SM [39–46] as the force carriers of new interactions. Indeed, massive gauge bosons are a feature of the SM itself. Moreover, the dark photon inherits the axion’s broad experimental prospects [47]: while detecting the axion’s mixing with the SM photon requires catalysis by a background magnetic field, the dark photon’s kinetic mixing with the SM photon takes place in vacuum. Every axion experiment is therefore also a dark photon experiment.

In this work, we investigate how theoretical considerations motivate particular parts of the extensive dark photon parameter space accessible to upcoming searches. We focus on a fundamental requirement for any dark matter candidate: a consistent mechanism for generating its relic abundance. In particular, the low-energy effective theory of a massive, kinetically mixed vector appropriate to describe its phenomenology for direct detection may well be inadequate to describe its cosmological production at early times (i.e., at higher energy). In minimal models where the ultraviolet (UV) completion of the dark photon’s mass is a Higgs mechanism, the cutoff scale is directly tied to the kinetic mixing strength. Reference [48] demonstrated that breaching this cutoff has severe consequences: topological defects (Nielsen-Olesen strings [49]) form, converting any coherent dark photon background into string kinetic and potential energy. The resulting string network is neither a viable dark matter candidate nor detectable by haloscopes. In the minimal scenario of vector production from inflationary fluctuations [50], the entire experimentally accessible parameter space is excluded on these grounds [48]. Here we extend this analysis to constrain additional dark photon production mechanisms, propose extensions thereof and novel scenarios with enhanced experimental prospects—including an in-depth discussion and generalization of the models of scalar-mediated dark photon production introduced in Refs. [51, 52]—and identify theoretically motivated targets within the dark photon parameter space.

The first loophole one might consider is that the dark photon’s mass instead originates from the Stückelberg mechanism [53]. Typically, studies of dark photon dark matter that assume Stückelberg masses for simplicity in fact make a stronger assumption: that the theory is well described by Proca theory [see Eq. (2.2)], i.e., an Abelian gauge field with a bare mass term and nothing more. In known examples from string theory and supersymmetry, however, Stückelberg masses are accompanied

by radial degrees of freedom analogous to a Higgs [54], and the validity of the Proca theory is similarly restricted in energy. If this regime is breached at early times, at the very least we expect modifications to the dynamics of dark photon production that have not been studied. Here we consider only Higgs masses, since the relevant dynamics have been established [48], and comment further on Stückelberg masses in Sec. VI C.

In Sec. II, we derive model-independent bounds on kinetic mixing as a function of wave number and redshift of production, applying these bounds to various models proposed in prior literature. We then consider the clockwork mechanisms as a production-agnostic means to relax these bounds in Sec. III, demonstrating that they introduce no additional fine-tuning issues. In Sec. IV, we revisit dark photon production from oscillating axions and describe mechanisms that unify enhanced production efficiency with dynamics that avoid string formation. Finally, in Sec. V we consider a class of models coupling the dark photon to a new singlet scalar, discussing the scalar’s potential to alleviate backreaction constraints by modulating the fundamental parameters of the Abelian-Higgs theory. We show that the Damour-Polyakov mechanism [55] can weaken bounds on inflationary production, allowing accessible kinetic mixing for dark photons heavier than an eV. We further discuss two qualitatively distinct postinflationary production mechanisms driven by the scalar [51, 52] that, with some fine-tuning, may open all kinetic mixing parameter space accessible to upcoming haloscopes. In Sec. VI, we summarize and discuss the implications of our findings and conclude in Sec. VII. A number of appendices provide additional details on scalar–Abelian-Higgs models (Appendix A), quantum corrections to the scalar effective potential in these models (Appendix B), the strong-coupling (Appendix C) and narrow-resonance (Appendix D) regimes of dark photon production from axions, and the effect of the Standard Model plasma on the narrow scalar resonance discussed in Sec. VD (Appendix E).

Throughout this paper, we use natural units in which $\hbar = c = 1$, define the reduced Planck mass $M_{\text{pl}} = 1/\sqrt{8\pi G}$, fix a cosmic-time Friedmann-Lemaître-Robertson-Walker (FLRW) metric $ds^2 = dt^2 - a(t)^2 \delta_{ij} dx^i dx^j$ with $a(t)$ the scale factor, and employ the Einstein summation convention for spacetime indices. Dots denote derivatives with respect to cosmic time t , and the Hubble rate is $H \equiv \dot{a}/a$. We use boldface for spatial three vectors.

II. BACKREACTION, DEFECT FORMATION, AND A SURVEY OF PRODUCTION SCENARIOS

We begin by reviewing Abelian-Higgs theory and the thresholds associated with backreaction onto the dark Higgs and defect formation [48]. We then identify generic conditions for postinflationary cosmological production of dark photons that evade these thresholds. We discuss defect bounds on inflationary production of dark photons in Sec. II A, considering the effects of modified postinflationary expansion histories (Sec. II A 1) and possible nonminimal couplings to gravity and the inflaton itself (Sec. II A 2). In Sec. II B we derive model-independent bounds from a dark photon’s kinetic mixing with the hot Standard Model plasma, and in Sec. II C we discuss dark photon production via an oscillating axion. We briefly consider vector misalignment in Sec. II D.

In this work, we consider a dark sector described by various extensions of the Abelian-Higgs model. We denote the dark photon with A , not to be confused with the Standard Model photon A_{SM} . The dark Higgs field Φ that provides the dark photon its mass is a complex scalar charged under A with gauge coupling g_D and a vacuum expectation value (VEV) v . We refer to the dark Higgs simply as the Higgs, since the SM Higgs is not relevant to our discussion. The action of

Abelian-Higgs model is $S = \int d^4x \sqrt{-g} \mathcal{L}$ with Lagrangian

$$\mathcal{L} = -\frac{1}{4}F_{\mu\nu}F^{\mu\nu} + \frac{1}{2}D_\mu\Phi(D^\mu\Phi)^* - \frac{\lambda}{4}\left(|\Phi|^2 - v^2\right)^2, \quad (2.1)$$

where $F_{\mu\nu} = \partial_\mu A_\nu - \partial_\nu A_\mu$ is the dark photon field strength, $D_\mu = \partial_\mu - ig_D A_\mu$ is the gauge-covariant derivative, and λ is the Higgs self-coupling.

In general, we seek to identify the conditions under which a cosmological abundance of dark photons in the early Universe—typically, their maximum density which they reach when first produced—invalidates the low-energy effective theory given by the Proca Lagrangian,

$$\mathcal{L} = -\frac{1}{4}F_{\mu\nu}F^{\mu\nu} + \frac{1}{2}m_A^2 A_\mu A^\mu, \quad (2.2)$$

and whatever description of dark photon production that relies upon it. The Proca Lagrangian derives from the low-energy limit of Eq. (2.1) when the dark photon’s U(1) symmetry is broken. In the broken phase, the dark photon and Higgs have masses $m_A = g_D v$ and $m_h = \sqrt{2\lambda}v$, where the Higgs is decomposed as $\Phi \equiv (v + h)e^{i\Pi/v}$. In unitary gauge, which sets $\Pi = 0$, the dark photon acquires a longitudinal mode as it eats the Higgs phase, i.e., $A_\mu - \partial_\mu \Pi/m_A \rightarrow A_\mu$. The theory is then described by the action

$$\mathcal{L} = -\frac{1}{4}F_{\mu\nu}F^{\mu\nu} + \frac{1}{2}\partial_\mu h \partial^\mu h - V_{\text{eff}}(h, A), \quad (2.3)$$

where the effective potential for the Higgs and dark photon is

$$V_{\text{eff}}(h, A) = \frac{\lambda v^4}{4} \left[1 + \left(\frac{h}{v} + 1 \right)^4 \right] - \frac{1}{2} \left(\frac{h}{v} + 1 \right)^2 (\lambda v^4 + m_A^2 A_\mu A^\mu). \quad (2.4)$$

The first term in the effective potential is a pure quartic with a unique minimum at the symmetric point $h = -v$. The latter term generates the symmetry-breaking minimum at $h = 0$ provided that the dark photon amplitude is not too large—that is, the dark photon backreacts strongly onto the Higgs if

$$|m_A^2 A_\mu A^\mu| \gtrsim \lambda v^4. \quad (2.5)$$

As pointed out in Ref. [56], beyond this threshold the dark photon is no longer well described by the Proca Lagrangian Eq. (2.2), and whatever dynamics are responsible for producing the dark photon are (presumably) substantially modified.

More recently, Ref. [48] showed that the consequences of violating Eq. (2.5) can be severe. The vacuum state of the Abelian-Higgs theory is characterized by a ring of degenerate vacua, allowing for topological line defects—namely, Nielsen-Olesen strings [49]. Each string has a quantized magnetic flux $\Phi_0 = 2\pi/g_D$; the strings therefore interact with the background dark electromagnetic field, converting the would-be dark matter into string energy.¹ For the purpose of understanding string formation, the dark photon, which otherwise would have constituted the cold dark matter, can often be approximated as a constant, homogeneous magnetic field (see Ref. [48] for a more comprehensive discussion). Magnetic flux in excess of one unit ($2\pi/g_D$) prefers to be confined to a topological defect by a phenomenon known as flux trapping [57]. That is, strings are the energetically preferable field configuration when the magnetic field exceeds the first critical field $B_{c1} \sim g_D v^2$, corresponding to a magnetic flux $2\pi/g_D$ inside an area $\sim 1/m_A^2$. However, there is an energy barrier to string

¹ Though strings only have an intrinsic magnetic moment per unit length, moving strings also possess an electric dipole moment; they therefore interact with both electric and magnetic fields of the dark photon.

formation (due to the differing spacetime symmetry and topology before and after string formation), which only vanishes when the magnetic field exceeds the parametrically larger “superheating” field $B_{\text{sh}} = \sqrt{\lambda}v^2$.² In this case, the magnetic flux confines to strings with interstring spacing much larger than the string core, $1/\sqrt{g_D B_{\text{sh}}} \gg m_h^{-1}$, so $U(1)$ symmetry is restored *locally*. Only once the external magnetic field exceeds the second critical field $B_{c2} \sim (\lambda/g_D^2)^{1/2}m_h^2$ do the string cores overlap, restoring symmetry globally.

The idealized limit of a purely magnetic, homogeneous background field is not precisely applicable to all scenarios for dark photon production, some of which produce semirelativistic or nonrelativistic modes (with wave numbers $k \lesssim m_A$) that are coherent on scales $1/m_A$ (or larger) but also contain electric fields. Reference [48] demonstrated with numerical simulations that defects nucleate nonetheless for tachyonic dark photon production (see Sec. II C) at energy densities above the superheating threshold. The superheating threshold also turns out to match that for strong backreaction onto the Higgs identified in Eq. (2.5). We therefore take Eq. (2.5) as generic upper limit on the dark photon field amplitude: as Proca theory is an invalid description of the Abelian-Higgs model in this regime either way, and the dynamics intended to produce massive dark photons are in all likelihood disrupted. In the rest of this section we discuss exceptions to this argument as needed.

To study the implications of Eq. (2.5) as a consistency limit on dark photon cosmologies, we first note that in almost all the cases we consider, dark photons are produced with a peaked spectrum. Namely, the relic abundance is dominated by dark photons over a narrow range of wave numbers centered about the peak k_* , which enables rephrasing the backreaction bound in terms of the dark photon energy density $\rho_{A'}$. Heuristically (see Appendix A for more formal expressions),

$$\lambda v^4 \gg -m_A^2 g^{\mu\nu} A_\mu A_\nu \sim \frac{m_A^2}{m_A^2 + k_*^2/a^2} \rho_{A,\perp} + \rho_{A,\parallel}, \quad (2.6)$$

where $\rho_{A,\perp}$ and $\rho_{A,\parallel}$ denote the contributions from transverse and longitudinal modes, respectively. Equation (2.6) shows that for equal energy densities, relativistic, transverse dark photons couple more weakly (at fixed energy density) to the Higgs than nonrelativistic ones by a factor of $(am_A/k_*)^2$. But the energy density in relativistic modes redshifts as a^{-4} , one factor of a faster than nonrelativistic modes, and must therefore be produced with a larger initial energy density to match the observed dark matter density. The backreaction constraint is therefore relaxed, albeit modestly, if transverse dark photons dominate ρ_A and become nonrelativistic as late as possible; Eq. (2.6) is relatively more constraining if relativistic longitudinal modes dominate. Figure 1 depicts the scaling of Eq. (2.6) for freely evolving dark photons in all possible regimes of wave number k/am_A and Hubble rate H/m_A .

We derive a concrete bound on g_D from Eq. (2.6) by taking dark photons to be produced at a time t_* in the radiation era (when the Hubble rate is $H_* = 1/2t_*$) with typical wave number k_* and energy density $\rho_A(t_*)$. The energy density of the dominant modes scales like a^{-4} until it becomes nonrelativistic when $\sqrt{H_{\text{NR}}/H_*}k_*/a_* = m_A$ (where $H \propto a^{-2}$ during radiation domination). Afterward, the dark photon’s energy density dilutes like matter ($\propto a^{-3}$). For a present-day abundance of dark photons $\Omega_A = \rho_A(t_0)/\rho(t_0)$ with $\rho(t_0)$ the critical density, and Ω_m defined likewise for the total matter density,

$$\frac{\Omega_A}{\Omega_m} \frac{3M_{\text{pl}}^2 H_{\text{eq}}^2}{2} \approx \left(\frac{H_{\text{eq}}}{H_{\text{NR}}} \right)^{3/2} \left(\frac{H_{\text{NR}}}{H_*} \right)^2 \rho_A(t_*), \quad (2.7)$$

where H_{eq} is the Hubble rate at matter-radiation equality, equal to 2.26×10^{-28} eV in *Planck*’s

² The phase transition is entirely nonthermal, making “superheating” a misnomer.

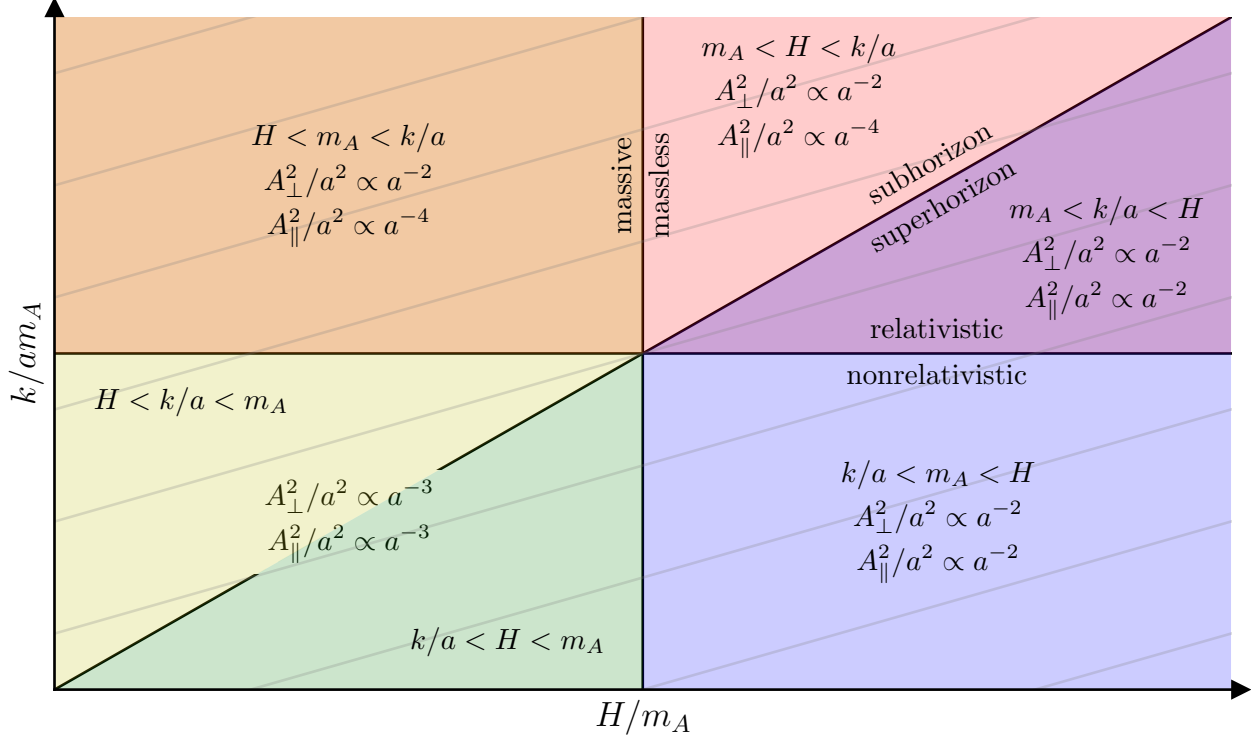


Figure 1. Redshifting of the dark photon's contribution to the Higgs's effective potential, $\propto m_A^2 A_\mu A^\mu$, in various regimes of free evolution. The horizontal and vertical axes are the physical Hubble scale and the physical momentum of a given mode. Gray lines depict the trajectory of modes of a fixed comoving wave number in time (from the top right to the bottom left). The relationship between H and k/a fixes a radiation-dominated Universe with $H \propto a^{-2}$; modifications to the expansion history would merely alter the line separating the sub- and superhorizon regimes.

best-fit cosmology [58]. Solving for $\rho_A(t_*)$ and plugging into Eq. (2.6) gives

$$g_D \lesssim 10^{-14} \lambda^{1/4} \left(\frac{m_A}{\mu\text{eV}} \right)^{5/8} \left(\frac{m_A}{H_\star} \right)^{3/8} \left(\frac{\Omega_A}{\Omega_m} \right)^{-1/4} \begin{cases} \left(\frac{H_{\text{NR}}}{H_\star} \right)^{-1/8}, & \rho_{A,\perp} \gg \rho_{A,\parallel}, \\ \left(\frac{H_{\text{NR}}}{H_\star} \right)^{1/8}, & \rho_{A,\perp} \ll \rho_{A,\parallel}. \end{cases} \quad (2.8)$$

Independent of polarization, the bounds on g_D are least severe when H_\star is as small as possible, as illustrated by Fig. 2. That is, the later dark photons are produced, the lower their peak energy density. The case with purely transverse dark photons benefits from remaining relativistic until as late as is allowed, while longitudinal-mode production is least constrained if nonrelativistic at the start; the dependence on H_{NR}/H_\star is modest in either case. As we show in the following, models of nonthermal production typically take place when $H_\star \gtrsim m_A$, setting a useful benchmark.

Crucially, reducing the gauge coupling g_D to avoid backreaction comes at the cost of also decreasing the strength of kinetic mixing between the dark and SM photons. In the simplest scenarios, kinetic mixing is generated by loops of fermions charged under both the visible and dark photons and is therefore proportional to their charge under both groups [59]:

$$\varepsilon \sim \frac{eg_D}{16\pi^2}, \quad (2.9)$$

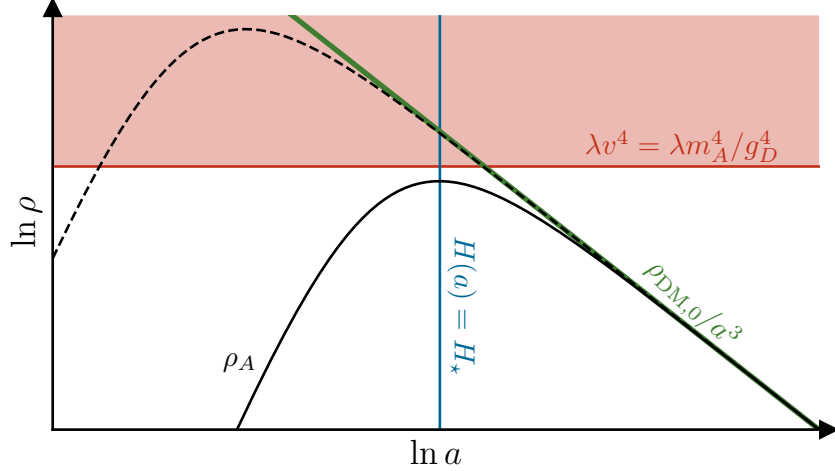


Figure 2. Illustration of dark photon production that avoids backreaction onto the Higgs by delaying the time of production (see also Ref. [52]). After it is produced and becomes nonrelativistic, the dark matter has a known energy density at any scale factor a (indicated by the green line) extrapolated from its present-day value. For any choice of model parameters, its energy density would exceed the threshold for backreaction (in the red shaded region) at some early time. By sufficiently delaying the production of dark photons, i.e., until some critical Hubble rate H_* (indicated by the blue line), they never backreact onto the Higgs (per the solid black curve). Dark photons produced too early (as in the dashed black curve) backreact onto the Higgs, possibly cutting off production before the total dark matter energy density is produced, and possibly collapsing into a string network that is not viable cold dark matter.

with loop factor $16\pi^2$ chosen to match Ref. [48]. On the other hand, kinetic mixing is a dimension-four operator, and from the perspective of effective field theory there is no fundamental obstruction to simply choosing $\varepsilon \gg g_D$. However, in the basis with diagonal kinetic and mass terms ($A_{\text{SM}} \rightarrow A_{\text{SM}} - \varepsilon A$), the SM fermions have a charge $Q \sim \varepsilon/eg_D$ under the dark gauge group—i.e., choosing an arbitrary value of ε is equivalent taking the SM fermions to have an arbitrarily large charge measured in units of the dark Higgs charge (g_D). A prototypical mechanism to mechanize a large hierarchy in charges from a theory with order-unity parameters is clockwork [60], which we consider in detail in Sec. III.

Taking Eq. (2.8) as a fiducial benchmark, Fig. 3 depicts bounds for several benchmark scenarios in the ε - m_A parameter space, superimposed with current limits [61–109] and the prospective reach of DMRadio [110], Dark E-field [111], ALPHA [112], MADMAX [113], BREAD [114] and an extension using a highly excited cyclotron [115], LAMPOST [116], SuperCDMS [117], and LZ [118]. Much of the open, experimentally accessible parameter space lies in the range $10^{-16} \lesssim \varepsilon \lesssim 10^{-10}$; only the lower end of this range, however, is within the reach of future searches for scenarios with $H_* \gtrsim m_A$.

A maximally conservative bound might assume that the dark matter existed no earlier than directly evidenced by data—namely, no earlier than required by observations of the cosmic microwave background (CMB) anisotropies. The visible CMB is sensitive to scales that enter the horizon in the few decades of expansion around matter-radiation equality; we take $H_* \approx 10^{-22}$ eV as a reasonable threshold. Figure 3 shows that a hypothetical scenario delaying production to so late a time is viable in nearly all the parameter space of future searches. Interestingly, bounds on dark photon dark matter from cosmological observations [72–76] (labeled “dark matter from cosmology/astrophysics” in Fig. 3) reside within this conservative exclusion region—that is, in the parameter space excluded by Refs. [72–76], dark photons with kinetic mixing Eq. (2.9) and a standard Higgs mass could not be the dark matter anyway.

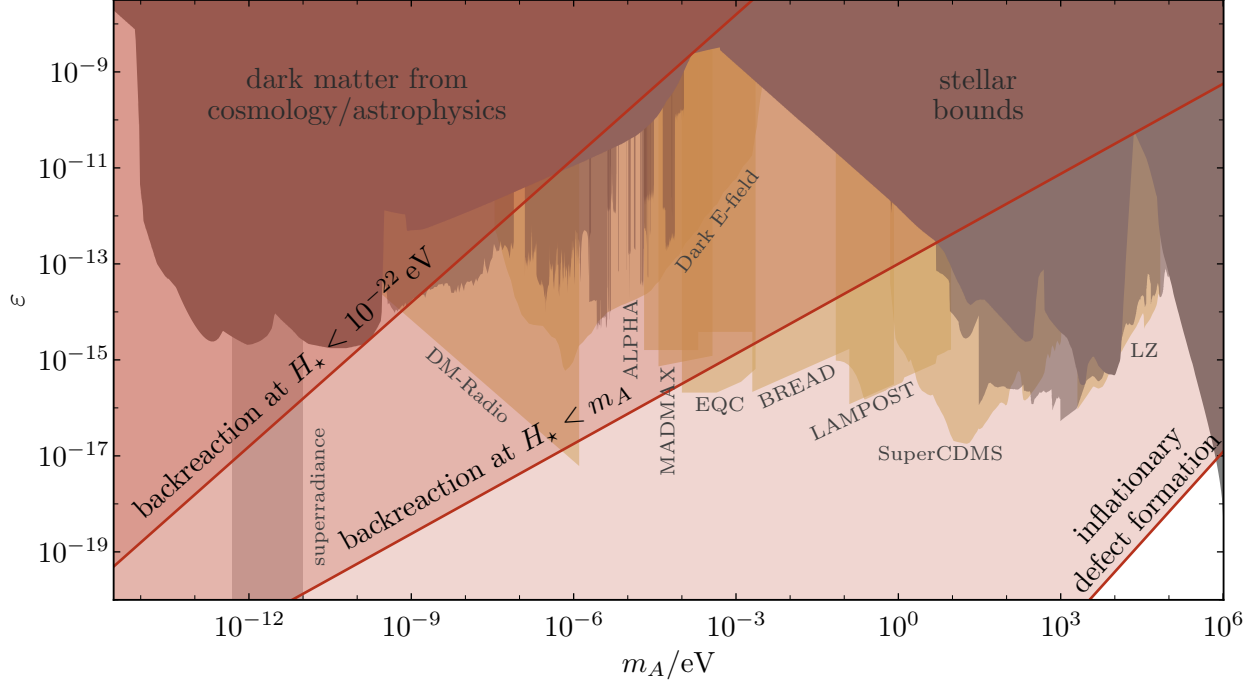


Figure 3. Parameter space for kinetically mixed dark photons. Current exclusions from astrophysical [61–71] and cosmological [72–76] probes are depicted in dark gray and those from haloscope and other laboratory searches [79–109] in light gray. The projected reaches [47] of DMRadio [110], Dark E-field [111], ALPHA [112], MADMAX [113], BREAD [114] and an extension using a highly excited cyclotron [115], LAMPOST [116], SuperCDMS [117], and LZ [118] are depicted in yellow. The red regions depict various benchmark thresholds for which the dark photon substantially backreacts onto the dark Higgs’s effective potential [Eq. (2.8)] and can collapse into a string network, taking the fiducial kinetic mixing of Eq. (2.9). These benchmark scenarios include inflationary production [Eq. (2.12)]; nonrelativistic, postinflationary production taking place when the Hubble $H_\star < m_A$; and a maximally conservative bound that only requires avoiding backreaction only around the time when scales relevant to CMB anisotropies enter the horizon.

A. Inflationary production

The most minimal mechanism for cosmological particle production is gravitational [119]. During inflation, minimally coupled degrees of freedom are excited as their wave number exits the horizon, so long as their action breaks conformal symmetry. Though the transverse polarizations of a vector are conformally symmetric up to their small mass $m_A \ll H_I$, the longitudinal mode of a massive vector is equivalent to a minimally coupled scalar field; its action thus violates conformal symmetry no matter how small its mass. Reference [50] showed that longitudinal modes exit the horizon during inflation with amplitude $kH_I/2\pi m_A$; per Fig. 1, they remain frozen until they either become massive (i.e., when $H \leq m_A$) or enter the horizon. A mode with wave number k reenters the horizon at $a_\times = k/H(a_\times)$ and becomes nonrelativistic at $a_{\text{NR}} = k/m_A$. Assuming that the radiation era began immediately after inflation (so that $H \propto a^2$) and using Eq. (A16), the energy density per logarithmic wave number thus scales as

$$\frac{d\rho_\parallel}{d\ln k} \propto \frac{m_A^2}{a^2} \frac{d|A_\parallel|^2}{d\ln k} \sim m_A^2 \left(\frac{H_I}{2\pi}\right)^2 \left(\frac{H(a)}{m_A}\right)^{3/2} \cdot \begin{cases} \left(\frac{k}{a_\star m_A}\right)^2, & k < a_\star m_A, \\ \left(\frac{k}{a_\star m_A}\right)^{-1}, & k > a_\star m_A \end{cases} \quad (2.10)$$

at late times $a > a_*$ and $a > a_\times$. The present abundance of longitudinal dark photons produced gravitationally is thus dominated by the mode that enters the horizon when $H = m_A$ and takes the form [50]

$$\Omega_A = \Omega_{\text{DM}} \left(\frac{m_A}{0.1 \text{ meV}} \right)^{1/2} \left(\frac{H_I}{5 \times 10^{13} \text{ GeV}} \right)^2. \quad (2.11)$$

Dark photons with mass m_A below 0.1 meV cannot be sufficiently produced during inflation due to bounds on the tensor-to-scalar ratio from recent *Planck* and *BICEP/Keck* observations [120].³

During inflation, unsuppressed formation of topological defects takes place if $H_I^2 \gtrsim \mu = \pi v^2 \ln(\min[\lambda/g_D^2, \sqrt{\lambda}v/H_I])$ [48, 121], where μ is the string tension.⁴ After inflation, these strings approach a scaling solution and absorb any remaining coherent dark photon field. Thus, if inflation is to account for vector dark matter, then the scale of inflation H_I must be below the Higgs VEV v , in turn bounding the dark gauge coupling by [48]

$$g_D \lesssim \frac{m_A}{H_I} \lesssim 2 \times 10^{-22} \left(\frac{m_A}{\text{eV}} \right)^{5/4} \left(\frac{\Omega_A}{\Omega_{\text{DM}}} \right)^{-1/2}. \quad (2.12)$$

The corresponding kinetic mixing [Eq. (2.9)] is well out of range of any foreseeable experiment (Fig. 3).⁵

The abundance in Eq. (2.11), as computed in Ref. [50], assumes instantaneous reheating, i.e., that the radiation era begins immediately following inflation. There is no guarantee that a prolonged era dominated by matter (or something more exotic) did not occur first after inflation, which modifies the relationship between the inflationary scale H_I and the relic abundance when the dark photon's mass m_A exceeds the Hubble rate at reheating H_{RH} . (Here by reheating we mean the moment the radiation era began, not necessarily that when the SM itself is populated and thermalized.) Modified expansion histories therefore shift the bound on g_D in Eq. (2.12) (as well as the minimal allowed dark photon mass m_A given an upper bound on H_I from CMB observations).

1. Postinflationary expansion history

The results of Ref. [50] were extended to an arbitrary reheating temperature in Refs. [124, 125] and to arbitrary expansion histories before reheating in Ref. [126]. In the simplest inflationary scenarios, once slow roll ends, the inflaton retains the entirety of the Universe's energy as it oscillates about the minimum of its potential (which is typically taken to be quadratic, such that the inflaton is matterlike in this period). The Universe only reheats once the inflaton's dominant decay channel becomes efficient relative to the expansion rate. Since the inflaton's energy density redshifts more slowly than the SM radiation it eventually decays into, the relative abundance of dark photons is lower for later reheating. Achieving the full relic abundance of the dark matter at a fixed dark photon mass then requires a larger inflationary scale H_I , such that avoiding defect formation imposes an even stronger limit on g_D . In fact, the relic abundance is independent of m_A for $m_A > H_{\text{RH}}$ [124–126], instead scaling with $\sqrt{H_{\text{RH}}} H_I^2$. Requiring the dark photon to make up all of the dark matter then places a lower bound on the Hubble rate when the radiation era began as a

³ Namely, taking the amplitude of the scalar power spectrum $A_s = 2.1 \times 10^{-9}$ [58] and the tensor-to-scalar ratio $r < 0.036$ [120] bounds $H_I = \sqrt{\pi^2 r A_s / 2 M_{\text{Pl}}} < 4.7 \times 10^{13} \text{ GeV}$.

⁴ References [122, 123] extended the study of inflationary dark photon production to account for a Higgs mass, though without considering the implications for direct detection.

⁵ Reference [48] points out that this bound may in fact be conservative, as even if string production is exponentially suppressed ($H_I \lesssim v$) strings may continue to grow in the background of the dark electromagnetic field to reach a scaling solution. In fact, this concern is also relevant for Eq. (2.8): large fluctuations, though exponentially unlikely, can produce strings. The precise threshold value of H_I or $\rho_A(t_*)$ for which strings would be cosmologically relevant today requires further study.

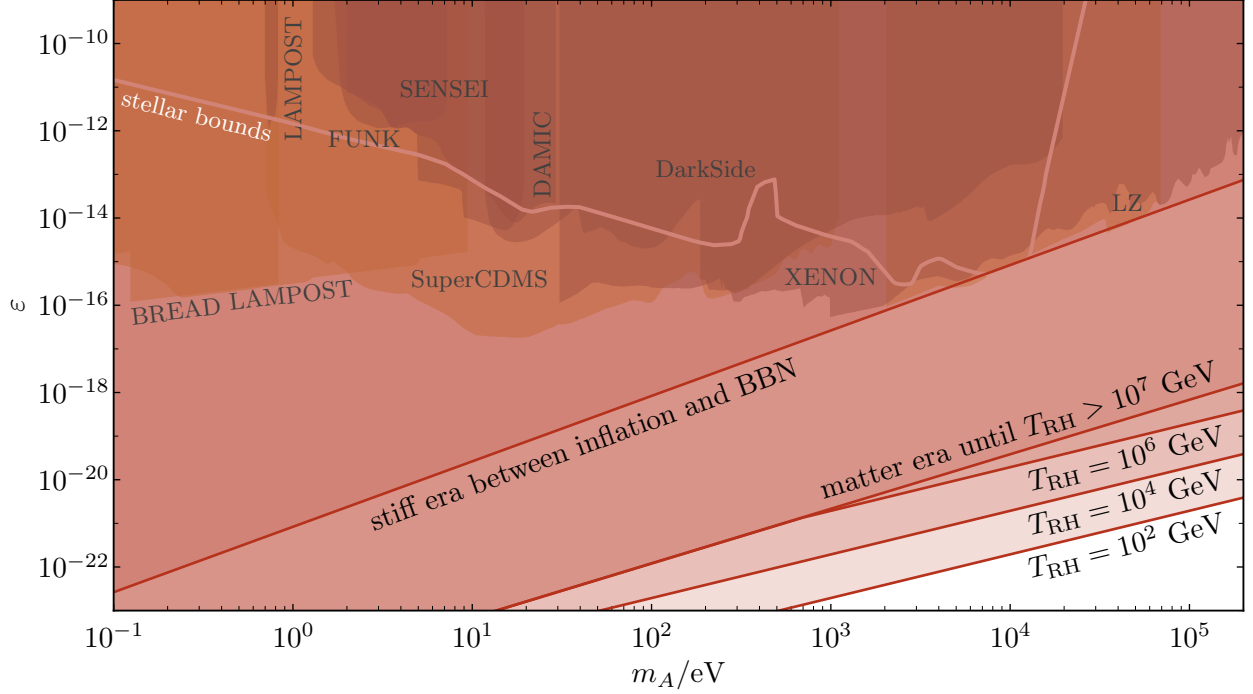


Figure 4. Kinetic mixing parameter space [Eq. (2.9)] of dark photon dark matter produced during inflation. Red regions depict parameter space that are constrained by defect formation under various assumptions on the expansion history between inflation and nucleosynthesis, as labeled on the figure: the standard case of instantaneous reheating, an extreme case in which the Universe is kination-dominated ($w = 1$) until BBN, and various extended epochs of matter domination with reheating temperatures indicated on the figure. Current limits from LAMPOST [94], FUNK [90], SENSEI [91], DAMIC [87], DarkSide [101], and XENON [86, 93, 97, 98] are depicted in gray and the projected reach [47] of BREAD [114], LAMPOST [116], SuperCDMS [117], and LZ [118] in yellow. Joint bounds from stellar probes are outlined in white.

function of H_I . The bound on the dark gauge coupling Eq. (2.12) is then penalized by a factor of $(m_A/H_{\text{RH}})^{-1/4}$ for dark photons heavier than H_{RH} (Fig. 4).

More generally, any early epoch with equation of state $w < 1/3$ further reduces the maximal gauge coupling that avoids inflationary defect formation. For stiffer equations of state $w > 1/3$, the Universe’s energy density redshifts faster than radiation, instead easing constraints on g_D . The net enhancement in abundance in the $w \rightarrow 1$ limit is $\sim \sqrt{m_A/H_{\text{RH}}}$ [126], requiring a lower inflationary scale to match the dark matter relic abundance and alleviating bounds on g_D by a factor $\sim \sqrt[4]{m_A/H_{\text{RH}}}$. The minimum reheat temperature allowed by big bang nucleosynthesis (BBN) is of order 10 meV [127–133], corresponding to $H_{\text{RH}} \approx 10^{-14}$ eV and an enhancement in allowed g_D of about three orders of magnitude for $m_A \sim \text{eV}$. Figure 4 shows that, while no viable parameter space is accessible to current or future searches assuming an instantaneous onset of radiation domination, a stiff era indeed marginally allows for kinetic mixing within reach of LZ [118] and only just below current exclusions from XENON [86, 93, 97, 98]. On the other hand, if the Universe were instead matter-dominated for some or all of the epoch between inflation and BBN (a possibility one has little reason to exclude *a priori*), viable kinetic mixings are up to ~ 2.5 decades further out of reach of these experiments, depending on how late reheating occurs.⁶

⁶ Note that $T_{\text{RH}} = 444$ GeV is the lowest possible reheating temperature for which dark photons (of any mass) produced gravitationally during inflation may make up the entire dark matter abundance when taking $H_I < 4.7 \times 10^{13}$ GeV (see Footnote 3).

2. Nonminimal couplings

Nonminimal couplings to gravity may affect the relic abundance of dark photons generated during inflation [134, 135]. However, nonminimally coupled Proca theories of the form

$$\mathcal{L} = -\frac{1}{4}F_{\mu\nu}F^{\mu\nu} + \frac{1}{2}m_A^2 A_\mu A^\mu - \frac{1}{2}\xi_1 R A_\mu A^\mu - \frac{1}{2}\xi_2 R^{\mu\nu} A_\mu A_\nu \quad (2.13)$$

exhibit ghost instabilities [136–138]. References [139, 140] more recently discuss these runaway instabilities during inflation, arguing that they are present if the nonminimal couplings ξ_1 and ξ_2 are larger than $\sim (m_A/H_I)^2$ in magnitude; the dynamics have only been solved numerically, preventing a simple analysis of the effect on defect formation bounds. References [139, 140] claim that radiative corrections in Abelian-Higgs theories generate nonminimal couplings of order $(m_A/m_h)^6 = g_D^6/(2\lambda)^3$. The runaway instability is then absent if $g_D/\sqrt{2\lambda} < \sqrt[3]{m_A/H_I}$, which is a dramatically weaker requirement than that to evade inflationary defect formation [Eq. (2.12)].

Moreover, the nonminimal couplings in Eq. (2.13) must ultimately descend from gauge-invariant operators. (Otherwise, technical naturalness would not protect the dark photon’s mass from large radiative corrections.) The only gauge-invariant operator linear in A_μ is $D_\mu\Phi$; the nonminimally coupled Abelian-Higgs theory therefore must take the form

$$\mathcal{L} = -\frac{1}{4}F_{\mu\nu}F^{\mu\nu} + \frac{1}{2}\left(g^{\mu\nu} - \frac{\xi_1}{m_A^2}Rg^{\mu\nu} - \frac{\xi_2}{m_A^2}R^{\mu\nu}\right)D_\mu\Phi(D_\nu\Phi)^* - \frac{\lambda}{4}\left(|\Phi|^2 - v^2\right)^2. \quad (2.14)$$

As mentioned by Ref. [48], such a nonminimal coupling for the dark Higgs drives its VEV to larger values during inflation, which would mitigate defect formation if an increase in the inflationary scale were not required to compensate for a suppression incurred in the dark photon abundance (as derived in Sec. VB1). Furthermore, the effective Higgs mass squared is also suppressed by a factor $\sim m_A^2/\xi_i R$, not to mention the additional derivative couplings induced by the time dependence of the coefficient of the Higgs’s kinetic term. Unless m_h/H_I is even larger than $\sqrt{|\xi_i|H_I/m_A}$, the Higgs is thus light during inflation and would be produced gravitationally to a comparable degree; since the Higgs is much heavier at late times, it would dominate the dark sector density. When requiring the Higgs to remain heavy during inflation (i.e., $m_A^2 m_h^2/|\xi_i|H_I^4 > 1$), if $|\xi_i| \sim (m_A/m_h)^6$ as expected from radiative corrections then $|\xi_i| < (m_A/H_I)^3$ and the runaway instability is absent.

Though Eq. (2.14) is written in terms of ξ_i/m_A^2 to match the form of Eq. (2.13), in reality we expect the coefficient of these dimension-6 operators to be $1/\Lambda^2$ where Λ is the energy scale of the physics that generates the nonminimal couplings. (Written in terms of Λ , the $m_A \rightarrow 0$ limit explicitly restores gauge symmetry and the dark photon mass’s technical naturalness remains manifest.) In order that the low-energy theory remain a valid description of gravity during inflation, H_I (if not the energy scale $\sqrt{H_I M_{\text{pl}}} \gg H_I$) should be below Λ ; one would thus expect that $\xi_i \sim (m_A/\Lambda)^2 < (m_A/H_I)^2$, even discounting powers of the dark gauge coupling expected from vertex factors. It is therefore not even clear whether the radiatively generated ξ_i should be large enough to trigger the runaway instability in the first place without breaching the validity of the effective field theory. Because it is unclear whether nonminimal couplings can have a significant impact on dark photon dark matter production without overproducing the dark Higgs, triggering vortex formation, or violating perturbativity, we do not consider them further (except when referencing their invocation in past literature on vector misalignment in Sec. IID).

3. Direct inflaton couplings

The dark photon (or one of the particles it interacts with) could also directly couple to the inflaton, enabling more efficient production of dark photon fluctuations and therefore a lower scale of inflation to achieve the dark matter relic abundance [141–147]. These mechanisms are nonetheless constrained at least to the same extent as any late-time production mechanism, i.e., Eq. (2.8) with $H_\star = m_A$; however, the maximal energy density is necessarily higher than that assumed in Eq. (2.8) given that the dark photons were produced before the end of inflation. Referring to Fig. 1, $A_\mu A^\mu$ redshifts no more slowly than a^{-2} , and while $H > m_A$ all modes redshift as such except for subhorizon, longitudinal ones for which $A_\mu A^\mu \propto a^{-4}$. Taking a general equation of state w in this epoch such that $H \propto a^{-3(1+w)/2}$, Eq. (2.8) is penalized by an additional factor $(m_A/H_I)^{1/3(1+w)}$. If longitudinal modes enter the horizon at a scale factor a_\times before $H = m_A$, a further penalty of $(a_\times/a_\star)^{1/2}$ is incurred. These factors only account for the dark photons existing at the end of inflation; production earlier in inflation yields yet stronger bounds (but with model dependence that is difficult to capture on general grounds).

Similar scenarios where the dark photon instead couples to a rolling spectator field during inflation [146] are subject to the same bounds. However, Refs. [142–144, 146] considered only phenomenological parametrizations of the time dependence of the coupling function to the inflaton or spectator, neglecting the production that occurs (in concrete models) as the coupled scalar eventually oscillates about the minimum of its potential—i.e., preheating. This contribution most likely substantially modifies the results in these models, given that preheating would produce dark photons on scales as small as $k \sim a_e H_I$ where a_e is the scale factor at the end of inflation. On the other hand, the results of Refs. [141, 145, 147] are limited to the linear regime in which backreaction effects are negligible; full nonlinear dynamics of such models were treated in Refs. [148–157], albeit not specialized to dark photons specifically as the dark matter.

B. Irreducible thermal fluctuations

Dark photons that kinetically mix with the SM photon are inevitably thermally excited to some degree; depending on the thermal history of the Universe, these fluctuations can be large enough to restore symmetry to the dark Higgs such that topological defects form via the Kibble-Zurek mechanism [158]. The dynamics of the photon–dark-photon system are described by the Lagrangian

$$\mathcal{L} = -\frac{1}{4}F_{\mu\nu}F^{\mu\nu} - \frac{1}{4}F_{\text{SM}\mu\nu}F_{\text{SM}}^{\mu\nu} + \frac{1}{2}m_A^2 A_\mu A^\mu - \frac{\varepsilon}{2}F_{\mu\nu}F_{\text{SM}}^{\mu\nu} - eJ_{\text{SM}}^\mu A_{\text{SM}\mu}, \quad (2.15)$$

where J_{SM} is the current of electrically charged SM particles. Charged SM particles are sterile with respect to the combination $S = A + \varepsilon A_{\text{SM}}$, making the $\{A_{\text{SM}}, S\}$ basis a convenient choice to discuss the propagation of (dark) photons in the SM plasma [61]. The dispersion relation of the active state A_{SM} receives corrections in the background of the Standard Model plasma, resulting in the well-known effective mixing angle between A_{SM} and S [61],

$$\epsilon_{\text{eff},\lambda}^2 = \frac{\varepsilon^2 m_A^4}{(m_\lambda^2 - m_A^2)^2 + \omega^2 \Gamma_\lambda^2} + \mathcal{O}(\varepsilon^4), \quad (2.16)$$

where m_λ and Γ_λ are the plasma frequency and damping rate of SM photons with polarization state λ and ω is the frequency of the photons.

At sufficiently early times, the plasma frequency of transverse modes far exceeds the bare mass of the dark photon, i.e., $m_\perp^2 \propto e^2 T^2 \gg m_A^2$; the effective mixing angle is then suppressed relative to

its vacuum value as $\varepsilon_{\text{eff},\perp} \sim \varepsilon m_A^2/m_\perp^2$. In other words, the transverse photon $A_{\text{SM},\perp}$ is not only an interaction eigenstate but also nearly a propagation eigenstate. The amplitude of the sterile state S is therefore suppressed relative to the SM photon by a factor $\varepsilon m_A^2/m_\perp^2$ and hence

$$A_\perp \approx -\varepsilon [1 + \mathcal{O}(m_A^2/m_\perp^2)] A_{\text{SM},\perp}. \quad (2.17)$$

The dark photon fluctuations of order $\varepsilon A_{\text{SM},\perp}$ do not set the late-time relic dark matter abundance—they are strongly coupled to the plasma and continually reabsorbed—rather, the sterile state itself adiabatically transitions into the dark photon as the Universe cools and the plasma frequency drops. These A_\perp fluctuations do, however, backreact onto the dark Higgs, and at sufficiently large temperature and dark gauge coupling the small, thermal dark photon fluctuations are enough to restore symmetry globally to the Higgs. That is, the active state A_{SM} receives a small effective mass from the Higgs field $\varepsilon g_D |\Phi|$, leading to a thermal effective potential for the Higgs [159] $V_{\text{eff}}(|\Phi|^2) \supset \varepsilon^2 g_D^2 |\Phi|^2 T^2/24$. This effective potential restores symmetry to the Higgs when Standard Model temperature is sufficiently large, and consequently defects form by the Kibble-Zurek mechanism, precluding the formation of dark photon dark matter at some later epoch. Requiring that symmetry remains broken when SM temperature is its largest (T_{max}) sets a bound

$$\varepsilon \lesssim 1.1 \times 10^{-6} \lambda^{1/6} \left(\frac{m_A}{\mu\text{eV}} \right)^{1/3} \left(\frac{T_{\text{max}}}{10 \text{ MeV}} \right)^{-1/3} \left(\frac{16\pi^2 \varepsilon}{eg_D} \right)^{2/3}. \quad (2.18)$$

This limit is depicted in Fig. 10 (red lines labeled by values of T_{max}) and discussed in Sec. VI.

C. Axion oscillations and tachyonic resonance

While inflationary and thermal dark photon production are both minimal scenarios in their physical content and assumptions, neither can produce dark photon dark matter at small masses and large couplings—nor can either produce viable dark photon dark matter below 0.1 meV at all. Detectably large kinetic mixing in the sub-meV mass range requires a nonthermal, postinflationary, and nonminimal production mechanism (or an *ad hoc* mechanism to boost ε relative to g_D ; see Sec. III). One possibility is that the dark photon inherits the relic abundance of a misaligned scalar field via resonant particle production. A canonical example is a coupling to an axion $\phi_a = f_a \theta$ with mass m_a and decay constant f_a through the axial term $\tilde{F}_{\mu\nu} F^{\mu\nu}/4 = \mathbf{E} \cdot \mathbf{B}$ [56, 160–162],

$$\mathcal{L} \supset \frac{1}{2} f_a^2 \partial_\mu \theta \partial^\mu \theta - V(\theta) + \frac{\beta}{4} \theta \tilde{F}_{\mu\nu} F^{\mu\nu}, \quad (2.19)$$

where $\tilde{F}_{\mu\nu} \equiv \epsilon_{\mu\nu\rho\sigma} F^{\rho\sigma}$ is the dual field strength tensor. The axion lives in a compact field space, and its potential often takes the simple periodic form

$$V = m_a^2 f_a^2 (1 - \cos \theta). \quad (2.20)$$

After a period of inflation with $m_a \ll H_I \ll f_a$, the axion field assumes a nearly homogeneous initial condition $\theta(0, \mathbf{x}) \equiv \theta_0$ selected from the interval $[0, 2\pi)$ with approximately uniform probability. To linear order in spatial fluctuations, the equations of motion for the circular polarizations of the dark

photon A_\pm [Eq. (A7c)] and the spatially averaged axion $\bar{\theta}(t)$ are

$$0 = \ddot{\theta} + 3H\dot{\theta} + m_a^2\theta - \frac{\beta}{f_a^2}\langle\mathbf{E}\cdot\mathbf{B}\rangle \quad (2.21a)$$

$$0 = \ddot{A}_\pm + H\dot{A}_\pm + \left(\frac{k^2}{a^2} + m_A^2 \pm \beta\dot{\theta}\frac{k}{a}\right) A_\pm, \quad (2.21b)$$

neglecting nonlinearities in the axion potential.

Provided β is large enough that $\beta\dot{\theta} \geq 2m_A$, the effective frequency of one of the two transverse polarization states is negative, leading to the exponential growth of A_\pm due to a tachyonic resonance [56, 160]. In the simplest scenarios, the axion’s damped and (nearly) harmonic oscillations begin around the time when $H = m_a$. The maximum velocity of an axion oscillating in a quadratic potential is set by its mass, i.e. $|\dot{\theta}| \leq m_a\theta_0$; tachyonic resonance then occurs if $\beta\theta_0 > 2m_A/m_a$. A more precise determination of the conditions for efficient resonance requires solving the equations of motion (see Appendix D); the so-called “broad resonance” regime requires

$$\beta\theta_0 \gg \max\{1, 4m_A/m_a\}. \quad (2.22)$$

In the broad resonance regime, the dark photon mode that grows the most has wave number $\mathcal{O}(\beta m_a)$.⁷

Assuming $\theta_0 \sim 1$, efficient dark photon production requires β larger than unity to some degree. If β is just large enough for production to be efficient [Eq. (2.22)], then by kinematics the dark photon cannot be heavier than the axion and production must occur at $H_\star \gtrsim m_A$. This regime is well studied [56, 160–162]. The resulting limit on the kinetic mixing that avoids backreaction onto the Higgs is displayed in Fig. 3 [assuming the fiducial relationship between g_D and ε , Eq. (2.9)] and coincides with the constraint taken in Ref. [56] to ensure backreaction onto the Higgs’s mass is negligible. Production at $H_\star \gtrsim m_A$ does offer substantially improved detection prospects compared to minimal inflationary production. Notably, however, most of the experimental prospects are only for masses above an meV—a range already accessible to inflationary production (i.e., given an *ad hoc* enhancement of the kinetic mixing in the latter case; see Sec. III). Thus, the sub-meV mass range (as probed by axion haloscopes) remains out of reach without additional machinery.

When the dark photon’s energy density becomes comparable to that of the axion, it backreacts onto the axion via nonlinear processes, altering the rate and direction of energy transfer. For resonant production mechanisms from massive, oscillating (pseudo)scalars in general, the final energy partition between the dark photon and the scalar ultimately must be quantified by numerical simulations. Those presented in Ref. [56] show that whether the majority of the axion’s energy density ends up in the dark photon depends on the mass ratio and becomes less efficient as m_a/m_A becomes large, though the range of ratios that have been simulated is limited. The nonlinear dynamics of backreaction do not generically yield a large hierarchy in abundance; Ref. [160] discusses a number of model-dependent remedies to dilute any remaining axion energy density.

In standard constructions where the axion-photon coupling is generated via Peccei-Quinn (PQ) fermions, order-unity couplings β are not the natural expectation. The anomaly coefficient to the PQ charge of the $U(1)_D$ -charged fermions is [56, 164]

$$C_{\theta AA} \sim \sum_{i=1}^{N_f} Q_i^2 \sim N_f Q_f^2, \quad (2.23)$$

⁷ The dynamics of broad parametric resonance via an oscillating, parity-even scalar [51] (or the dark Higgs itself [163]) are qualitatively similar. Production via scalars does allow for a number of qualitatively distinct regimes, which we discuss in detail in Sec. V.

where Q_i is the PQ charge of the i th fermion, and N_f is the total number of fermions. In terms of $C_{\theta AA}$ and the dark fine-structure constant $\alpha_D = g_D^2/4\pi$, the axial coupling is

$$\beta = C_{\theta AA} \frac{\alpha_D}{2\pi}. \quad (2.24)$$

For modest charges and number of PQ fermions, $\beta \sim g_D^2 \ll 1$, in extreme tension with the requirement for tachyonic resonance [Eq. (2.22)]. Namely, for gauge couplings that evade backreaction onto the Higgs [Eq. (2.8)],

$$C_{\theta AA} \gtrsim 10^{31} \frac{\beta}{10} \sqrt{\frac{\Omega_A}{\Omega_{\text{DM}}}} \left(\frac{m_A}{\mu\text{eV}} \right)^{-5/4} \left(\frac{m_A}{m_a} \right)^{-1/4}. \quad (2.25)$$

References [56, 164, 165] discuss several model-building avenues to enhance the axial coupling relative to the nominal expectation, including taking N_f and Q_f large as well as the clockwork mechanism [60]. We discuss clockwork and its consequences for backreaction onto the Higgs in more detail in Sec. III. Abelian clockwork may also simultaneously account for large hierarchies between ε and g_D and between β and α_D [56].

D. Vector misalignment

Much like scalar fields, the energy density of a homogeneous vector field dilutes as a^{-3} when $H \lesssim m_A$, and the resulting condensate behaves as cold dark matter [166]. But in contrast to a scalar, a vector's energy density dilutes as a^{-2} at early times ($H \gtrsim m_A$) when it is not oscillating, as can be inferred from the $k/a \ll m_A$ limit in Fig. 1. Successful vector misalignment after inflation therefore requires a nonminimal coupling to gravity of the form Eq. (2.13) with $\xi_1 = -1/6$ and $\xi_2 = 0$ to avoid this additional a^{-2} dilution [72]. Setting aside the theoretical issues with nonminimal couplings discussed in Sec. II A 2, vector misalignment provides a useful benchmark for nonthermal production of dark photons—in particular, one whose initial conditions lack magnetic fields.

In the absence of spatial gradients, the temporal component A_0 vanishes and the dark photon is purely electric. Defining the rescaled field $\tilde{A}_i = \bar{A}_i/a$, each component of \tilde{A}_i satisfies the equation for the evolution of a homogeneous scalar with additional terms proportional to $1 + 6\xi_1 \equiv 1 - \kappa$:

$$0 = \ddot{\tilde{A}}_i + 3H\dot{\tilde{A}}_i + \left[m_A^2 + (1 - \kappa) \left(\dot{H} + 2H^2 \right) \right] \tilde{A}_i. \quad (2.26)$$

During inflation, the solutions to this equation all decay exponentially if $\kappa < 1$, while one instead grows exponentially if $\kappa > 1$; the vector field \tilde{A}_i is only constant if κ is tuned very close to one. Fixing $\kappa = 1$, vector misalignment and scalar misalignment are mathematically identical in vacuum.

A homogeneous dark photon field contains no magnetic flux, offering misalignment a possible loophole to avoid the defect bound Eq. (2.5). On the other hand, if $m_A^2 \tilde{A}_i(0)^2 \gtrsim \lambda v^4$, the dark photon condensate causes the Higgs field to oscillate about the symmetric point $\Phi = 0$; the dark photon itself then slowly rolls due to its oscillating (and decreasing) mass. Perturbations in one of Φ or Φ^* experience a tachyonic instability that ultimately fragments the Higgs, although whether misalignment would seed topological defects is a question that can only be addressed by numerical simulations (see Appendix B of [48]).

III. CLOCKWORKED COUPLINGS AND BACKREACTION

The fiducial kinetic mixing Eq. (2.9) is comparable to the dark gauge coupling, as prescribed by the simple, canonical model that kinetic mixing is generated by N_f heavy fermions charged under both the SM and dark gauge groups [59, 167]:

$$\varepsilon = \frac{eg_D}{12\pi^2} \sum_{i=1}^{N_f} Q_{e,i} Q_{D,i} \ln \frac{m_i^2}{\mu^2}, \quad (3.1)$$

where m_i are the masses of the so-called “portal matter” fermions, each with charges $Q_{e,i}$ and $Q_{D,i}$ under electromagnetism and the dark U(1), respectively. The additional constraint

$$\sum_{i=1}^{N_f} Q_{e,i} Q_{D,i} = 0 \quad (3.2)$$

is often imposed so that ε is independent of the renormalization scale μ . Assuming that the portal matter masses are comparable and their charges are order unity leads to the parametric estimate of Eq. (2.9). Clearly, taking a large number of fermions and/or their charges large enhances ε/g_D . A less contrived possibility, perhaps, is the clockwork mechanism [48, 60]. In this section we consider the viability of clockwork as a means to evade backreaction onto the Higgs and possible defect formation when invoked both to enhance the kinetic mixing itself (Sec. III A) and to generate the hierarchically large axion couplings required for successful tachyonic production (Sec. III B), as discussed in Sec. II C.

The Abelian clockwork mechanism employs a chain of $N + 1$ U(1) gauge symmetries that are broken to a single U(1) when N charged scalars (Higgses) acquire VEVs. Each gauge field A_i is labeled by an integer $i \in \{1, \dots, N + 1\}$, and each Higgs $\Phi_{i,i+1}$ is charged under two neighboring U(1)s on the chain with charges 1 and $-Q$. We denote the additional dark Higgs that couples only to the dark photon A (and generates its mass) by Φ without subscripts, and for clarity we never refer to the clockwork gauge fields without an index subscript (leaving A to denote only “the” dark photon). The clockwork Lagrangian is explicitly

$$\begin{aligned} \mathcal{L} = & \frac{1}{2} |(\partial^\mu - igA_{N+1}^\mu) \Phi|^2 + \frac{\lambda}{4} (|\Phi|^2 - v^2)^2 + gJ_\mu A_1^\mu \\ & - \frac{1}{4} \sum_{i=1}^{N+1} F_i^{\mu\nu} F_{\mu\nu}^i + \sum_{i=1}^N \left[\frac{1}{2} |D_{i,i+1} \Phi_{i,i+1}|^2 - \frac{\lambda_{i,i+1}}{4} (|\Phi_{i,i+1}|^2 - v_{i,i+1}^2)^2 \right], \end{aligned} \quad (3.3)$$

where the gauge-covariant derivative is

$$D_{i,i+1}^\mu = \partial^\mu + igA_i^\mu - iQgA_{i+1}^\mu \quad (3.4)$$

and J_μ is the current of particles charged under A_1 (e.g. the portal fermions). We also take all gauge couplings g and charges Q independent of i for simplicity. We take the N Higgses $\Phi_{i,i+1}$ to have VEVs $v_{i,i+1}$ larger than the VEV v of the Higgs Φ that ultimately breaks the last U(1) and gives the dark photon its mass.

The effective potential for the gauge fields is a sum of independent quadratics $g^2 \sum_i v_{i,i+1}^2 (A_i - QA_{i+1})^2$ that is minimized when each term in the sum is independently zero. At low enough energies, integrating out the heavy Higgses and heavy gauge fields therefore sets $|\Phi_{i,i+1}| = v_{i,i+1}$

and $A_i = QA_{i+1}$ for all $i < N + 1$. The resulting low-energy effective theory is

$$\mathcal{L} = \frac{1}{2} |(\partial_\mu - ig_D A_\mu) \Phi|^2 + \frac{\lambda}{4} (|\Phi|^2 - v^2)^2 - \frac{1}{4} F^{\mu\nu} F_{\mu\nu} + g_D Q^N J_\mu A^\mu, \quad (3.5)$$

where the canonically normalized dark photon field is identified as

$$A^\mu = \sqrt{\sum_{i=0}^N Q^{2i}} A_{N+1}^\mu = \sqrt{\frac{Q^{2(N+1)} - 1}{Q^2 - 1}} A_{N+1}^\mu \quad (3.6)$$

with a dark gauge coupling

$$g_D = g \sqrt{\frac{Q^2 - 1}{Q^{2(N+1)} - 1}}. \quad (3.7)$$

Particles charged under the first clockwork site have an effective charge under the dark photon Q^N times larger than their charge under A_1 itself, exponentially enhancing the kinetic mixing relative to the Higgs coupling g_D :

$$\varepsilon \sim Q^N \frac{eg_D}{16\pi^2}. \quad (3.8)$$

Implementing clockwork to explain large kinetic mixing with a small effective charge for the dark Higgs Φ is the reverse of the traditional invocation—to account for a small kinetic mixing with order-unity gauge couplings.

While Eq. (3.5) takes the form of the standard Abelian-Higgs model Eq. (2.1) (plus a current), it is only strictly correct while the final gauge symmetry remains unbroken. After Φ acquires its VEV, the ground state configuration of the clockwork gauge fields is modified from that above ($A_i = QA_{i+1}$ for all $i < N + 1$) because the effective potential has an additional contribution $g^2 v^2 A_{N+1}^2 / 2$. Whereas in Eq. (3.5) the massless mode couples to no clockwork Higgses in the low-energy theory, the lightest mass eigenstate [after the final U(1) is broken] couples to them all—and, with a large abundance, can in principle backreact strongly on any of the clockwork Higgses. In Sec. III A we assess whether the dark photon backreacts on any of the clockwork Higgses at a lower threshold than it does onto the dark Higgs Φ , i.e., whether clockwork modifies the backreaction condition Eq. (2.5). In Sec. III B we then consider whether the heavier clockwork gauge fields themselves may be produced (as a byproduct of the dynamics that produce the lightest mode, the dark photon) and themselves trigger backreaction onto any of the clockwork scalar fields.

A. Large kinetic mixing

In the absence of the additional dark Higgs Φ , the massless mode of the clockwork fields is precisely that which couples to none of the clockwork Higgses $\Phi_{i,i+1}$. Breaking the last gauge symmetry (with Φ) only generates effective couplings to the clockwork Higgses by perturbing the lightest mode in the clockwork spectrum away from the would-be massless mode identified in Eq. (3.5). The size of the dark photon's couplings to the clockwork Higgses must therefore be controlled by that of the dark Higgs, g_D [168]. Since $v_{i,i+1} \gtrsim v$, the threshold dark photon density at which any of the other clockwork gauge symmetries are restored is manifestly higher than that of the dark photon and dark Higgs, i.e., the dark Higgs still provides the strongest condition to evade backreaction and defect formation.

To verify this expectation, we explicitly compute the dark photon's couplings to the clockwork

Higgses by expanding in small $v/v_{i,i+1}$. The gauge fields have an unperturbed mass matrix

$$M^2 = g^2 \begin{pmatrix} v_{1,2}^2 & -Qv_{1,2}^2 & & & \\ -Qv_{1,2}^2 & Q^2v_{1,2}^2 + v_{2,3}^2 & -Qv_{2,3}^2 & & \\ & \ddots & \ddots & \ddots & \\ & & -Qv_{N-1,N}^2 & Q^2v_{N-1,N}^2 + v_{N,N+1}^2 & -Qv_{N,N+1}^2 \\ & & & -Qv_{N,N+1}^2 & Q^2v_{N,N+1}^2 \end{pmatrix}. \quad (3.9)$$

Independent of the VEVs of the $\Phi_{i,i+1}$, by inspection this matrix always has a null eigenvector

$$\mathbf{e}_0 = \sqrt{\frac{1 - Q^{-2}}{1 - Q^{-2(N+1)}}} [1, Q^{-1}, \dots, Q^{-N}], \quad (3.10)$$

which, for $v = 0$, is the (massless) dark photon field A . However, specifying the other eigenvectors requires specifying the VEVs of the clockwork Higgses. To simplify the calculation, we assume all the VEVs are the same, $v_{i,i+1} = v$, in which case the remaining eigenvectors have the form [60]

$$[\mathbf{e}_k]_j = \sqrt{\frac{2g^2v^2}{(N+1)m_k^2}} \left(Q \sin \frac{\pi j k}{N+1} - \sin \frac{\pi(j+1)k}{N+1} \right), \quad (3.11)$$

where the mass-squared eigenvalues are

$$m_k^2 = g^2v^2 \left[Q^2 + 1 - 2Q \cos \frac{\pi k}{N+1} \right]. \quad (3.12)$$

Note that all the masses of the broken U(1)s are parametrically $g^2Q^2v^2$.

When $v \ll v$, breaking the final gauge symmetry modifies the mass matrix Eq. (3.9) by a small perturbation

$$\delta M^2 = g^2 \text{diag} (0, \dots, 0, v^2). \quad (3.13)$$

The perturbation to the eigenvectors can be computed at first order in v^2/v^2 as

$$\delta \mathbf{e}_k = \sum_{j \neq k} \frac{\mathbf{e}_k^T \delta M^2 \mathbf{e}_j}{m_k^2 - m_j^2} \mathbf{e}_j. \quad (3.14)$$

The lightest of these states, which we identify as the dark photon, is then

$$[\delta \mathbf{e}_0]_i = - \left(\frac{v}{v} \right)^2 \frac{g_D}{g} \frac{2Q}{N+1} \sum_{j=1}^N \sin \frac{\pi N j}{N+1} \frac{Q \sin \frac{\pi i j}{N+1} - \sin \frac{\pi(i+1)j}{N+1}}{\left[Q^2 + 1 - 2Q \cos \frac{\pi j}{N+1} \right]^2}. \quad (3.15)$$

We may straightforwardly infer the dark photon's couplings to all the clockwork Higgses via their kinetic terms, projecting each clockwork photon onto the dark photon (i.e., the mass eigenstate $\mathbf{e}_0 + \delta \mathbf{e}_0$):

$$\mathcal{L} \supset \frac{1}{2} g^2 A_\mu A^\mu \sum_{i=1}^N ([\delta \mathbf{e}_0]_i - Q [\delta \mathbf{e}_0]_{i+1})^2 |\Phi_{i,i+1}|^2, \quad (3.16)$$

which we empirically observe to evaluate to

$$\mathcal{L} \supset \frac{1}{2} g_D^2 \left(\frac{v}{v}\right)^4 A_\mu A^\mu \sum_{i=1}^{N-1} \left(Q^{N-i} \frac{Q^{2(i+1)} - 1}{Q^{2(N+1)} - 1} \right)^2 |\Phi_{i,i+1}|^2. \quad (3.17)$$

In the limit of large Q^2 ,

$$\mathcal{L} \supset \frac{1}{2} g_D^2 \left(\frac{v}{v}\right)^4 A_\mu A^\mu \sum_{i=1}^{N-1} \frac{|\Phi_{i,i+1}|^2}{Q^{2(N-i)}} = \frac{1}{2} m_A^2 A_\mu A^\mu \left(\frac{v}{v}\right)^2 \sum_{i=1}^{N-1} \frac{|\Phi_{i,i+1}/v|^2}{Q^{2(N-i)}}. \quad (3.18)$$

The dark photon A backreacts significantly onto $\Phi_{i,i+1}$ when the corresponding terms in Eq. (3.18) exceed λv^4 . Not only is the dark photon's contribution to the clockwork Higgses' effective potentials in Eq. (3.18) suppressed relative to that for the dark Higgs Φ by $(v/v)^2$ and at least two powers of Q , their backreaction thresholds are parametrically higher by a factor of $(v/v)^4$. If only the A field is produced and no other eigenstate, clockwork therefore remains a viable means to boost kinetic mixing without requiring a large hierarchy $v/v \sim g/g_D$, contrary to the claim made in Appendix C.1 of Ref. [48].

B. Large axion coupling

While the preceding section establishes that the dark photon itself does not backreact strongly onto any of the clockwork Higgses before it does so to the dark Higgs, any production channel via an interaction-basis gauge field could, in principle, produce mass eigenstates other than the dark photon. (Production could simply occur via a coupling directly to the linear combination of clockwork fields that make up the lightest mode, but this possibility seems rather contrived.) So long as the clockwork gauge fields' masses lie above a kinematic threshold for production, these heavier states are not directly produced. In principle, however, the interactions directly responsible for production may also generate interactions between the dark photon and other mass eigenstates.

We now show that such effects are negligible for production of dark photons from an oscillating axion (Sec. II C) as a concrete example. Efficient dark photon production from an oscillating axion typically requires couplings β that are parametrically large compared to that expected to arise by integrating out heavy, PQ-charged fermions charged under the $U(1)$ gauge group of A , for which $\beta \propto g_D^2 \ll 1$. If these fermions couple to the more strongly coupled end of the clockwork chain [as in Eq. (3.5)], then β is enhanced to $\beta \propto Q^{2N} g_D^2 \sim g^2$, after which only a moderate enhancement to β is necessary to reach $\beta \gtrsim 40$ (see the discussion in Sec. IV and Ref. [56]).

Following the notation of the previous section, the Chern-Simons term for the clockwork vector A_1^μ expands to

$$F_1^{\mu\nu} \tilde{F}_{\mu\nu}^1 = \sum_{i,j=0}^N [\mathbf{e}_i]_1 [\mathbf{e}_j]_1 F_i^{\mu\nu} \tilde{F}_{\mu\nu}^j, \quad (3.19)$$

where we use A_i^μ to denote the i th mass-basis vector and $F_i^{\mu\nu}$ its field strength. The equations of motion for the mass-basis fields are then

$$\ddot{A}_{i,\pm} + H \dot{A}_{i,\pm} + \left[\frac{k^2}{a^2} + m_i^2 \pm \beta \dot{\theta} \frac{k}{a} ([\mathbf{e}_i]_1)^2 \right] A_{i,\pm} = \mp \beta \dot{\theta} \frac{k}{a} \sum_{j=0, j \neq i}^N [\mathbf{e}_i]_1 [\mathbf{e}_j]_1 A_{j,\pm}. \quad (3.20)$$

Following Sec. II C, if the massive modes are sufficiently heavy ($m_i \sim gv > \beta \dot{\theta} \sim \beta m_a \theta_0$), only the lightest mode (the dark photon) is produced. The mixing term on the right-hand side of Eq. (3.20) is therefore dominated by the $j = 0$ term in the sum. This source generates heavy modes with amplitude of order

$$\mathbf{A}_{i,\pm} \sim \frac{\beta \dot{\theta} k/a}{k^2/a^2 + m_i^2} [\mathbf{e}_i]_1 [\mathbf{e}_0]_1 \mathbf{A}_{0,\pm} \propto (m_a/m_i)^2 [\mathbf{e}_i]_1 [\mathbf{e}_0]_1 \mathbf{A}_{0,\pm}, \quad (3.21)$$

noting that $\dot{\theta} \sim m_a \theta_0$ and $k/a \sim m_a$ in the broad resonance regime. The eigenvector elements are each no larger in magnitude than $\sim 1/Q$, so the backreaction thresholds for the clockwork Higgses are order $\lambda v^4 \gtrsim m_i^2 A_i^\mu A_\mu^i \sim m_a^4 \mathbf{A}_{0,\pm}^2 / m_i^2$. Taking the dark photon's own kinematic threshold from Eq. (2.22) for order-unity axion misalignments, $m_a \gtrsim m_A/\beta$, shows that avoiding backreaction onto the clockwork Higgses requires $\lambda v^4 \gtrsim (m_A/m_i)^2 / \beta^4 \cdot m_A^2 \mathbf{A}_{0,\pm}^2$. Since $\beta > 1$ and $m_A < m_i$ (and $v < v$) by construction, avoiding backreaction onto the dark Higgs for the dark photon itself is a parametrically stronger condition than for the other clockwork gauge symmetries; the backreaction bound Eq. (2.5) is therefore not modified by clockwork.

IV. DETECTABLE DARK PHOTONS FROM AXIONS

As discussed in Sec. II C, the dimensionless axion-photon coupling is typically $\beta \sim \alpha_D/2\pi \ll 1$, and without additional model building, tachyonic resonance from axion oscillations does not occur. Suitable model building can generate a hierarchy in β/α_D , as achieved by Abelian clockwork mechanism described in Sec. III. The enhancement from clockwork alone, however, is limited to $\beta \lesssim 1$ by perturbative unitarity (i.e., of scatterings with the fermions with largest charge); an additional mechanism must further enhance β to the values $\gg 10$ required for efficient resonance [56, 164, 165]. Even taking a viable origin of arbitrarily large β for granted, backreaction constraints still limit production in much of the experimentally accessible parameter space (Fig. 3), since production typically occurs no later than when $H \approx m_A$. The same mechanisms that boost β can also enhance ε relative to g_D , and in principle axions can produce dark photons across all experimentally accessible parameter space [56, see also Sec. III B]. However, a 10^{30} enhancement to the axion-photon coupling is rather implausible *a priori* [see Eq. (2.25)].

In this section, we explore scenarios that simultaneously facilitate efficient dark photon production and weaken backreaction and defect formation limits. We demonstrate that models that delay production (thereby relaxing these bounds, as described in Sec. II) can also enable efficient tachyonic resonance at smaller values of β . In this regime, both objectives work in tandem: delayed production allows for larger g_D , raising the expected axion coupling $\alpha_D/2\pi \propto g_D^2$, and also reduces the degree to which β must be enhanced relative to this expectation. We also consider how the opposite regime—strong coupling—can itself delay production and may require less model-building machinery than the moderately large values of β considered in prior literature. Figure 5 illustrates these various dynamical regimes in parameter space.

A. Narrow resonance

In the standard scenario described in Sec. II C, only dark photon modes with $m_A < k/a < \beta |\dot{\theta}| \propto a^{-3/2}$ undergo tachyonic growth. As the Universe expands, modes continuously exit the resonance band since their wave numbers redshift more slowly than does the width of the resonance band itself. Because the expansion rate H is only just below the axion's frequency m_a , resonance is efficient only during the axion's first few oscillations before unstable modes redshift out of the

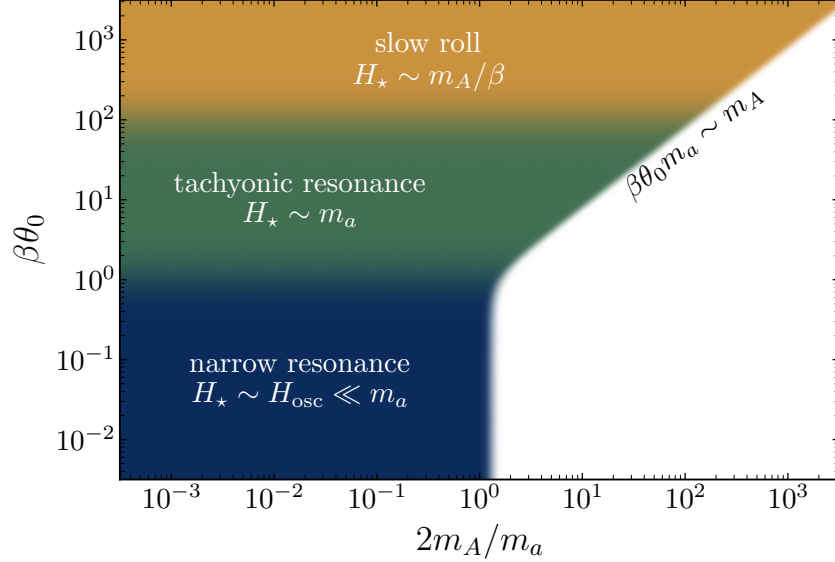


Figure 5. Illustration of the parameter space in which an axion may transfer its energy efficiently to a dark photon. The green region represents the usual range of moderate axion couplings considered, for example, in Refs. [56, 160, 163]. The blue region corresponds to the narrow resonance discussed in Sec. IV A and Ref. [162], in which delayed axion oscillations lead to a more efficient resonance and thus allow for $\beta \ll 1$. In the yellow region, the axion–dark-photon coupling is so large that the axion’s oscillations are overdamped and energy transfer takes a parametrically long time. A rigorous understanding of this regime, however, requires numerical simulations (see Sec. IV B). Such large couplings could possibly be realized if the axion is coupled to the dark photon in the magnetic basis [169, 170], but this possibility also remains speculative and requires further model-building study.

band and are no longer tachyonic. However, if axion oscillations begin when H is parametrically lower than m_a , modes grow over a proportionally larger number of oscillations, making resonance efficient at smaller $\beta\theta_0$.

As derived in Appendix D 1 and Ref. [162], when axion oscillations begin at an arbitrary Hubble rate $H_{\text{osc}} < m_a$, the resonance condition relaxes to

$$\beta\theta_0 \sqrt{\frac{m_a}{2H_{\text{osc}}}} \gg 1. \quad (4.1)$$

Delaying axion oscillations until $H \ll m_a$ thus not only reduces the required enhancement of the axion coupling β , but also weakens constraints on the dark gauge coupling from backreaction onto the Higgs [per Eq. (2.8)]. Because resonance is narrow in wave number about $a_{\text{osc}}m_a/2$, resonantly produced dark photons become nonrelativistic when $H_{\text{NR}}/H_\star = (a_\star/a_{\text{NR}})^2 = (2m_A/m_a)^2$. Figure 6 shows that a sufficiently long delay allows for viable kinetic mixing in reach of all future searches.

To quantify the joint impact on the required hierarchy in β and α_D , combine the efficient resonance condition Eq. (4.1) with the backreaction bound Eq. (2.8):

$$\frac{\beta}{\alpha_D/2\pi} \gg 10^{10} \theta_0^{-1} \lambda^{-1/2} \sqrt{\frac{\Omega_A}{\Omega_{\text{DM}}}} \frac{2m_A}{m_a} \left(\frac{m_A}{\mu\text{eV}}\right)^{-5/2} \left(\frac{H_{\text{osc}}}{10^{-22} \text{ eV}}\right)^{5/4}. \quad (4.2)$$

Equation (4.2) represents a significant reduction in the required hierarchy relative to the standard scenario, traded instead for a large hierarchy in m_a/H_{osc} . The requirement is further reduced from the fiducial values in Eq. (4.2) by taking a heavier axion or dark photon, but at the expense of exacerbating the hierarchy in m_a/H_{osc} . For instance, the fiducial hierarchy is order unity for dark

photons with mass 10 meV, for which $m_a/H_{\text{osc}} > 10^{20}$. Delayed oscillations require a dynamical hierarchy rather than a parameter hierarchy, but candidate models may well require parameter hierarchies or tunings of their own.

There are numerous concrete models that delay the onset of axion oscillations [162, 171–174], although mechanisms relying on attractive self-interactions [171, 172] result in axion fragmentation, spoiling the dark photon’s tachyonic resonance (see Appendix D 2). Repulsive self-interactions suppress axion perturbations, but constructing an axion potential with repulsive self-interactions (while possible [175]) is its own challenge because the periodic axion field always has attractive self-interactions at large enough field excursions. Equation (4.2) tacitly assumes axion self-interactions do not disrupt dark photon production.

Example models whose dynamics can plausibly delay axion oscillations while also avoiding axion fragmentation may arise in axiverse scenarios [43]. Given a large number of axions logarithmically distributed in mass, there is a reasonable chance that a pair of axions have masses within an order-unity factor of each other [173]; candidate pairs indeed appear in concrete string theory compactifications [176]. Such “friendly” pairs can undergo nonlinear autoresonance, in which the axion with the smaller decay constant f_a oscillates with fixed amplitude until a parametrically late time, after which it dilutes like matter [173, 174]. Importantly, autoresonance may occur whether axion self-interactions are attractive or repulsive [173]. The time between $H = m_a$ and when the axion starts diluting is controlled by the ratio of decay constants between the friendly axions, $\mathcal{F} \gg 1$, as $H_{\text{osc}} \sim m_a \mathcal{F}^{-4/3}$. Quantified in decades, a hierarchy in m_a/H_{osc} translates to one 3/4 as severe in decay constants.

B. Slow roll

Given that dark photon production from axion oscillations already requires a significant enhancement of β beyond its natural expectation, one may as well consider enhancements yet larger than the bare minimum required for efficient resonance. We now point out the possibility that such large β (much greater than, say, 50) may yield a new dynamical regime in which dark photon production is delayed. Moreover, because such delayed production allows for larger g_D without backreaction or defect formation, requiring larger β itself does not necessarily exacerbate the hierarchy in β/α_D , a claim we quantify below.

The cosmological evolution of massive, noninteracting scalars is relatively simple: the (homogeneous) field is frozen when Hubble friction dominates over the curvature of its potential ($H \gg m_a$) and subsequently undergoes underdamped oscillations once H drops below m_a . The axion’s interaction with dark photons, however, yields a source term $\propto \beta \langle \mathbf{E} \cdot \mathbf{B} \rangle$ in its equation of motion Eq. (2.21a). The relative importance of dark photon backreaction may be parametrically estimated by comparing energy densities, i.e., comparing $\beta \rho_A$ and ρ_a . For the moderate values of β considered in the standard scenario (Sec. II C), tachyonic resonance of dark photons only becomes efficient in the oscillatory regime, and their backreaction onto the homogeneous axion only becomes important as energy transfer completes. However, for sufficiently large β , even the axion’s parametrically small velocity at early times,

$$\dot{\theta} = -m_a \theta_0 [m_a/5H + \mathcal{O}([m_a/H]^3)], \quad (4.3)$$

is enough to produce dark photons. As derived in Appendix C, if

$$\theta_0 \beta \gg 48.5 + 3.2 \ln \frac{f_a^4}{m_a^4 \theta_0^2 \beta^6}, \quad (4.4)$$

then not only does the slowly rolling axion efficiently produce dark photons, but the dark photons that are produced induce significant backreaction—not just because larger β increases the magnitude of their backreaction at fixed energy density, but also because dark photons are produced at earlier times $m_a t_{\text{BR}} \sim (\beta\theta_0)^{-1/2}$. Rather than proceeding to oscillate when $H \leq m_a$, the axion may instead undergo an extended phase of slow roll.

Neglecting spatial axion perturbations (a strong assumption we comment on shortly), the structure of Eq. (2.21)—where the dark photon’s backreaction grows with a rate proportional to the axion velocity—suggests the possibility of a quasiequilibrium state where the rolling axion produces a dark photon background that exerts friction on the axion, in turn regulating the axion’s velocity. In particular, when $\dot{\theta} = 2m_A/\beta$, the axion rolls just fast enough that one dark photon polarization is massless. (The other is massive and may be ignored.) If $\dot{\theta}$ were to roll any faster, the massless mode would become tachyonic, the energy in the rolling axion would be converted into dark photons, and θ would slow down. Under these assumptions, the totality of the axion energy density would gradually drain into the dark photon by the time $H_\star \approx m_A/\beta$, realizing both efficient and delayed dark photon production at once. Because $\dot{\theta}$ is nearly constant, the axion rolls to its minimum almost entirely during the last e -fold of production; the majority of the dark photon energy density is then concentrated at wavelengths $k = m_A a_\star$.⁸

In Appendix C, we show that the axion enters the overdamped regime just as its perturbations become comparable to its homogeneous component. If the axion indeed fully fragments, the tachyonic resonance is disrupted, meaning the slow-roll solution is not realized. On the other hand, this effective slow-roll regime is indeed realized in numerical simulations of preheating into massless gauge bosons after axion inflation [149, 150, 152, 153, 155–157, 177], indicating that axion perturbations may be regulated at large axion-photon coupling—in which case the axion would remain approximately homogeneous and overdamped as it rolls to the bottom of its potential. Suggestive as these results are, it remains to be shown whether they extend to the radiation-dominated epoch relevant for dark photon dark matter production, a possibility only testable with nonlinear simulations. Given the magnitude of β required, the initial resonance is quite broad and nonlinear interactions between modes should be strong (even if they do not disrupt the homogeneous mode); robust simulations may require significant computational resources. We leave this investigation to future work and reiterate the uncertainty that any conclusions are subject to.

Slow roll, should it occur, requires larger couplings, but not necessarily in units of α_D . That is, the increase in the maximum g_D that evades backreaction onto the Higgs and defect formation can offset the required increase in β itself. Taking $H_\star = m_A/\beta$ and substituting Eq. (2.8),

$$\frac{\beta}{\alpha_D/2\pi} \gtrsim 10^{34} \lambda^{-1/2} \sqrt{\frac{\Omega_A}{\Omega_{\text{DM}}}} \left(\frac{m_A}{\mu\text{eV}}\right)^{-1} \left(\frac{H_\star}{10^{-22} \text{ eV}}\right)^{-1/4}, \quad (4.5)$$

which is in the same ballpark as the standard case [Eq. (2.25)], though with slightly different mass dependence. However, axion–dark-photon couplings $\beta \gg 1$ may in fact require less model building than moderate $\beta \sim \mathcal{O}(10) \gg \alpha_D$. If the axion couples to PQ-charged fermions that have both dark electric and magnetic charges (dyons), then β may be proportional to (the square of) the dark magnetic charge $4\pi/g_D$ rather than the electric charge g_D [178]. As a result, β would naturally be of order $1/\alpha_D$, realizing the slow-roll regime. Because β is determined by the dark gauge coupling and itself sets the time of dark photon production $H_\star \sim m_A/\beta$, the magnetically coupled axion is potentially viable only in a narrow range of kinetic mixing bounded from above and below.

⁸ At extremely large β and m_a/m_A , the axion velocity at the onset of slow roll is parametrically larger than its quasiequilibrium value by an amount proportional to $\sqrt{\beta\theta_0}m_a/m_A$. It is therefore likely that much of the axion’s initial energy converts to highly relativistic dark photons before it slows to its quasiequilibrium velocity; a large axion decay constant may thus be necessary to achieve the correct dark photon relic abundance.

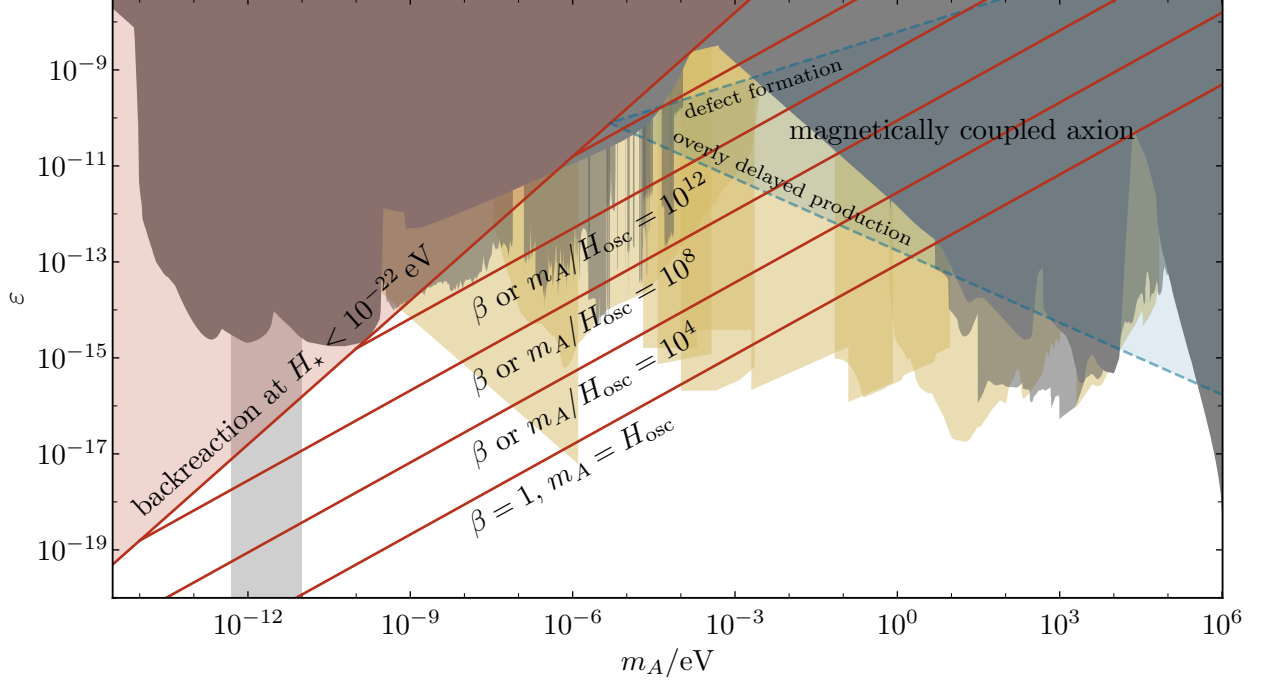


Figure 6. Kinetic mixing parameter space of dark photon dark matter produced from rolling axions. Red lines depict the maximum kinetic mixing [Eq. (2.9)] that evades backreaction onto the Higgs when either the axial coupling β is large enough to realize slow roll (Sec. IV B) or when axion oscillations are delayed (relative to $m_A \lesssim m_a$) sufficiently long by other means (Sec. IV A). The blue region depicts the parameter space available when the axion coupling is $\beta \propto 1/\alpha_D$, as may be for an axion coupled in the magnetic basis. We note that the slow-roll scenario is subject to theoretical uncertainty regarding nonlinear dynamics and, for the magnetic axion, the consistency of large magnetic couplings (both discussed in Sec. IV B). The red region depicts parameter space for which backreaction onto the Higgs occurs when scales relevant to CMB anisotropies enter the horizon, i.e., when the dark photon must behave as dark matter; current bounds and projected search space are depicted in gray and yellow as labeled in Fig. 3.

Substituting $H_* = \alpha_D m_A / 2\pi$ into Eq. (2.8) yields

$$g_D \lesssim 2 \times 10^{-8} \lambda^{1/7} \left(\frac{m_A}{\mu\text{eV}} \right)^{5/14} \left(\frac{\Omega_A}{\Omega_{\text{DM}}} \right)^{-1/7}. \quad (4.6)$$

On the other hand, if the dark gauge coupling is too small, then (at a given m_A) β would be so large that dark photon production is delayed until after we know the dark matter must exist. This places a *lower* bound on the gauge coupling of

$$g_D \gtrsim 9 \times 10^{-8} \left(\frac{m_A}{\mu\text{eV}} \right)^{-1/2} \left(\frac{H_{*,\text{min}}}{10^{-22} \text{ eV}} \right)^{1/2}. \quad (4.7)$$

We plot the resulting parameter space in Fig. 6. Intriguingly, production from a magnetically coupled axion may only both evade defect formation and occur early enough for masses $m_A \gtrsim \mu\text{eV}$. Moreover, the available parameter space is already largely excluded, but numerous future axion haloscopes, such as ALPHA [112], MADMAX [113], Dark E-field [109], BREAD [114], LAMPOST [116], and SuperCDMS [85, 117] could easily detect or exclude the parameter space that remains below an eV. LZ [118] could also potentially detect viable parameter space around 10 keV.

The viability of a magnetic-basis coupling as a means to boost the axion-photon coupling remains

unsettled at present [169, 170]. Although most of the objections raised by Ref. [169] are specific to the case of the QCD axion coupled to the Standard Model photon, questions remain even for the case of axionlike particles coupled to a dark photon. Because of the dual Witten effect [179], as the axion rolls from 0 to 2π , the magnetic charge of every dyon changes by one unit, implying the existence of an infinite dyonic tower. Not only must the magnetically charged dyons be very heavy to avoid magnetic Schwinger pair production [180, 181], but Ref. [169] also suggests that integrating out such a tower generically drives the theory to weak coupling. The coupling to heavy dyons would also generate a large mass for the axion, though because H_\star is independent of m_a once the axion has achieved its equilibrium, slow-roll velocity, production may still proceed as described even if the axion were quite heavy. The dark Higgs is one such electrically charged state that would form the basis of such a dyonic tower [182]. The possibility of axions strongly coupled to dark photons—perhaps with a Stückelberg rather than a Higgs mass—remains an intriguing possibility, and further investigation is required to establish its viability. Finally, note that even if one ignores possible backreaction onto the radial mode associated with the Stückelberg mass, the lower bound [Eq. (4.7)] on ε remains.

V. DARK PHOTON DARK MATTER IN SCALAR–ABELIAN-HIGGS THEORIES

Unlike axions, whose couplings are restricted to those that perturbatively preserve their continuous shift symmetry, scalars can couple to any operator and therefore offer more possible means to produce dark photons and evade strong backreaction. In particular, a scalar field effectively modulates the fundamental parameters of a theory throughout spacetime [183, 184]. A homogeneous and dynamical scalar field coupled to the Abelian-Higgs model may therefore modulate the backreaction threshold [Eq. (2.5)] and the string production threshold [Eq. (2.12)] over time. For example, the dark Higgs VEV could be larger when dark photons are first produced than it is today, raising the backreaction and defect formation thresholds at early times when the dark photon energy density is largest.

We begin this section by introducing a useful parametrization of a scalar’s interactions with the Abelian-Higgs Lagrangian in Sec. V A. In Sec. V B, we illustrate how “universal” scalar couplings can alleviate defect bounds in existing scenarios, focusing on gravitational production during inflation; in Sec. V B 2, we show that this scenario can be realized in well-motivated physics models such as the string dilaton [55]. Scalar couplings also offer unique mechanisms for particle production: in Secs. V C and V D, we explore two models that avoid backreaction and defect formation through the same physics that drives dark photon production [51, 52].

A. Equations of motion

The classical Lagrangian describing an Abelian-Higgs theory coupled to a scalar ϕ may be parametrized as⁹

$$\mathcal{L}_{\text{SAH}} = \frac{1}{2} \partial_\mu \phi \partial^\mu \phi - V(\phi) - \frac{W(\phi)}{4} F_{\mu\nu} F^{\mu\nu} + \frac{X(\phi)}{2} D_\mu \Phi (D^\mu \Phi)^* - \frac{\lambda Y(\phi)}{4} (|\Phi|^2 - v^2)^2, \quad (5.1)$$

⁹ Equation (5.1) neglects a possible fourth coupling that modulates the quadratic term of the dark Higgs potential independent of the quartic. However, our choice of parametrization is sufficient to modulate all the Abelian-Higgs parameters independently and also includes all possible (two-)derivative interactions.

generalizing Eq. (2.1). As discussed in Appendix A, written in terms of radial fluctuations h of the Higgs about its VEV in unitary gauge ($\Pi = 0$), Eq. (5.1) expands to

$$\begin{aligned} \mathcal{L}_{\text{SAH}} = & \frac{1}{2} \partial_\mu \phi \partial^\mu \phi - V(\phi) - \frac{W(\phi)}{4} F_{\mu\nu} F^{\mu\nu} + \frac{X(\phi)}{2} \left(1 + \frac{h}{v}\right)^2 m_A^2 A_\mu A^\mu \\ & + \frac{X(\phi)}{2} \partial_\mu h \partial^\mu h - Y(\phi) \left(\frac{\lambda}{4} h^4 + \lambda v h^3 + \frac{1}{2} m_h^2 h^2 \right). \end{aligned} \quad (5.2)$$

The coupling functions W , X , and Y could in general depend on multiple scalar fields; for simplicity we consider only a single scalar field, but the extension to multiple is straightforward.

To rewrite the theory with canonically normalized kinetic terms, we rescale the vector and Higgs fields as $A_\mu = \mathcal{A}_\mu / \sqrt{W(\phi)}$ and $h = \mathfrak{h} / \sqrt{X(\phi)}$. Then, suppressing the explicit ϕ dependence of W , X , and Y for brevity,

$$\begin{aligned} \mathcal{L}_{\text{SAH}} = & \frac{1}{2} \partial_\mu \phi \partial^\mu \phi - V(\phi) - \frac{1}{4} (\mathcal{F}_{\mu\nu} + \mathcal{G}_{\mu\nu}) (\mathcal{F}^{\mu\nu} + \mathcal{G}^{\mu\nu}) + \frac{1}{2} \frac{X m_A^2}{W} \left(1 + \frac{\mathfrak{h}}{\sqrt{X} v}\right)^2 \mathcal{A}_\mu \mathcal{A}^\mu \\ & + \frac{1}{2} \partial_\mu \mathfrak{h} \partial^\mu \mathfrak{h} - \frac{1}{2} \mathfrak{h} \partial^\mu \mathfrak{h} \frac{\partial_\mu X}{X} + \frac{1}{8} \mathfrak{h}^2 \frac{\partial_\mu X \partial^\mu X}{X^2} - \frac{\lambda Y}{X^2} \left(\frac{\mathfrak{h}^4}{4} + v \sqrt{X} \mathfrak{h}^3 \right) - \frac{1}{2} \frac{Y}{X} m_h^2 \mathfrak{h}^2, \end{aligned} \quad (5.3)$$

where

$$\mathcal{F}_{\mu\nu} \equiv \partial_\mu \mathcal{A}_\nu - \partial_\nu \mathcal{A}_\mu \quad (5.4a)$$

and

$$\mathcal{G}_{\mu\nu} \equiv \frac{1}{2W} (\mathcal{A}_\mu \partial_\nu W - \mathcal{A}_\nu \partial_\mu W). \quad (5.4b)$$

To treat scenarios where a homogeneous, classical background scalar field effectively modulates the fundamental parameters of the Abelian-Higgs model through its cosmological evolution, we expand $\phi(t, \mathbf{x}) = \bar{\phi}(t) + \delta\phi(t, \mathbf{x})$ where $\delta\phi$ is a small perturbation. The form of Eq. (5.3) therefore motivates absorbing the $\bar{\phi}$ dependence of the theory into its fundamental parameters as

$$m_A(\bar{\phi}) \equiv m_A \sqrt{X(\bar{\phi})/W(\bar{\phi})}, \quad (5.5a)$$

$$v(\bar{\phi}) \equiv v \sqrt{X(\bar{\phi})}, \quad (5.5b)$$

$$\lambda(\bar{\phi}) \equiv \lambda Y(\bar{\phi})/X(\bar{\phi})^2, \quad (5.5c)$$

and, as a consequence,

$$m_h(\bar{\phi}) = \sqrt{2\lambda(\bar{\phi})} v(\bar{\phi}) = m_h \sqrt{Y(\bar{\phi})/X(\bar{\phi})} \quad (5.5d)$$

and

$$g_D(\bar{\phi}) = m_A(\bar{\phi})/v(\bar{\phi}) = g_D/\sqrt{W(\bar{\phi})}. \quad (5.5e)$$

From this point on, we take the dark photon to have no homogeneous component and set the Higgs to zero for simplicity (with results including the Higgs presented in Appendix A). In an FLRW

spacetime [Eq. (A6)], the linearized equations of motion in Fourier space read

$$0 = \ddot{\bar{\phi}} + 3H\dot{\bar{\phi}} + V'(\bar{\phi}) \quad (5.6a)$$

$$0 = \ddot{\mathcal{A}}_{\pm} + H\dot{\mathcal{A}}_{\pm} + \left[\frac{k^2}{a^2} + m_A(\bar{\phi})^2 - \frac{H}{2} \frac{\partial_t W(\bar{\phi})}{W(\bar{\phi})} - \frac{\partial_t^2 \sqrt{W(\bar{\phi})}}{\sqrt{W(\bar{\phi})}} \right] \mathcal{A}_{\pm} \quad (5.6b)$$

$$0 = \ddot{A}_{\parallel} + \frac{[3H + \partial_t \ln X(\bar{\phi})] k^2 + [H + \partial_t \ln W(\bar{\phi})] a^2 m_A(\bar{\phi})^2}{k^2 + a^2 m_A(\bar{\phi})^2} \dot{A}_{\parallel} + \left[\frac{k^2}{a^2} + m_A(\bar{\phi})^2 \right] A_{\parallel}. \quad (5.6c)$$

Equation (5.6) has also decomposed the vector onto a basis of transverse (\mathcal{A}_{\pm}) and longitudinal (A_{\parallel}) polarization; see Appendix A for full details. Note that the equation of motion for the longitudinal component Eq. (5.6c) is written in terms of the noncanonical field, as the rescaling applied for transverse modes does not fully remove scalar couplings from the longitudinal mode's friction term. Equation (5.6c) also more transparently demonstrates that the relativistic and nonrelativistic limits of the longitudinal dynamics coincide with those of scalars and of transverse vectors, respectively, in accordance with the Goldstone equivalence theorem.

The structure of Eq. (5.6) is quite general, allowing for a number of qualitatively distinct dark photon production mechanisms. Large field excursions (relative to whatever relevant energy scale), for instance, allow for large variation in the Abelian-Higgs parameters [Eq. (5.5)], in which case both the backreaction threshold and the kinematic conditions for efficient particle production become time dependent. We specialize to two examples that illustrate each of these possibilities. In Sec. VB we show that a universally coupled dilaton broadens the parameter space available to inflationary production by modulating the Higgs VEV, simultaneously weakening the defect bound and making production more efficient. In Sec. VC we consider the model presented in Ref. [52] of a scalar coupled to the dark photon kinetic term. Such a coupling can both exponentially suppress the dark photon mass at early times and induce a tachyonic instability that achieves extremely delayed production. Finally, in Sec. VD we discuss an alternative particle production mechanism that was pointed out by Ref. [51]: for a particular (and finely tuned) mass ratio between the dark photon and an oscillating scalar, parametric resonance can efficiently produce dark photons even with arbitrarily slow resonance, providing another realization of delayed production. This scenario, in contrast to the aforementioned, only depends on the leading-order behavior of the scalar's couplings about the minimum of its potential. Throughout, we also discuss various unique signatures predicted by each model and their relation to the dark photon's direct-detection parameter space.

B. Universal coupling

In this section, we show that defect constraints on inflationary production are weakened if particle masses (possibly including SM particles) are ϕ dependent. A scalar's interactions with matter, be it the dark matter or SM matter, generate for it an effective potential that naturally drives the field to values that minimize the free energy of the system. Absent a bare potential, the scalar ϕ rolls to values that either minimize particle masses (for ϕ -dependent masses) or decouple the theory (for ϕ -dependent couplings). For the dark Abelian-Higgs theories we consider, the latter possibility would make g_D , which already must be small to avoid defect formation, decrease yet further as the Universe evolves toward its ground state. On the other hand, a larger dark Higgs VEV during inflation works in favor of weaker defect bounds: defect formation is suppressed when all degrees of freedom are heavier, while cosmological evolution makes them lighter at late times.

The particular choice of coupling functions that endows only the theory's mass scales with ϕ

dependence is $W(\phi) = 1$ and

$$Y(\phi) = X(\phi)^2 \equiv Z(\phi)^2, \quad (5.7)$$

for which, using Eq. (5.5), the Abelian-Higgs parameters all scale with $Z^{d/2}$ where d is the mass dimension of the particular parameter. In Sec. VB1 we outline the model-independent features that weaken defect bounds from inflationary production, and in Sec. VB2 we discuss one particularly well-motivated realization from string theory, in which all parameters in the theory depend on the so-called dilaton [55]. While we focus on inflationary production because of its minimalism, the mechanism of Sec. VB2 could suppress backreaction onto the Higgs for a number of other production mechanisms discussed in this paper.

1. Inflationary production and varying masses

To study the impact of evolving mass scales on defect formation and the dark photon relic abundance on a model-agnostic basis, we first work in terms of a time-dependent mass $m_A(a)$. The energy density of the longitudinal mode [Eq. (A16)] scales as

$$\frac{d\rho_{\parallel}}{d\ln k} \sim \frac{1}{2a^2} m_A(a)^2 \frac{d|A_{\parallel}|^2}{d\ln k} \quad (5.8)$$

in both the relativistic and nonrelativistic limits. When $m_A(a)$ evolves slowly compared to H , the longitudinal-mode equation of motion [Eq. (5.6c)] simplifies to

$$0 = \ddot{A}_{\parallel} + \frac{3k^2 + a^2 m_A(a)^2}{k^2 + a^2 m_A(a)^2} H \dot{A}_{\parallel} + \left(\frac{k^2}{a^2} + m_A(a)^2 \right) A_{\parallel}. \quad (5.9)$$

In the relativistic limit $k \gg am_A(a)$, A_{\parallel} 's dynamics are independent of $m_A(a)$, but once A_{\parallel} is nonrelativistic its dynamics depend nontrivially on the evolution of its mass. If the dark photon's mass evolves adiabatically [such that a Wentzel-Kramers-Brillouin (WKB) solution is valid] after it becomes nonrelativistic, its amplitude then scales $\propto 1/\sqrt{m_A(a)}$. This distinction between the relativistic and nonrelativistic regimes is crucial to determining the dynamics of $m_A(a)$ that alleviate defect formation bounds.

Equation (2.10) shows that the mode that dominates the abundance of dark photons produced gravitationally during inflation is that which enters the horizon at the same time it becomes nonrelativistic—that is, the mode with wave number $k_{\star} = a_{\star} H(a_{\star}) = a_{\star} m_A(a_{\star})$. Assume that the peak remains at this mode, evaluated when $H(a)$ first drops below $m_A(a)$.¹⁰ At $a > a_{\star}$ its energy density scales as

$$\frac{d\rho_{\parallel}(k_{\star})}{d\ln k} \sim \frac{m_A(a)^2}{2} \left(\frac{k_{\star} H_I}{2\pi a_{\star} m_{AI}} \right)^2 \left(\frac{a}{a_{\star}} \right)^{-3} \frac{m_A(a_{\star})}{m_A(a)}. \quad (5.10)$$

These four factors respectively encode the longitudinal modes' (current) mass; its initial conditions from inflation [50], during which its mass takes the value m_{AI} ; its redshifting upon reentering the horizon (when it simultaneously becomes nonrelativistic); and the adiabatic evolution induced by its evolving mass. Assuming this mode enters the horizon during the radiation era and setting

¹⁰ In principle, the mass could subsequently decrease rapidly enough that this mode becomes temporarily relativistic and no longer dominates the energy spectrum. We neglect this possibility for simplicity, since it is avoided if m_A 's evolution either is sufficiently slow or begins sufficiently late.

$$k_\star = a_\star m_A(a_\star),$$

$$\frac{d\rho_\parallel(k_\star)}{d\ln k} \sim \frac{m_A(a)^2}{2} \left(\frac{m_A(a_\star)}{m_{AI}} \right)^2 \left(\frac{H_I}{2\pi} \right)^2 \left(\frac{H}{m_A(a_\star)} \right)^{3/2} \frac{m_A(a_\star)}{m_A(a)}. \quad (5.11)$$

If m_A only changes while the longitudinal mode is still relativistic, then the WKB factor in Eq. (5.11) reduces to unity and the abundance scales with the square of its late- and early-time masses:

$$\frac{d\rho_\parallel(k_\star)}{d\ln k} \sim \frac{m_A^2}{2} \left(\frac{H_I}{2\pi} \right)^2 \left(\frac{H}{m_A} \right)^{3/2} \left(\frac{m_A}{m_{AI}} \right)^2. \quad (5.12)$$

Compensating for the $(m_A/m_{AI})^2$ suppression of the dark photon abundance (at a given present-day mass) requires increasing $H_I \propto m_{AI}$, which nullifies any relaxation of defect constraints [Eq. (2.12)], as noted by Ref. [48].¹¹

Now consider the scenario where m_A instead remains at its inflationary value m_{AI} until *after* the dominant dark photon mode becomes nonrelativistic. In this case, the second factor in Eq. (5.11) (which encodes the superhorizon initial condition seeded during inflation) simplifies to unity. As a result, m_A 's evolution only affects the dark photon mode amplitude through adiabatic evolution and an earlier onset of subhorizon redshifting:

$$\frac{d\rho_\parallel(k_\star)}{d\ln k} \sim \frac{m_A^2}{2} \left(\frac{H_I}{2\pi} \right)^2 \left(\frac{H}{m_A} \right)^{3/2} \left(\frac{m_A}{m_{AI}} \right)^{1/2}. \quad (5.13)$$

Therefore, H_I need only be $(m_{AI}/m_A)^{1/4}$ times larger to maintain the correct relic abundance, while the defect bound on H_I is weakened by m_{AI}/m_A . Matching ρ_\parallel to the dark matter relic density requires

$$\frac{m_{AI}}{m_A} = \frac{m_A}{0.1 \text{ meV}} \left(\frac{H_I}{5 \times 10^{13} \text{ GeV}} \right)^4, \quad (5.14)$$

while the defect bound limits

$$g_D \leq \frac{m_{AI}}{H_I} \lesssim 2 \times 10^{-19} \left(\frac{m_A}{\text{eV}} \right)^2 \left(\frac{H_I}{5 \times 10^{13} \text{ GeV}} \right)^3. \quad (5.15)$$

The requisite early-late mass ratio is

$$\frac{m_{AI}}{m_A} = 10^4 \left(\frac{g_D}{2 \times 10^{-19}} \right)^{1/2} \left(\frac{H_I}{5 \times 10^{13} \text{ GeV}} \right)^{5/2} = 10^4 \left(\frac{g_D}{2 \times 10^{-19}} \right)^{4/3} \left(\frac{m_A}{\text{eV}} \right)^{-5/3}. \quad (5.16)$$

Equation (5.15) is parametrically weaker than in the minimal scenario [Eq. (2.12)] and is in fact weakest for the highest allowed inflationary scale because the relic abundance is more sensitive to H_I than to the drop in the dark photon's mass. Further, the bound scales with a higher power of m_A than Eq. (5.15) because the relic abundance no longer requires a unique inflationary scale as a function of m_A ; heavier (present-day) dark photons may therefore be accommodated at larger H_I when simultaneously increasing m_{AI}/m_A .

¹¹ As mentioned in Sec. II A 2, Ref. [48] (in Appendix C.2) considers a nonminimal coupling of the dark Higgs, $\xi R|\Phi|^2$, as a means to drive the Higgs VEV to larger values during inflation, which then returns to its vacuum value shortly afterward. The evolution of the mass scales in the theory thus necessarily terminates long before the dominant dark photon mode becomes nonrelativistic.

2. Damour-Polyakov dilaton

We now show that the model of the string dilaton proposed by Damour and Polyakov [55] can realize cosmological evolution of the dark photon mass that weakens defect bounds, as described phenomenologically in the previous section. We briefly review the mechanism of Ref. [55]. In general, the string dilaton ϕ is expected to couple to all Standard Model operators, essentially promoting the constants of nature to field-dependent quantities $\zeta \rightarrow \zeta(\varphi)$ (where $\varphi \equiv \phi/\sqrt{2}M_{\text{pl}}$). If the “constant” has sufficiently large linear dependence on the dilaton, then it mediates a force between objects whose mass depends on the value of ζ ; such fifth forces are strongly constrained by tests of equivalence principle violation (unless ϕ is sufficiently heavy) [185–187]. If the dilaton only enters the action via the single function $\zeta(\phi)$ or by a collection of functions all with the same extrema (and has a canonical kinetic term), then one may shift its value such that it has no linear couplings, i.e., $\zeta(\varphi) = \zeta_0 + \kappa\varphi^2/2 + \mathcal{O}(\varphi^3)$.

The now-leading quadratic coupling still mediates a fifth force, but one proportional to φ ’s expectation value. Reference [55] identified a mechanism that efficiently drives ϕ to its minimum: if the mass m_X of a particle species X is generated by the confinement of a strongly coupled gauge group whose gauge coupling depends on ϕ , then m_X depends strongly on the dilaton:

$$m_X(\phi) = m_X \exp \left[\kappa \ln \left(\frac{e^{1/2} \hat{\Lambda}_s}{m_X} \right) \frac{\varphi^2}{2} + \mathcal{O}(\varphi^3) \right], \quad (5.17)$$

where m_X is the particle mass when ϕ is at the minimum of its effective potential, $\hat{\Lambda}_s$ is the string scale (chosen to be 3×10^{17} GeV, in line with Ref. [55], though our results are only logarithmically sensitive to this choice), and κ is an $\mathcal{O}(1)$ coefficient of the Taylor expansion of the gauge coupling of the confining sector with respect to ϕ . Because $\hat{\Lambda}_s \gg m_X$, the constant of proportionality

$$\beta_X \equiv \kappa \ln(e^{1/2} \hat{\Lambda}_s/m_X) \approx \kappa \left(40.75 - \ln \frac{m_X}{\text{GeV}} \right) \quad (5.18)$$

can be quite large, making this attractor mechanism efficient (as required for the dilaton to evade fifth force bounds). The confining gauge group coupling changes by $\mathcal{O}(1)$ over a field range $\Delta\phi \sim M_{\text{pl}}/\sqrt{\kappa}$, ensuring perturbative control even as $m_X(\phi)$ [and, for our purposes, $m_A(\phi)$] change by multiple orders of magnitude. If indeed the dilaton modulates the dark photon mass in this way, then per Sec. VB1 these dynamics are sufficient to alleviate inflationary defect formation bounds.

The dilaton’s cosmological dynamics are governed by its interactions with the SM plasma, which induce an effective potential that takes the form [159, 188, 189]

$$V(\phi) \approx \sum_{\{X|m_X(\phi) \lesssim T\}} \frac{g_X}{24} T^2 m_X(\phi)^2 \cdot \begin{cases} 1, & \text{boson,} \\ 1/2, & \text{fermion} \end{cases} \quad (5.19)$$

at one-loop order, where g_X is the number of degrees of freedom associated with species X and the sum runs over all particles whose masses are below the plasma temperature and depend on ϕ via the confining gauge group. The homogeneous component of ϕ evolves according to

$$0 = \ddot{\bar{\phi}} + \frac{3}{2t} \dot{\bar{\phi}} + \sum_{m_X(\bar{\phi}) \lesssim T} \frac{g_X}{24} T^2 m_X^2 \beta_X e^{\beta_X \bar{\phi}^2/2M_{\text{pl}}^2} \frac{\bar{\phi}}{M_{\text{pl}}^2}, \quad (5.20)$$

which may be integrated directly in the slow-roll approximation, $\ddot{\bar{\phi}} \rightarrow 0$. The heaviest coupled species that has not annihilated away dominates the effective potential, meaning the dilaton starts rolling

from its initial condition around when the heaviest species begins to annihilate. The temperature at that time is

$$T_{\text{roll}} \approx \sum_{m_X(\phi_0) \lesssim T_{\text{roll}}} \sqrt{\frac{g_X}{g_\star}} m_X(\phi_0) \frac{\beta_X \phi_0}{M_{\text{pl}}}. \quad (5.21)$$

After this point, particle masses drop in proportion to the temperature,

$$m_X(\phi(t)) \approx m_X(\phi_0) \frac{T(t)}{T_{\text{roll}}}. \quad (5.22)$$

No particle falls out of thermal equilibrium as long as its mass continues to scale in proportion to its temperature, effectively pausing the thermal evolution of that species (or of the Universe if all masses are ϕ dependent) until the dilaton reaches the minimum of its effective potential,¹² at which point all masses take on their present-day values. These dynamics rely only on the slow-roll approximation and not the particular form of the ϕ dependence of m_X —only that m_X is a sufficiently steep function of ϕ and that the scalar’s bare potential is negligible. The same phenomenon occurs in, for example, Brans-Dicke [190]–inspired models (see e.g., Ref. [191]).

To have any impact on the available parameter space of dark photon dark matter, both m_A and at least one thermalized species must acquire a ϕ -dependent mass in the manner described above (though, in principle, all masses could depend on ϕ). Defect formation limits are thus alleviated by whatever amount the dark photon mass drops after $H = m_{A,I}$, per Sec. VB 1; however, the dilaton can, in principle, begin rolling earlier, which would not contribute any relaxation of defect limits but would still require a larger H_I to set the correct relic abundance. In order for the dark photon mass to start shrinking only after the dominant mode has become nonrelativistic, the dilaton must start rolling at a Hubble rate $H_{\text{roll}} = \sqrt{\pi^2 g_\star / 90} T_{\text{roll}}^2 / M_{\text{pl}}$ below $m_{A,I}$. Using Eq. (5.21), the relic abundance constraint Eq. (5.14), and $m_{A,I}/m_A = \exp(\beta_X \phi_0^2 / 4M_{\text{pl}}^2)$:

$$\begin{aligned} \frac{H_{\text{roll}}}{m_{A,I}} &\approx \frac{\beta_X}{30} \left(\frac{m_X}{125 \text{ GeV}} \right)^2 \left(\frac{m_A}{0.1 \text{ meV}} \right)^{-2} \frac{g_X}{4} \left(\frac{g_\star}{106.75} \right)^{-1/2} \left(\frac{H_I}{5 \times 10^{13} \text{ GeV}} \right)^{-4} \\ &\times \ln \left[\left(\frac{m_A}{0.1 \text{ meV}} \right) \left(\frac{H_I}{5 \times 10^{13} \text{ GeV}} \right)^4 \right]. \end{aligned} \quad (5.23)$$

The expanded parameter space available to “dilaton-assisted” inflationary production is depicted in Fig. 7 and could be probed by LZ [118]. This accessible parameter space would require inflationary scales so large that primordial gravitational waves would be easily detected by future CMB observations [192–194] (but are not already excluded). However, there are currently no direct-detection prospects at masses below a keV. Finally, as described in Ref. [55], this model predicts violations of the weak equivalence principle, which are stronger for $\kappa \lesssim 1$ and potentially observable in successors to Eöt-Wash [185, 186] or MICROSCOPE [187, 195].

C. Rapidly varying dark gauge coupling

Whether dark photons are produced gravitationally during inflation or via an oscillating axion afterward, the dark sector is populated at the end of inflation (if not earlier). What distinguishes the two scenarios is that gravitationally produced dark photons redshift even during inflation, whereas

¹² The energy density of the dilaton during its subsequent oscillations about its minimum dilute faster than matter because its mass drops with T , ensuring it never contributes significantly to the dark matter density.

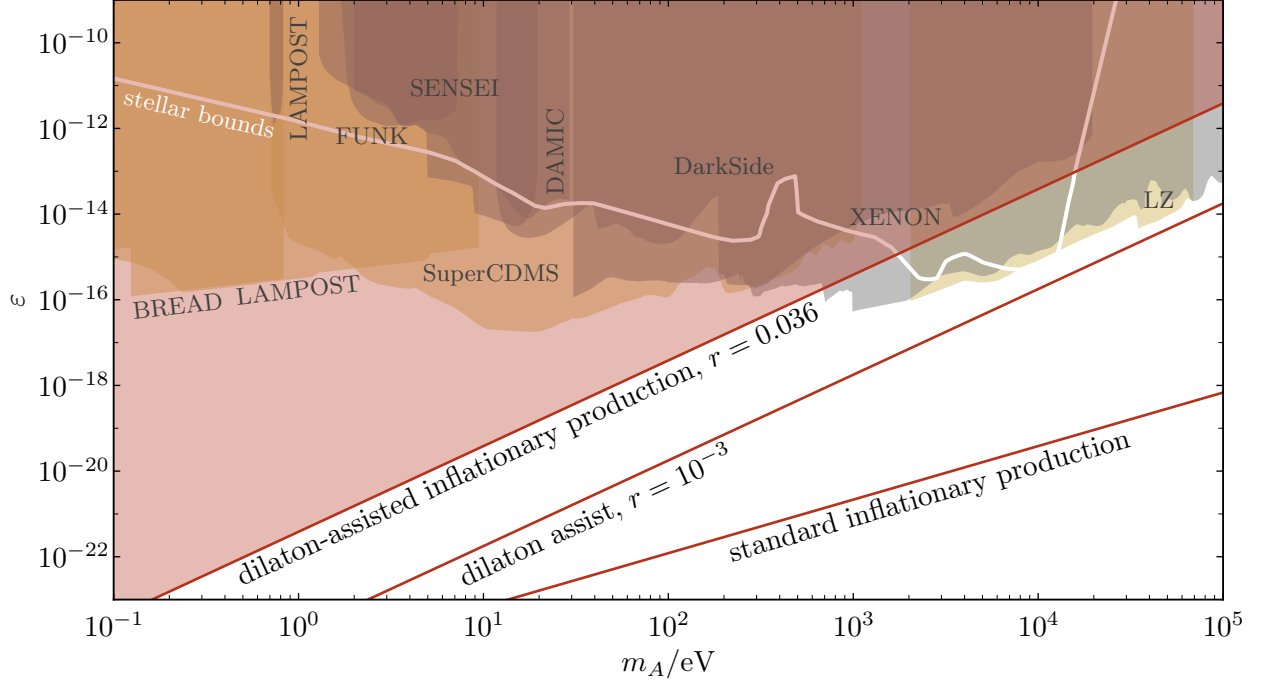


Figure 7. Kinetic mixing parameter space [Eq. (2.9)] of dark photon dark matter produced during inflation. The red region depicts parameter space that is constrained by defect formation for dilaton-assisted inflationary production for the maximal inflationary scale presently allowed (corresponding to a tensor-to-scalar ratio $r = 0.036$ [120]), and the upper limit for $r = 10^{-3}$ (a value that can be probed by future CMB observations [192–194]) appears as labeled. The upper limit for standard inflationary production (without any mass evolution) is also plotted in red. Limits and projects are displayed as in Fig. 4.

in the latter case the dark sector density remains frozen in the misaligned axion condensate until $H = m_a$. In this way, the axion effectively acts as a reservoir, allowing for a lower maximum dark photon density and reducing backreaction onto the dark Higgs once dark photons are produced. Kinematic efficiency ultimately limits how long dark photon production from axions may be delayed (Sec. IIC), requiring larger couplings or field excursions ($\beta\theta_0 \gg 1$) and typically also a boost of the axion–dark-photon coupling by *ad hoc* means (but see Sec. IVB for a possible exception). In this section, we show that a scalar coupled to the kinetic term of the dark photon can realize further delayed dark photon production by eliminating the kinematic barrier (Sec. VC1). We present the dynamics in a concrete scenario (Sec. VC2), and we find that such scenarios do not require parametrically large dimensionless numbers, in contrast to axion production (Sec. VC3); however, we do not identify a concrete UV completion. We then discuss unique signatures of delayed dark photon production in Sec. VC4.

1. Resonant production with kinetic couplings

Whereas dilaton-assisted inflationary production (Sec. VB) relied on couplings that modulate mass scales alone, the kinetic couplings W and X (to the dark photon and Higgs, respectively) modulate the dark photon mass without changing the backreaction threshold $\lambda v^4 \propto Y$ [Eq. (5.5)]. Thus, instead of raising the threshold for defect formation relative to the required dark photon energy density, kinetic couplings could suppress the dark photon mass, eliminating the kinematic barrier to resonance and delaying production to late times $H \sim m_\phi \ll m_A$. Moreover, kinetic

couplings are derivative couplings, and the requisite evolution of X or Y by orders of magnitude (between their early-time and present-day values) can mechanize tachyonic resonance that could itself source the dark photon relic abundance.

The scalar-dependent dark photon mass $m_A(\bar{\phi}) = m_A \sqrt{X(\bar{\phi})/W(\bar{\phi})}$ is small compared to its present-day value if either X is initially very small or W very large. (We normalize the values of X and Y today to unity without loss of generality.) The massless limit of Eq. (5.6c) is

$$0 = \ddot{A}_{\parallel} + \partial_t \ln X(\bar{\phi}) \dot{A}_{\parallel} + k^2 A_{\parallel}, \quad (5.24)$$

neglecting cosmic expansion for illustration's sake. Exponential growth requires a negative friction term, but the longitudinal mode's friction term is positive when X increases with time. The coupling W , on the other hand, does decrease in our hypothesized scenario. Setting $X = Y = 1$, the canonical, transverse equation of motion Eq. (5.6b) takes the simplified form

$$0 = \ddot{\mathcal{A}}_{\pm} + H \dot{\mathcal{A}}_{\pm} + \omega_{\pm}(k)^2 \mathcal{A}_{\pm}, \quad (5.25)$$

where the dark photon's effective frequency squared is

$$\omega_{\pm}(k)^2 = \frac{k^2}{a^2} + \frac{m_A^2}{\bar{W}} - \frac{H}{2} \frac{\dot{\bar{W}}}{\bar{W}} - \frac{\partial_t^2 \sqrt{\bar{W}}}{\sqrt{\bar{W}}}. \quad (5.26)$$

Transverse modes thus have a negative squared effective mass if $\dot{\bar{W}}^2 < 2\ddot{\bar{W}}\bar{W}$; functions that are both large in magnitude and accelerating yield the fastest growth. If the rate of change of W is proportional to the scalar's effective mass m_{ϕ} , i.e., $\dot{\bar{W}}/\bar{W} = \dot{\bar{\phi}}\partial_{\bar{\phi}} \ln W \sim m_{\phi} \partial \ln W / \partial \ln \phi$, the tachyonic growth condition $\omega_{\pm}^2 \leq 0$ requires the kinetic function to be larger than the squared dark-photon–scalar mass ratio, $W(\phi_0) \gtrsim (m_A/m_{\phi})^2$. This, however, is an underestimate: efficient production requires that ω_{\pm}^2 is negative for a period long enough to build up all of the dark matter. Therefore, W must decrease for a parametrically long time and so by many orders of magnitude. We next present a concrete realization of tachyonic production via a rapidly varying dark gauge coupling, i.e., a suitable choice of coupling function W and scalar potential V as first presented in Ref. [52].

2. Dynamics

Realizing functions W that vary by orders of magnitude generally requires exponential dependence on the scalar and that the scalar rolls over a fairly large distance (in appropriate units). We therefore choose a potential that is compatible with large field excursions: the “runaway,” exponential potential

$$V(\phi) = M^2 f^2 e^{-\phi/f} \equiv m_{\phi}^2 f^2 e^{-(\phi-\phi_0)/f}, \quad (5.27)$$

which is motivated by certain constructions in string theory [196–199] and whose self-similarity stabilizes it against quantum corrections from self-interactions [200]. The latter equality in Eq. (5.27) merely defines m_{ϕ} to coincide with the scalar's effective mass when at its homogeneous initial condition $\phi = \phi_0$ (whereas M is that when ϕ crosses zero). The evolution of a homogeneous scalar in Eq. (5.27) is approximately

$$\bar{\phi}(t) \approx \phi_0 + f \ln [1 + (m_{\phi} t)^2], \quad (5.28)$$

up to oscillations that fall off with $(m_\phi t)^{-1/4}$.¹³

Many possible coupling functions satisfy the tachyonic resonance condition $\partial_t^2 \sqrt{W}/\sqrt{W} < 0$, but an exponential does so even as ϕ 's time derivatives become small [as for Eq. (5.28)] and for all field values of ϕ . However, were W a pure exponential, nothing would prevent the dark photon's mass from continuing to decrease to the present day. To stabilize the vector's mass, one could augment the scalar potential with a minimum at some finite ϕ or modify the coupling function W to asymptote to a constant at late times. We choose the latter option (for reasons explained at the end of this section), taking

$$W(\phi) = 1 + e^{-\eta\phi/f}, \quad (5.29)$$

normalized such that $W = 1$ as ϕ rolls toward $+\infty$ and with η parametrizing the coupling strength. The initial condition ϕ_0 must thus be negative so that $W(\phi_0) \gg 1$.

Production begins when $H \approx m_\phi$ and continues until the latter term in Eq. (5.29) drops below unity, at which point the scalar and dark photon decouple, the dark photon's mass reaches its present-day value, and production completes (when the Hubble rate is H_\star by definition). Per the approximate solution Eq. (5.28), the scalar crosses zero (i.e., W approaches unity) at $t_\star \approx e^{-\phi_0/2f}/m_\phi = 1/M$. While $\phi < 0$, we may take $W(\phi) \approx e^{-\eta\phi/f}$ and the time dependence of the effective frequency is approximately

$$\frac{\omega_{\text{eff}}(k)^2}{m_\phi^2} \approx \frac{k^2}{a^2 m_\phi^2} + \frac{m_A^2}{W(\phi) m_\phi^2} - \frac{\eta(2\eta + 1)m_\phi^2 t^2 - 3\eta}{2(1 + m_\phi^2 t^2)^2}. \quad (5.30)$$

While W remains much larger than $(m_A/m_\phi)^2$, the dark photon's bare mass is negligible; modes with $k/a \lesssim \eta m_\phi (m_\phi t)^{-1}$ therefore have a negative ω_{eff}^2 and grow by a tachyonic resonance.

For modes with negligible wave numbers and at early enough times that the bare mass term can be neglected, the equation of motion Eq. (5.25) with effective frequencies given by Eq. (5.30) has the analytic solution (with $\dot{\mathcal{A}}_\pm$ initially zero)

$$\mathcal{A}_\pm(t, 0) = \mathcal{A}_\pm(0, 0) [1 + (m_\phi t)^2]^{-\eta/2}. \quad (5.31)$$

This result may be extended to small, nonzero k with a perturbative expansion in the parameter k/m_ϕ . Setting $a(t) = \sqrt{m_\phi t}$, we take the ansatz

$$\mathcal{A}_\pm(t, k) = \mathcal{A}_\pm(0, k) [1 + (m_\phi t)^2]^{-\eta/2} [1 + (k/m_\phi)^2 \delta\mathcal{A}(t)] \quad (5.32)$$

and solve for the dimensionless perturbation $\delta\mathcal{A}(t)$. The equation of motion then reduces to one for $\delta\mathcal{A}$ of the form

$$0 = \delta\ddot{\mathcal{A}} - \frac{(m_\phi t)^2(4\eta - 1) - 1}{2t[1 + (m_\phi t)^2]} \delta\dot{\mathcal{A}} + \frac{m_\phi}{t} + \frac{k^2}{m_\phi t} \delta\mathcal{A}. \quad (5.33)$$

The last term is negligible at leading order in k/m_ϕ , and in this limit the equation is solved by an integral of a hypergeometric function:

$$\delta\mathcal{A}(t) = \int_0^{m_\phi t} dx (1 + x^2)^\eta {}_2F_1(1/4, \eta, 5/4; -x^2) + \mathcal{O}(k^2/m_\phi^2). \quad (5.34)$$

¹³ These oscillations are logarithmic in time and change the resulting dark photon mode amplitude at the $\mathcal{O}(1)$ level. Since $\mathcal{O}(1)$ changes to the mode amplitude may be compensated by similar changes to parameter values, we neglect this subtlety for the sake of clarity.

Eventually, either the gradient or bare mass term overtakes the W -derivative term as the dominant contribution to $\omega_{\text{eff}}(k)^2$ and growth ceases. This behavior may be approximated by cutting off the integral Eq. (5.34) at the earlier of the two possibilities,

$$t_{\text{cut}}(k) \approx \min \left[\frac{1}{M} \left(\sqrt{\eta^2 + \eta/2} \frac{M}{m_A} \right)^{\frac{1}{\eta+1}}, \frac{(\eta^2 + \eta/2)m_\phi}{k^2} \right]. \quad (5.35)$$

As long as $m_\phi t_{\text{cut}}(k) \gg 1$, the integral in Eq. (5.34) is dominated by $x \gg 1$, making it an excellent approximation to substitute $1 + x^2 \approx x^2$. The integral may then be evaluated analytically, yielding $\mathcal{A}_\pm(t, k) \propto (k/m_\phi)^2 (m_\phi t)^{\eta+1/2}$. After this point, the mode amplitude begins to decrease as $\mathcal{A}_\pm \propto W^{1/4}/a^{1/2}$ while the dark photon mass continues to increase toward its vacuum value, per the WKB approximation.

In summary, the mode amplitude evaluated at t_\star is a product of factors encoding its initial condition $\mathcal{A}_\pm(0, k) \propto 1/\sqrt{2k/a}$, the $k=0$ solution [Eq. (5.31)] and the leading-order correction $\delta\mathcal{A}$ for nonzero k [Eq. (5.32)], and factors encoding the adiabatic evolution between $t_{\text{cut}}(k)$ and t_\star :

$$\frac{\mathcal{A}_\pm(t_\star, k)}{\mathcal{A}_\pm(0, k)} = \frac{\mathcal{A}(t_{\text{cut}}, 0)}{\mathcal{A}(0, 0)} \left(\frac{k}{m_\phi} \right)^2 \delta\mathcal{A}(t_{\text{cut}}) \sqrt[4]{\frac{W(\bar{\phi}(t_\star))}{W(\bar{\phi}(t_{\text{cut}}))}} \sqrt{\frac{a(t_{\text{cut}}(k))}{a(t_\star)}}. \quad (5.36)$$

Inserting the preceding results in the $m_\phi t \gg 1$ limit yields

$$\frac{\mathcal{A}_\pm(t_\star, k)}{\mathcal{A}_\pm(0, k)} = [m_\phi t_{\text{cut}}(k)]^{-\eta} \left(\frac{k}{m_\phi} \right)^2 [m_\phi t_{\text{cut}}(k)]^{2\eta+1/2} \frac{2\Gamma(\frac{5}{4})\Gamma(\eta-\frac{1}{4})}{\Gamma(\eta)(4\eta+1)} [2H_\star t_{\text{cut}}(k)]^{\eta/2+1/4}, \quad (5.37)$$

where the Hubble rate at production

$$H_\star \equiv 1/2t_\star = M/2 \quad (5.38)$$

is set by the time when ϕ crosses 0 and the scalar decouples.

The relic density of dark photons is obtained by a suitable integral of Eq. (5.37) over wave number [Eq. (A16)]. The mode with peak power is that for which the mass and gradient terms are equally responsible for cutting off the resonance:

$$k_\star \approx \sqrt{(\eta^2 + \eta/2)Mm_\phi} \left(\sqrt{\eta^2 + \eta/2} \frac{M}{m_A} \right)^{-\frac{1}{2\eta+2}}. \quad (5.39)$$

The mode amplitude is peaked at this wave number and falls off sharply at larger k , so the energy density is well approximated by integrating up to $k = k_\star$. The total dark photon energy density [Eq. (A16)] evaluated at $H = H_\star$ is thus approximately

$$\frac{\rho_\star}{H_\star^4} \approx \mathcal{N}_\eta \left(\frac{m_\phi}{M} \right)^{2\eta-1} \left(\frac{M}{m_A} \right)^{\frac{\eta-7/2}{\eta+1}}, \quad (5.40)$$

where the η -dependent coefficient is

$$\mathcal{N}_\eta = \frac{(\eta^2 + \eta/2)^{\frac{9(2\eta+1)}{4(\eta+1)}}}{6\pi^2} \frac{\Gamma(5/4)^2 \Gamma(\eta-1/4)^2}{(1+4\eta)^2 \Gamma(\eta)^2}. \quad (5.41)$$

In the large- η limit, the power spectrum peaks at $k_\star \sim \eta\sqrt{Mm_\phi} \lesssim m_A$, so the dark photons are nonrelativistic when their mass reaches its final value and growth ends. Redshifting the energy

density to matter-radiation equality, the dark photon relic abundance is

$$\frac{\Omega_A}{\Omega_{\text{DM}}} \approx \frac{2}{3} \mathcal{N}_\eta \left(\frac{m_\phi}{2H_\star} \right)^{2\eta-1} \left(\frac{2H_\star}{m_A} \right)^{\frac{\eta-7/2}{\eta+1}} \frac{H_\star^2}{M_{\text{pl}}^2} \sqrt{\frac{H_\star}{H_{\text{eq}}}}. \quad (5.42)$$

This result reproduces full numerical solutions within a couple of orders of magnitude for $-\phi_0/f \gtrsim 5$ [below which the errors are dominated by the approximation made in Eq. (5.28)]—accuracy more than sufficient for our purposes.

For η larger than a few, the relic abundance is most sensitive to m_ϕ/H_\star , which effectively encodes how long production takes or equivalently the scalar’s initial displacement, $\phi_0 = -2f \ln(m_\phi/H_\star)$. The ratio H_\star/m_A may then be chosen to delay production as long as desired. In addition, the initial dark photon mass must be far smaller than is necessitated by the kinematic condition $m_A(\phi_0) \ll m_\phi$: neglecting the η -dependent prefactor in Eq. (5.42) and taking the large- η limit (for which $H_\star \approx m_\phi$) with $\Omega_A = \Omega_{\text{DM}}$ yields the estimate

$$\frac{m_A^2}{W(\phi_0)m_\phi^2} \sim \frac{H_\star^4}{m_\phi^2 M_{\text{pl}}^2} \frac{m_A}{m_\phi} \sqrt{\frac{H_\star}{H_{\text{eq}}}} \ll 1. \quad (5.43)$$

In other words, the initial condition for ϕ is determined primarily by requiring a sufficient dark photon abundance rather than the kinematic requirement that $W(\phi_0) \gtrsim m_A^2/m_\phi^2$. The dynamics are thus effectively insensitive to the scalar–dark-photon mass ratio. This class of models thus certainly avoids backreaction onto the dark Higgs [Eq. (2.8)] in the same parameter space as standard axion production (Sec. IIC), corresponding to $H_\star \sim m_\phi \gtrsim m_A$ [as depicted in Fig. 3]. But the suppression of the kinematic barrier also allows dark photon much heavier (today) than m_ϕ . In fact, production may be delayed to at least as late as when $H_\star = 10^{-22}$ eV (i.e., roughly the earliest time observations require the dark matter to exist and behave like matter)¹⁴ and the kinetic coupling still eliminates the kinematic barrier for m_A as large as $\sim (H_{\text{eq}}/H_\star)^{1/2} M_{\text{pl}}^2/H_\star$.

The above calculations remain valid so long as the scalar’s dynamics are well approximated by Eq. (5.28), i.e., so long as backreaction of the dark photon onto the scalar and that of either field on the expansion history are negligible. The energy density of a scalar in a runaway potential tracks the critical density in both the radiation- and matter-dominated epochs: [201–203]:

$$\Omega_\phi(t) \equiv \frac{\bar{\rho}_\phi(t)}{3M_{\text{pl}}^2 H^2} \approx \left(\frac{2f}{M_{\text{pl}}} \right)^2. \quad (5.44)$$

The expansion history thus only departs from the radiation solution near the onset of the matter era, as in standard cosmology. Comparing the scalar’s energy density to η times the dark photon’s provides a decent proxy for whether backreaction onto the scalar is important. At production, the dark photon abundance (which redshifts more slowly than the radiation background by a power of a) is $\Omega_A \approx (H_{\text{eq}}/H_\star)^{1/2}/2$, so the scalar’s decay constant needs to be larger than

$$f \gtrsim 10^{-2} \sqrt{\eta} \left(\frac{H_\star}{10^{-22} \text{ eV}} \right)^{-1/4} M_{\text{pl}} \quad (5.45)$$

to ensure backreaction never occurs.

The scalar’s tracking behavior, moreover, provides a natural means for the dark photon’s abundance to exceed the scalar’s in the late Universe: the scalar redshifts as radiation, faster than

¹⁴ Dark photon subcomponents of dark matter could, in principle, be produced later with even larger kinetic mixing, but their direct-detection signals are also suppressed by their reduced abundance. Assessing precisely what fraction of dark matter could be produced at such late times, however, would require a dedicated cosmological analysis.

the nonrelativistic dark photons. In contrast, when dark photons are produced via a harmonically oscillating axion (Secs. [II C](#) and [IV](#)) or scalar, the parent field retains a sizable energy density at late times, as discussed in Sec. [II C](#). For this reason, we implemented the termination of production by modifying W from a pure exponential [Eq. (5.29)] rather than augmenting the potential [Eq. (5.27)] with a minimum at a finite field value. Barring some additional decay channel [[56](#), [160](#), [163](#)], production is terminated via nonlinear backreaction that can only be studied via 3 + 1-dimensional simulations [[56](#)] and generically leads to two-component dark matter.

3. Quantum corrections

Unlike the axion, whose continuous shift symmetry protects its potential from perturbative quantum corrections, the scalar theories discussed in this section are susceptible to quantum corrections. Additional heavy degrees of freedom (that arise in a UV completion of the theory) may overwhelm any phenomenologically viable tree-level scalar potential as it rolls over large field ranges. Nonetheless, so long as the scalar only has self-interactions and a kinetic coupling to the dark photon, quantum corrections can remain small because of the smallness of m_A at early times, only becoming important as m_A reaches its vacuum value. We compute the one-loop scalar effective potential in scalar–Abelian-Higgs theory in Appendix [B](#), from which we find that, for the particular choices of W and V above, the UV cutoff Λ_{UV} must be bounded above by

$$\frac{\Lambda_{UV}^2}{(4\pi f)^2} < \frac{3H_\star^2}{2m_A^2}. \quad (5.46)$$

The later production occurs, the lower the scalar’s potential and the smaller its quantum corrections must be to ensure the dynamics are not disrupted. Taking $\Lambda_{UV} \sim 4\pi f$ as a criterion for naturalness sets $H_\star \gtrsim m_A$ for scalar–dark-photon production—that is, we expect that below the postinflationary line in Fig. [3](#) the scalar models of dark photon production we discuss are both detectable and not fine-tuned in this sense. Larger kinetic mixing (without backreaction) is available to scalar-produced dark photons to the extent that one allows the models to be fine-tuned, as illustrated by Fig. [8](#).

The above discussion, taking only quadratically divergent contributions to the effective potential, derives from the one-loop computations in Appendix [B](#) which show that properly quantizing noncanonical field theories leads to a subtle cancellation of would-be quartic divergences (that one might intuitively expect to be present). Appendix [B](#) does not, however, attempt to determine whether such divergences are present at higher-loop order. Supposing that a quartic divergence was incurred at two loops by the kinetic coupling W , it would also be suppressed by g_D^2 . Requiring $g_D^2 \Lambda_{UV}^4 \lesssim H_\star^2 f^2$ imposes that $g_D \lesssim H_\star/f \cdot (f/\Lambda_{UV})^2$ —nominally quite a constraining bound, given that it combines with the lower bound on f [Eq. (5.45)] to set $g_D \lesssim 1.3 \times 10^{-20} (H_\star/\text{eV})^{5/4} / \sqrt{\eta}$ (taking $\Lambda_{UV} \approx f$). This bound happens to coincide with that on standard inflationary production [Eq. (2.12)] in scaling (with H_\star in place of m_A) and nearly in magnitude and is therefore extremely constraining for delayed production. Suppose, however, that $m_\phi \gg m_A$ (so that production is instead early) and that $k_\star/a_\star \sim H_\star$. The generic backreaction bound Eq. (2.8) on transverse production then scales quite weakly with H_\star : $g_D \lesssim 10^{-14} \lambda^{1/4} (m_A/\mu\text{eV})^{5/8} (m_A/H_\star)^{1/8}$. The parameter space that is natural can be made larger than that which avoids backreaction simply by increasing H_\star/m_A by, say, eight orders of magnitude, yielding a bound only one decade tighter than the fiducial case where $H_\star = m_A$. We therefore conclude that, even for the worst-case (and unconfirmed) UV divergences, the runaway scalar model allows for natural and backreaction-free parameter space in most of the fiducial postinflationary regime.

Since this class of production mechanism relies on the dark Abelian-Higgs sector being extremely

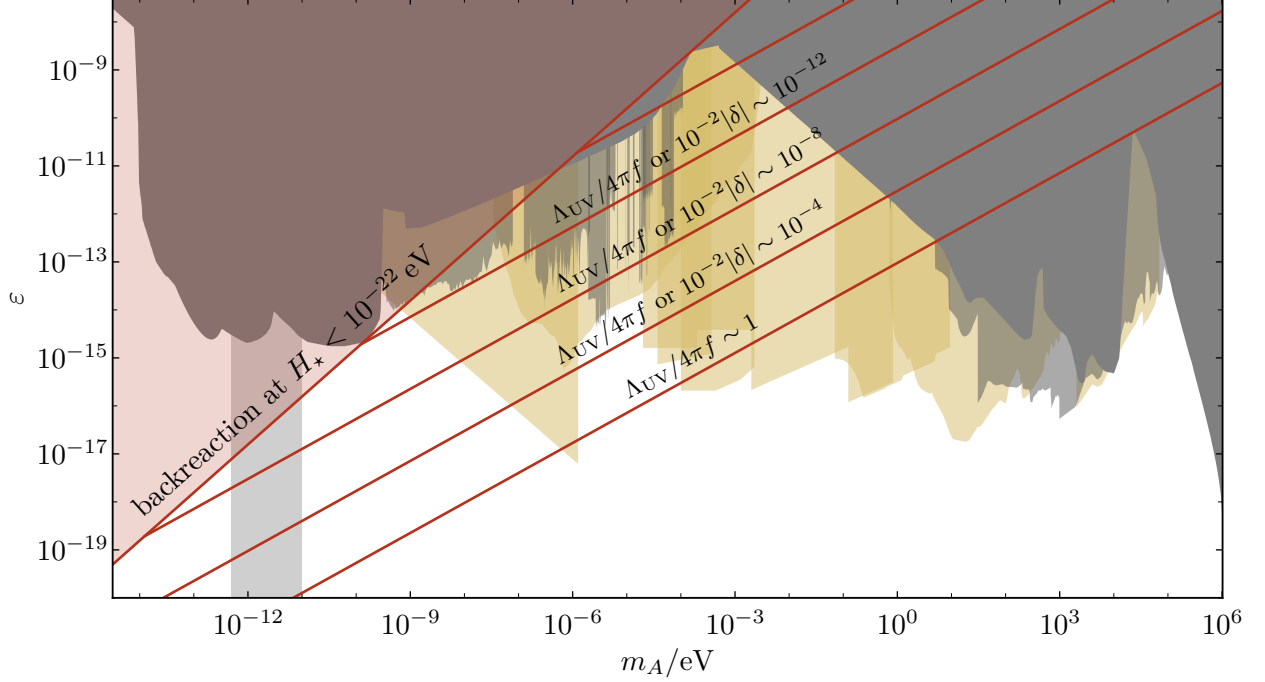


Figure 8. Parameter space in mass and kinetic mixing [Eq. (2.9)] of dark photon dark matter produced via kinetically coupled scalars. Thin red lines depict the maximum allowed kinetic mixing for a given degree of tuning (as labeled) of either the UV cutoff $\Lambda_{UV}/4\pi f$ for which one-loop quantum corrections are unimportant for runaway scalars (Sec. V C) or the dark-photon-scalar mass tuning δ [Eq. (5.61)] for oscillating scalars (Sec. V D). The red shaded region depicts parameter space in which backreaction or defect formation occurs even if the dark photon is produced as late as allowed by the CMB (roughly $H_* \approx 10^{-22}$ eV). Gray and yellow regions respectively depict the current limits and projected reach of various probes, as labeled in Fig. 3.

weakly coupled at early times, one might worry that it runs afoul of weak gravity conjectures (WGCs) [204]. While it is plausible but uncertain whether the WGCs constrain the gauge couplings for displaced moduli [182], were this the case, they would limit the field range of the scalar field and possibly interfere with dark photon production. The dark photon mass and hence the gauge coupling must be very small at early times; their sizes are quantified by Eq. (5.43), which translates to an estimate for the initial gauge coupling of

$$g_D(\phi_0) \sim g_D \frac{H_*}{M_{\text{pl}}} \sqrt{\frac{H_*}{m_A}} \sqrt[4]{\frac{H_*}{H_{\text{eq}}}} \quad (5.47)$$

in the large- η limit. The tower WGC [54, 205, 206] implies a UV cutoff of $g_D(\phi_0)^{1/3} M_{\text{pl}}$. Using the upper limit on g_D implied by the backreaction bound Eq. (2.8), we find that the UV cutoff associated with the WGC is

$$g_D \lesssim 3 \times 10^{-18} \cdot \lambda^{7/22} \left(\frac{m_A}{10^{-15} \text{ eV}} \right)^{25/22} \left(\frac{H_{\text{max}}}{10^{-15} \text{ eV}} \right)^{-9/22}, \quad (5.48)$$

where H_{max} is the maximum Hubble rate of the Universe and we have required $T_{\text{max}} \sim \sqrt{M_{\text{pl}} H_{\text{max}}} < \Lambda_{UV}$. Figure 9 depicts the range of parameter space in which this model would violate the WGC at early times for UV cutoffs of 1 TeV and 10^{16} GeV (the latter corresponding to the energy scale of high-scale inflation).

4. Signatures

In the regime of extremely delayed production, where the scalar potential must be protected by a low effective UV cutoff, the signatures of production via a rapidly varying gauge coupling are particularly striking. Small-scale structure is significantly enhanced for sufficiently small H_* and is potentially observable. In principle, since power below the peak (at which the power spectrum is order unity) scales as $(k/k_*)^3$, cosmological scales could also be enhanced above that of the baseline adiabatic fluctuations (whose power is $\sim 10^{-9}$) if k_* is within three decades of an observable scale. In our case, the peak wave number is $k_* \approx 2\eta H_*$ in the large- η limit. As a rough guide, at matter-radiation equality $k_*/a_{\text{eq}} \sim 2\beta H_{\text{eq}} \sqrt{H_*/H_{\text{eq}}}$. If production terminates long enough before equality (say, by three decades of expansion), then $\sqrt{H_*/H_{\text{eq}}} \gtrsim 10^3$; with $\beta \gtrsim 10$, enhanced power is important on scales at least an order of magnitude smaller than the horizon at equality. These scales are on the threshold of the sensitivity of *Planck*'s CMB observations and around those which the Lyman- α forest probe [207–209]. Further in the future, 21-cm intensity mapping could probe scales 1-2 orders of magnitude smaller [210]. Ultimately, quantitative cosmological constraints require a dedicated analysis of dark matter with such power spectra (as would a bound on the latest time the dark matter could be produced).

Enhanced power on yet smaller scales would approach the critical overdensity $\delta_c = 1.686$ during radiation domination [211], leading to the collapse of structures with radius $\sim \pi/(2k_*/a_{\text{eq}})$ around matter-radiation equality. (The peak of the density power spectrum is at roughly twice k_* .) The density of these structures is approximately 178 times that of the ambient matter at matter-radiation equality [212],

$$\rho_{\text{coll}} \sim 178 \cdot \frac{3}{2} M_{\text{pl}}^2 H_{\text{eq}}^2 \approx 2.7 \times 10^5 M_{\odot}/\text{pc}^3, \quad (5.49)$$

and these collapsed structures contain a mass¹⁵

$$M \sim \frac{3}{2} M_{\text{pl}}^2 H_{\text{eq}}^2 \cdot \frac{4\pi}{3} \left(\frac{\pi}{2k_*/a_{\text{eq}}} \right)^3 \approx 2.4 \times 10^5 M_{\odot} \left(\frac{\eta}{10} \right)^{-3} \left(\frac{H_*}{10^{-22} \text{ eV}} \right)^{-3/2}. \quad (5.50)$$

Power on larger scales is also moderately enhanced, resulting in the collapse of larger, more diffuse structures at later times. The structures collapsing at $z = 250$ are the largest that remain resilient against tidal stripping [214]; their density is again 178 times the matter density at the time of collapse, $\rho_{\text{coll}} \sim 9.2 \times 10^1 M_{\odot}/\text{pc}^3$. We may estimate their mass by extrapolating the density power spectrum from its peak to small wave number, i.e. $\sim (2k/k_*)^3$, where the factor of two accounts for the broad peak of the density power spectrum. Since the density power spectrum is proportional the square of the fractional overdensity, it grows with a^2 during the matter era, so modes of ever longer wavelength $a/k \propto a^{5/3}$ collapse as the Universe continues to expand. On the other hand, the matter density dilutes as a^{-3} . In total, the mass of structures collapsing at a given redshift grows with a^2 , and we estimate that structures collapsing at $z = 250$ have mass

$$M \sim \frac{3}{2} \frac{M_{\text{pl}}^2 H_{\text{eq}}^2}{(a/a_{\text{eq}})^3} \cdot \frac{4\pi}{3} \left(\frac{\pi}{k_{\text{col}}/a_{\text{eq}}} \right)^3 \sim 2.9 \times 10^9 M_{\odot} \left(\frac{\eta}{10} \right)^{-3} \left(\frac{H_*}{10^{-22} \text{ eV}} \right)^{-3/2}. \quad (5.51)$$

Figure 9 depicts the expected substructure mass for maximally delayed dark photon production as a function of m_A and ε , superimposed on the limits and prospective reach of direct-detection experiments. Note that production may well be delayed longer than strictly necessary to accommodate

¹⁵ Although gravitational interactions can change the subhalo's mass and density over time [213], we calculate their initial values at collapse for a conservative representation of their late-time properties.

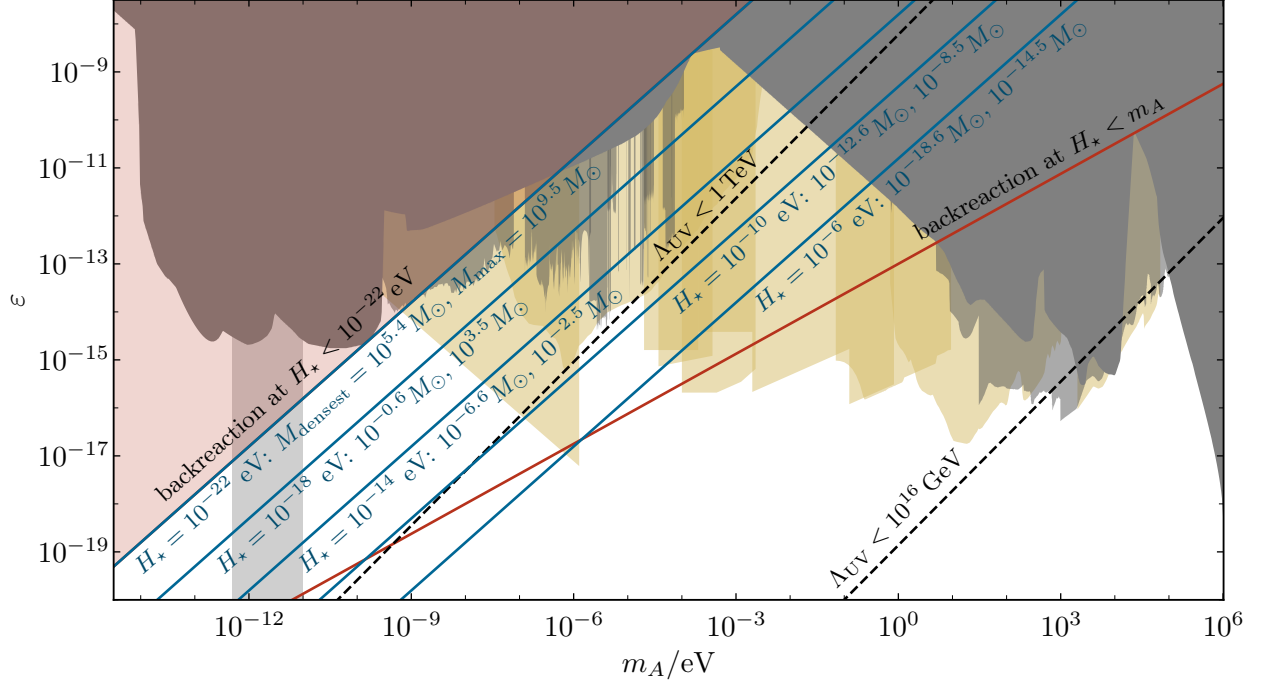


Figure 9. Minimum dark matter substructure sizes predicted by the kinetically coupled runaway scalar model in the direct-detection parameter space. Blue lines display substructure masses M_{densest} for structures collapsing at the onset of matter-radiation equality and M_{max} for structures collapsing at redshift $z = 250$ in scenarios where production is delayed until Hubble rates H_* as labeled on each line. Much of the expanded kinetic mixing parameter space—including that accessible to future direct-detection programs—features substructures that are potentially accessible to upcoming astrometric ($M > 10^{-3} M_\odot$) [213] and photometric searches ($10^{-15} M_\odot < M < 10^{-8} M_\odot$) [215]. Dashed black lines represent upper bounds on the dark gauge coupling implied by the tower weak gravity conjecture [54, 205, 206], should it apply to displaced moduli. Results are otherwise presented as in Figs. 3 and 8.

whatever kinetic mixing the dark photon happens to have; the substructure masses displayed in Fig. 9 are thus the minimum predicted by the model (rather than a unique value thereof).

Astrometric lensing, the correlated deflection in background stars induced by a dense, heavy halo passing through our line of sight, is a promising indirect signature of such substructure [216]. High-resolution telescopes like *Gaia* [217] and the *Hubble* Space Telescope [218], and future missions such as *Theia* [219], *Roman* [220], the Square Kilometre Array (SKA) [221], and the Thirty Meter Telescope [222], could detect these effects by measuring the correlated proper motions and accelerations of stars. *Gaia* is sensitive to subhalos heavier than $10^5 M_\odot$ for the densest subhalos that form around matter-radiation equality, while *Theia* and SKA will probe these dense substructures down to masses around $10^{-3} M_\odot$ and the more dilute structures forming at $z = 250$ down to $10^2 M_\odot$ [213]. Another signature is photometric microlensing, where changes in a star’s brightness suggest an intervening gravitational lens. This technique is particularly effective with highly magnified stars near critical lensing caustics of galaxy clusters. If dark matter subhalos are present, their virial motion introduces noise in the star’s position and brightness, depending on the subhalo mass spectrum [215]. However, these projections are subject to uncertainties from galactic evolution and tidal stripping of subhalos and require further simulation to confirm their viability [214].

The scalar coupled to the dark photon may yield its own signatures; their inherent model dependence could facilitate positively identifying the origin of dark photon dark matter. In the case of the runaway scalar considered in Sec. VC2, delaying production requires large enough

decay constants f to ensure resonant growth is not disrupted, as well as to supply the dark photon with sufficient energy to make up the dark matter. The model thus predicts some minimum cosmological abundance of the scalar in both the radiation and matter eras due to its tracking behavior [Eq. (5.44)], even if the dark photon dominates the dark matter abundance. The runaway scalar would alter cosmological dynamics to a degree controlled by f/M_{pl} . Recent work [223, 224] has quantitatively analyzed cosmology with tracking scalars as a means to resolve the Hubble tension, the mismatch between Hubble constants inferred from the early Universe (e.g., via CMB data [58]) and measured directly by the calibrated distance ladder [225]. In the scenarios studied in Refs. [223, 224], current data limit the fractional abundance of the scalar at early times at the few-percent level. Extrapolating this result to the runaway scalars we consider estimates that f must be below about a tenth of the Planck scale. Though these signatures are specific to runaway scalars, a scalar with a quadratic potential could just as well mechanize delayed production, but without a natural means to ensure dark photons dominate the dark matter density (since production terminates via nonlinear backreaction). Such scalars could instead provide astrophysical signatures as fuzzy subcomponents of dark matter.

Finally, though production must end sufficiently early that the dark matter exists well before matter-radiation equality, the dark photon’s mass need not necessarily stop evolving at this point. The coupling function [Eq. (5.29)], rather than asymptoting to unity, could instead transition to a slower evolution with time. While not necessary for the scenario we identify, a concrete realization thereof may well predict that the dark photon mass continues to evolve to some extent after production, a possibility that can also be tested by cosmological data [226, 227].

D. Narrow resonance with an oscillating scalar

The final possibility we consider is, rather than a runaway scalar, a scalar oscillating in a quadratic potential

$$V(\phi) = \frac{1}{2}m_\phi^2\phi^2. \quad (5.52)$$

Such a scenario was studied in Ref. [51], which showed that a kinetic coupling $W(\phi) = e^{\eta\phi/f}$ leads not just to broad tachyonic resonance familiar from analogous models of gauge preheating [148, 151, 152, 228] but also to a unique regime of narrow resonance when $m_A/m_\phi = 1/2$ that can, in principle, persist for arbitrarily small scalar field amplitudes (and so an arbitrarily long time). As a result, conversion of the scalar into dark photons eventually becomes fast compared to the Hubble rate without requiring large coupling [51]—indeed, only relying on the leading-order expansion $W(\phi) \approx 1 + \eta\phi/f$, which would be expected to dominate the behavior from the perspective of bottom-up effective field theory.

Moreover, smaller couplings delay the time that dark photons are efficiently produced, which Ref. [51] posited as a means to alleviate defect formation bounds. Before examining this possibility in detail, we briefly review the mechanics of this scenario, focusing on the novel regime of persistent resonance at small scalar field amplitudes.¹⁶ We also show that the structure of the equations of motion that gives rise to the small-amplitude regime is not unique to the kinetic coupling considered in Ref. [51].

The solution to the homogeneous equation of motion Eq. (5.6a) for a massive, misaligned scalar

¹⁶ The broad resonance scenario (i.e., $\eta\phi_0/f > 1$ for any mass $m_A \lesssim \eta m_\phi$) is certainly a viable production mechanism, but its phenomenology (in terms of allowed kinetic mixing, at least) is identical to axion production.

that begins oscillating in the radiation era [when $a(t) \propto \sqrt{t}$] is

$$\bar{\phi}(t) = \Gamma(5/4)\phi_0 \frac{J_{1/4}(m_\phi t)}{\sqrt[4]{m_\phi t/2}} \quad (5.53)$$

from initial conditions $\bar{\phi} = \phi_0$ and $\dot{\bar{\phi}} = 0$ at times $m_\phi t \rightarrow 0$. Define $a_{\text{osc}} = a(t_{\text{osc}})$ where $H(t_{\text{osc}}) = m_\phi$, such that $H(t) = m_\phi[a(t)/a_{\text{osc}}]^{-2}$. At late times $m_\phi t \gg 1$,

$$\bar{\phi}(t) \approx \frac{2^{3/2}\Gamma(5/4)\phi_0}{\sqrt{\pi}[a(t)/a_{\text{osc}}]^{3/2}} \sin(m_\phi t + \pi/8) \equiv \Phi(t) \sin(m_\phi t + \pi/8), \quad (5.54)$$

where the second equality defines the time-dependent oscillation amplitude $\Phi(t)$.

Expanding coupling functions in Eq. (5.6b) to leading order in small $\bar{\phi}$ and neglecting Hubble friction (as appropriate at the late times when resonance becomes efficient),

$$0 = \ddot{\mathcal{A}}_\pm + \left[\frac{k^2}{a^2} + m_A^2 + m_A^2 \bar{\phi}(t) \left(\frac{X'(\bar{\phi})}{X(\bar{\phi})} - \frac{W'(\bar{\phi})}{W(\bar{\phi})} \right) + \ddot{\bar{\phi}}(t) \frac{W'(\bar{\phi})}{2W(\bar{\phi})} \right] \mathcal{A}_\pm. \quad (5.55)$$

Substituting Eq. (5.54) and taking the time coordinate $z = m_\phi t/2 - 3\pi/16$, Eq. (5.55) takes the form of the Mathieu equation,

$$0 = \frac{d^2 \mathcal{A}_\pm}{dz^2} + [p - 2q \cos(2z)] \mathcal{A}_\pm, \quad (5.56)$$

with $m_\phi^2 p/4 = k^2/a^2 + m_A^2$ and

$$q = \Phi(t) \left[\frac{2m_A^2}{m_\phi^2} \left(\frac{X'(\bar{\phi})}{X(\bar{\phi})} - \frac{W'(\bar{\phi})}{W(\bar{\phi})} \right) - \frac{W'(\bar{\phi})}{W(\bar{\phi})} \right]. \quad (5.57)$$

If the mass ratio m_A/m_ϕ is precisely $1/2$ then a narrow resonance for $k \ll m_\phi$ persists to arbitrarily small q (i.e., field amplitudes) [51]. (Otherwise—as is typical of such scenarios—the resonance terminates once the scalar redshifts below some nonzero $\bar{\phi}$.)

Evidently, Eq. (5.57) is nonzero regardless of whether the coupling is via the kinetic term (W) or the mass term (X) or both (i.e., a universal coupling); only coupling functions contrived to make Eq. (5.57) identically zero would exhibit no such instability. Furthermore, longitudinal modes experience the same instability: as discussed below Eq. (5.6), in the $k \ll m_A(\bar{\phi})$ limit where the small-amplitude resonance would exist if present, the longitudinal mode's dynamics [Eq. (5.6c)] are identical to the transverse modes'.

The narrow-resonance scenario allows for dark photon production parametrically later than the standard expectation that $H_\star \gtrsim m_A$. Modes in the narrow-resonance band have exponential growth rate $\Gamma = \eta m_\phi \Phi(t)/8f$, which decays more slowly than the Hubble rate in the radiation era. Production therefore becomes efficient at a scale factor [51]

$$\frac{a_\star}{a_{\text{osc}}} = \left(\frac{3\eta\phi_0}{4f} \right)^{-2} \ln \left(\frac{m_\phi^2 \phi_0^2}{m_A^2 m_\phi^2} \right)^2, \quad (5.58)$$

where ϕ_0 is the initial misalignment of the scalar. The corresponding Hubble rate at production is

$$\frac{H_\star}{m_A} = 2 \left(\frac{3\eta\phi_0}{4f} \right)^4 \ln \left(\frac{m_\phi^2}{m_A^2} \frac{\phi_0^2}{m_\phi^2} \right)^{-4}. \quad (5.59)$$

Since nonrelativistic dark photons are produced, the energy density in the sector always redshifts as a^{-3} (after a_{osc}); the relic abundance is therefore simply that inherited from the scalar's misalignment:

$$\frac{\Omega_A}{\Omega_{\text{DM}}} \approx \left(\frac{m_A}{2 \times 10^{-18} \text{ eV}} \right)^{1/2} \left(\frac{\phi_0}{10^{16} \text{ GeV}} \right)^2. \quad (5.60)$$

As suggested by Ref. [51], such delayed production could allow for larger g_D while avoiding defect formation, akin to the mechanisms discussed above. Moreover, since $W(\phi)$ need not be particularly large (or small) for efficient production, the effect of the scalar on the parameters of the theory [Eq. (5.5)] is negligible. However, the persistence of narrow resonance to small amplitudes $\Phi(t)$ (and therefore at late times) depends how precisely the mass ratio m_A/m_ϕ is tuned to $1/2$. Concretely, the instability persists until a_\star only if the tuning parameter [51]

$$\delta \equiv (m_A/m_\phi)^2 - 1/4 \quad (5.61)$$

satisfies

$$|\delta| < \frac{3\eta\phi_0}{16f(a_\star/a_{\text{osc}})^{3/2}}. \quad (5.62)$$

Inserting Eq. (5.59) for $\eta\phi_0/f$, production thus may only be delayed to a Hubble rate

$$\frac{H_\star}{m_A} > 4|\delta| \ln \left(\frac{m_\phi^2}{m_A^2} \frac{\phi_0^2}{m_\phi^2} \right)^{-1} \gtrsim 0.02|\delta|, \quad (5.63)$$

using the relic abundance Eq. (5.60) evaluated with a fiducial scalar mass $m_\phi = 4 \times 10^{-18} \text{ eV}$. Using Eq. (2.8), the maximum dark gauge coupling that evades defect formation is then

$$g_D \lesssim 4 \times 10^{-14} \lambda^{1/4} |\delta|^{-3/8} \left(\frac{m_A}{\mu\text{eV}} \right)^{5/8} \left(\frac{\Omega_A}{\Omega_{\text{DM}}} \right)^{-1/4}. \quad (5.64)$$

The allowed kinetic mixing parameter space as a function of δ is depicted in Fig. 8.

1. Thermal masses and tuning

Even assuming the existence of a UV completion that guarantees such a mass tuning that is robust to quantum corrections, in-medium effects inevitably source a time-dependent mass for the dark photon via its kinetic mixing with the SM photon. To assess the impact of the SM plasma on this mechanism, we extend the scalar–Abelian-Higgs theory to explicitly include kinetic mixing as well as a current term representing nonrelativistic electrons:

$$\mathcal{L} = \mathcal{L}_{\text{SAH}} - \frac{\varepsilon}{2} F_{\mu\nu} F_{\text{SM}}^{\mu\nu} - \frac{1}{4} F_{\mu\nu}^{\text{SM}} F_{\text{SM}}^{\mu\nu} - e A_\mu^{\text{SM}} J^\mu, \quad (5.65)$$

where $J^\mu = n_e u_e^\mu$ and n_e is the electron number density and u_e^μ is their velocity. We remove the explicit kinetic mixing by redefining the SM photon field to

$$\mathbf{A}^\mu = A_{\text{SM}}^\mu + \varepsilon A^\mu \quad (5.66)$$

and define the electromagnetic field strength tensor $F_{\mu\nu} \equiv \partial_\mu A_\nu - \partial_\nu A_\mu$. In this basis, the Lagrangian takes the form

$$\mathcal{L} = \frac{1}{2} \partial_\mu \phi \partial^\mu \phi - V(\phi) - \frac{W(\phi) - \varepsilon^2}{4} F_{\mu\nu} F^{\mu\nu} + \frac{X(\phi)}{2} m_A^2 A_\mu A^\mu - \frac{1}{4} F_{\mu\nu} F^{\mu\nu} - e J_\mu (A^\mu - \varepsilon A^\mu). \quad (5.67)$$

The formalism developed in the absence of mixing must only be augmented by including the SM current in the equations of motion and replacing $W(\phi)$ with $W(\phi) - \varepsilon^2$.

For simplicity we consider only transverse modes; the equations of motion for \mathbf{A}_\pm and \mathcal{A}_\pm for the Lagrangian Eq. (5.67) are

$$e J_\pm = \ddot{\mathbf{A}}_\pm + H \dot{\mathbf{A}}_\pm + \frac{k^2}{a^2} \mathbf{A}_\pm \quad (5.68a)$$

$$-e\varepsilon(\bar{\phi}) J_\pm = \ddot{\mathcal{A}}_\pm + H \dot{\mathcal{A}}_\pm + \left[\frac{k^2}{a^2} + m_A(\bar{\phi})^2 - \frac{H}{2} \frac{\partial_t W(\bar{\phi})}{W(\bar{\phi}) - \varepsilon^2} - \frac{\partial_t^2 \sqrt{W(\bar{\phi}) - \varepsilon^2}}{\sqrt{W(\bar{\phi}) - \varepsilon^2}} \right] \mathcal{A}_\pm. \quad (5.68b)$$

In Appendix E, we show that the transverse modes of the current evolve approximately by

$$\dot{J}_\pm + \nu(t) J_\pm = \frac{\omega_p(t)^2}{e} \left[\dot{\mathbf{A}}_\pm - \varepsilon(\bar{\phi}) \dot{\mathcal{A}}_\pm \right], \quad (5.69)$$

where the damping coefficient $\nu(t)$ is defined in Eq. (E10a), and its value relative to the plasma frequency $\omega_p \equiv \sqrt{e^2 n_e / m_e}$ is given by Eq. (E13). For simplicity, we take $W = 1$ so that ε is constant. In this case, the factor of $1 - \varepsilon^2$ multiplying the kinetic term in Eq. (5.67) may be absorbed via a redefinition of g_D .

We reduce the system to a set of third-order equations of motion for \mathbf{A}_\pm and \mathcal{A}_\pm alone by differentiating Eq. (5.68) with respect to time, inserting Eq. (5.69) for \dot{J}_\pm , and then substituting Eq. (5.68a) for J_\pm . The resulting equations may then be written in the form

$$0 = \frac{d}{dt} \left(\ddot{\mathbf{A}}_\pm + [H + \nu] \dot{\mathbf{A}}_\pm + \left[\frac{k^2}{a^2} + \omega_p^2 - \dot{\nu} + H\nu \right] \mathbf{A}_\pm - \varepsilon \omega_p^2 \mathcal{A}_\pm \right) + \left(\ddot{\nu} - H\dot{\nu} + \nu \frac{k^2}{a^2} - \nu \dot{H} - 2\omega_p \dot{\omega}_p \right) \mathbf{A}_\pm + 2\omega_p \dot{\omega}_p \mathcal{A}_\pm \quad (5.70a)$$

$$0 = \frac{d}{dt} \left(\ddot{\mathcal{A}}_\pm + H \dot{\mathcal{A}}_\pm + \left[\frac{k^2}{a^2} + m_A(\bar{\phi})^2 + \varepsilon^2 \omega_p^2 \right] \mathcal{A}_\pm - \varepsilon \dot{\nu} \dot{\mathbf{A}}_\pm + [\dot{\nu} - H\nu - \omega_p^2] \varepsilon \mathbf{A}_\pm \right) + \varepsilon \left(2\omega_p \dot{\omega}_p + \left[\dot{H} - \frac{k^2}{a^2} + H\dot{\nu} - \ddot{\nu} \right] \right) \mathbf{A}_\pm - 2\varepsilon^2 \omega_p \dot{\omega}_p \mathcal{A}_\pm. \quad (5.70b)$$

If the second lines of each equality in Eq. (5.70) are negligible, then the system reduces to second order in time with additional damping and mass contributions from the plasma. Since $\dot{\omega}_p / \omega_p \propto H$ and $\dot{\nu} / \nu \propto H$, this condition is met by taking both H and k/a small compared to ω_p and $m_A(\bar{\phi})$.

Equation (5.70) then simplifies to

$$0 = \ddot{A}_\pm + \nu \dot{A}_\pm + \omega_p^2 A_\pm - \varepsilon \omega_p^2 \mathcal{A}_\pm \quad (5.71a)$$

$$0 = \ddot{\mathcal{A}}_\pm + [m_A(\bar{\phi})^2 + \varepsilon^2 \omega_p^2] \mathcal{A}_\pm - \varepsilon \nu \dot{A}_\pm - \varepsilon \omega_p^2 A_\pm. \quad (5.71b)$$

Equation (E13) (and the surrounding discussion) shows that the relevant regime for $T \ll m_e$ is that of negligible damping, $\nu \ll \omega_p$.¹⁷ In this case, were $m_A(\bar{\phi})^2 + \varepsilon^2 \omega_p^2$ constant we could simply diagonalize the equations and solve for the mode functions. Though $m_A(\bar{\phi})$ is explicitly not constant, in the narrow-resonance band its relative variations are small. Writing this small perturbation in the form $m_A(\bar{\phi})^2 = m_A^2 + \delta m_A(\bar{\phi})^2$, we may meaningfully define new fields

$$\begin{pmatrix} a_\pm \\ b_\pm \end{pmatrix} = \begin{pmatrix} \cos \varphi & \sin \varphi \\ -\sin \varphi & \cos \varphi \end{pmatrix} \begin{pmatrix} A_\pm \\ \mathcal{A}_\pm \end{pmatrix} \approx \begin{pmatrix} 1 & \varepsilon/[1 - m_A^2/\omega_p^2] \\ -\varepsilon/[1 - m_A^2/\omega_p^2] & 1 \end{pmatrix} \begin{pmatrix} A_\pm \\ \mathcal{A}_\pm \end{pmatrix}, \quad (5.72)$$

where

$$\frac{1}{2} \tan 2\varphi = \frac{\varepsilon}{1 - \varepsilon^2 - m_A^2/\omega_p^2} \quad (5.73)$$

and the second equality in Eq. (5.72) shows the result at leading order in ε . Then to quadratic order in ε and $\delta m_A(\bar{\phi})^2/m_A^2$, these fields evolve according to

$$0 = \ddot{a}_\pm + \omega_p^2 \left(1 + \frac{\varepsilon^2}{1 - m_A^2/\omega_p^2} \right) a_\pm - \varepsilon \frac{\delta m_A(\bar{\phi})^2}{1 - m_A^2/\omega_p^2} b_\pm \quad (5.74a)$$

$$0 = \ddot{b}_\pm + m_A(\bar{\phi})^2 \left(1 - \frac{\varepsilon^2}{1 - m_A^2/\omega_p^2} \right) b_\pm - \varepsilon \frac{\delta m_A(\bar{\phi})^2}{1 - m_A^2/\omega_p^2} a_\pm. \quad (5.74b)$$

If $\ddot{a}_\pm \sim \omega_p a_\pm$, then $a_\pm \sim \varepsilon \delta m_A(\bar{\phi})^2/(\omega_p^2 - m_A^2) \cdot b_\pm$. So long as $\delta m_A(\bar{\phi})^2$ is small compared to either ω_p^2 or m_A^2 (the latter of which is certainly the case), the contribution of a_\pm to the equation of motion for b_\pm is negligible and the two equations decouple. Plasma effects therefore do not disrupt resonance when their contribution to the effective mass of b_\pm is smaller than the required tuning [defined in Eq. (5.61)]:

$$\delta \gtrsim \varepsilon^2 \frac{\min(\omega_p^2, m_A^2)}{4 \max(\omega_p^2, m_A^2)}. \quad (5.75)$$

Note that this analysis breaks down if m_A crosses ω_p .

Since the thermal mass decreases monotonically with time, Eq. (5.75) need only hold at the latest possible production time allowed by the degree of bare mass tuning. Inserting Eq. (E12) for ω_p and then evaluating at H_\star according to Eq. (5.63) yields

$$\varepsilon \lesssim 1.76 \times 10^{-8} \begin{cases} \left(\frac{m_A}{6.28 \times 10^{-5} \text{ eV}} \right)^{-3/2} \left(\frac{H_\star}{10^{-22} \text{ eV}} \right)^{5/4} \sqrt{\frac{\eta_B}{6 \times 10^{-10}}}, & m_A \ll \omega_p, \\ \left(\frac{m_A}{6.28 \times 10^{-5} \text{ eV}} \right)^{1/2} \left(\frac{H_\star}{10^{-22} \text{ eV}} \right)^{-1/4} \sqrt{\frac{6 \times 10^{-10}}{\eta_B}}, & m_A \gg \omega_p, \end{cases} \quad (5.76)$$

¹⁷ As a matter of interest, the system decouples in the limit of infinite damping ($\nu \gg \omega_p$) because the SM photon slowly rolls in this case. That is, $\dot{A}_\pm \approx -(\omega_p^2/\nu)(A_\pm - \varepsilon \mathcal{A}_\pm)$ solves Eq. (5.71a) when A_\pm is neglected at leading order in ω_p/ν . As a result, $\dot{\mathcal{A}}_\pm \approx -m_A(\bar{\phi})^2 \mathcal{A}_\pm$. In other words, if the plasma is extremely resistive to currents, it decouples from the dark photon.

where η_B is the baryon-to-photon ratio. [The plasma frequency is 6.28×10^{-5} eV when $H_\star = 10^{-22}$ eV, so Eq. (5.76) is written relative to the most constrained dark photon mass.] Notably, the kinetic mixing can be much larger than the maximum that would otherwise be allowed by backreaction [Eq. (2.8)]. The detuning due to plasma effects redshifts faster than the tuning required for efficient resonance, and the more tuned the bare masses are, the later production may viably occur (i.e., by reducing η as much as possible). Moreover, at a fixed bare mass tuning, Eq. (5.76) is a weaker constraint than Eq. (5.64). Note also that we assumed the plasma is nonrelativistic because our interest is in maximally delayed production; production at earlier times when electrons are relativistic is certainly allowed, but a different analysis would be necessary.

2. Matter power spectrum

Although the narrow resonance is centered on $k = 0$, with time the resonance band only grows in width over comoving wave number since [51]

$$\left| \left(\frac{k}{am_\phi} \right)^2 + \delta \right| < \frac{\eta\phi_0}{f} \left(\frac{H}{m_\phi} \right)^{3/4}. \quad (5.77)$$

The dark photon's power spectrum thus peaks at the largest wave number that is unstable when the scalar starts oscillating (at $H \approx m_\phi$). As long as the detuning δ is negligible, which is certainly the case during the early phases of the resonance, the peak wave number is approximately $k_\star/a_{\text{osc}} \sim 2m_A\sqrt{\eta\phi_0}/f$. The density power spectrum is thus peaked as in Sec. VC4, with scales $\sim a_{\text{eq}}/2k_\star$ collapsing at matter-radiation equality. The resulting substructures have a characteristic mass of

$$M \sim \frac{3}{2} M_{\text{pl}}^2 H_{\text{eq}}^2 \frac{4\pi}{3} \left(\frac{\pi}{2k_\star/a_{\text{eq}}} \right)^3 \sim 1.5 \times 10^{-6} M_\odot \left(\frac{m_A}{10^{-12} \text{ eV}} \right)^{-9/8} \left(\frac{H_\star}{10^{-22} \text{ eV}} \right)^{-3/8}, \quad (5.78)$$

where we used Eq. (5.59) to solve for $\eta\phi_0/f$ and then used the relic abundance Eq. (5.60) to set a fiducial value for ϕ_0/m_ϕ in terms of m_A and H_\star at the benchmark parameters. (The above result thus neglects logarithmic dependence on m_A .) While these structures are smaller than those produced by the kinetic coupling in the previous section, they may be interesting targets for photometric microlensing [215].

VI. DISCUSSION

In this paper, we mapped the parameter space of kinetically mixed dark photon dark matter, charting regions that require varying degrees of assumptions and model complexity to mechanize cosmologically consistent dark photon production. Building off the results of Ref. [48], in Sec. II we reviewed how early-Universe backreaction onto the dark Higgs impacts the viability of established dark photon production mechanisms. A fundamental assumption is that the dark photon's mass is UV-completed by a dark Higgs mechanism, for which the dark gauge coupling and kinetic mixing would generally be of the same order. This minimal scenario faces stringent constraints due to the excitation of new degrees of freedom—namely, the dark Higgs, which disrupts production, and the formation of magnetic strings, whose presence rules out cold dark photon dark matter [48]. Our atlas of the Higgsed dark photon parameter space is summarized by Fig. 10; in the remainder of this section we review our main results.

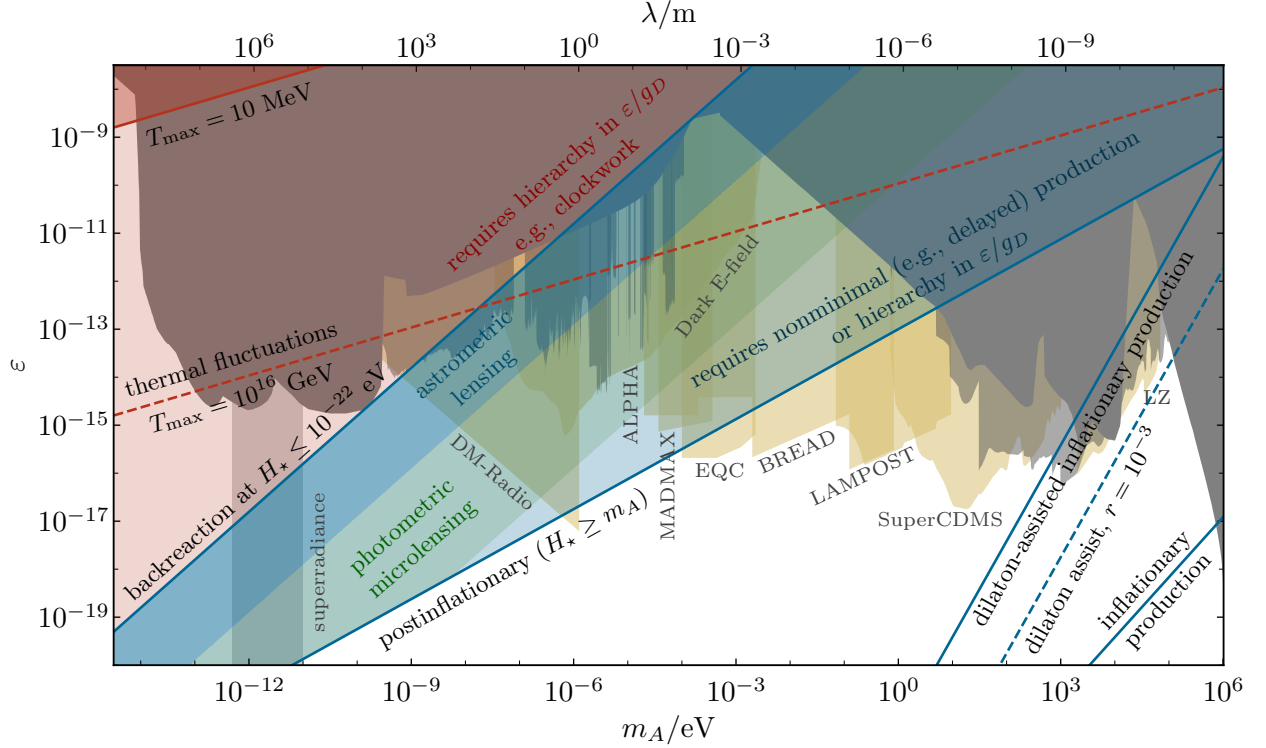


Figure 10. Summary of various limits on viable kinetic mixing [Eq. (2.9)] of dark photon dark matter. From right to left, blue lines correspond to the upper bounds for the various production scenarios outlined in the text: gravitational production during inflation (Sec. II A); inflationary production assisted by a dilaton mechanizing an evolving dark photon mass (Sec. V B); postinflationary production taking place at a fiducial Hubble rate $H_* \approx m_A$, as exemplified by tachyonic production via axion oscillations (Sec. II C); and maximally delayed postinflationary production, as realized by multiple models with rolling scalars (Secs. IV, V C, and V D). The red region above this last line cannot be realized by modified dark photon production, as the Proca theory breaks down even while modes observed in the CMB enter the horizon ($H_* \lesssim 10^{-22}$ eV); this parameter space instead requires a hierarchy in ϵ and g_D (see Sec. III). Above the red lines, defects nucleate due solely to the Standard Model plasma’s mixing with the dark photon, independent of whatever other mechanisms produce dark photons (see Sec. II B); solid and dashed lines depict bounds assuming the minimum and maximum possible reheating temperatures within currently viable inflationary cosmologies. Signatures of the various nonminimal production scenarios become more prominent toward the upper boundaries of their allowed parameter space. For dilaton-assisted inflationary production, larger kinetic mixing requires larger inflationary scales and therefore could be corroborated by a detection of primordial gravitational waves with future CMB observations; this scenario also predicts equivalence principle violation. Dark matter substructure probed via astrometric lensing (darker blue) or photometric microlensing (green) could corroborate delayed production via, e.g., a runaway scalar (Fig. 9) with kinetic mixing above the fiducial postinflationary production line; the enhancement of small-scale structure could also be probed by future cosmological observations. Current exclusions from astrophysical [61–71] and cosmological [72–76] probes are depicted in dark gray and those from haloscope and other laboratory searches [79–109] in light gray.

A. Inflationary production

The minimal scenario of gravitational dark photon production during inflation [50] is the most strongly constrained [48]—no planned experiments come close to detecting viable kinetic mixing in this case. Section II A discussed the dependence of this result on the postinflationary expansion history, showing that a prolonged period of postinflationary kination (rather than

instantaneous reheating) allows for kinetic mixings that are just marginally accessible to LZ [118] and XENON [86, 93, 97, 98] (see Fig. 4). A perhaps more plausible early-Universe cosmology—a prolonged matter era after inflation—leads instead to even more stringent upper limits.

In Sec. V we explored a class of models extending the Abelian-Higgs sector with a singlet scalar, whose couplings induce field-dependent modulation of the theory’s parameters. In such models, the scalar’s dynamics could directly alter the backreaction bound Eq. (2.6) throughout cosmological history—for instance, between inflation and the present day. In Sec. VB we showed that a universal coupling, for which the mass scales in the theory depend on the scalar, can expand the parameter space available to inflationary production if the dark photon’s mass drops after it becomes nonrelativistic. Further, we demonstrated that the dilaton model of Damour and Polyakov [55] provides a realization of such dynamics: if the dilaton is also universally coupled to Standard Model particles, it only starts rolling at late times when Standard Model particles begin to annihilate. Optimally weakening the backreaction bounds requires the inflationary scale to approach the upper limit permitted by CMB constraints, $H_I \sim 5 \times 10^{13}$ GeV [58]. This “dilaton assist” model therefore predicts that if LZ detects a dark photon, future CMB experiments will detect primordial gravitational waves from inflation (see Figs. 7 and 10). Furthermore, the dilaton’s coupling to Standard Model matter potentially violates the equivalence principle and could be probed in future space-based experiments [187, 229].

B. Postinflationary and delayed production

While gravitational production during inflation is inevitable, inflation need not occur at an energy scale high enough for inflationary dark photon production to fully account for the dark matter abundance. Postinflationary mechanisms, while less minimal, allow for dark photon dark matter not only over a much broader range of masses [56, 141, 160, 163] but also, as explained in Sec. II, a much broader range of kinetic mixing. The general bound of Eq. (2.8) demonstrates that backreaction on the dark Higgs and the formation of topological defects are evaded at larger couplings the later dark photon production occurs. Dark matter must exist in time for the standard Λ CDM model to describe the observed CMB; a reasonable benchmark is that production occurs no later than a Hubble rate of $H_\star \sim 10^{-22}$ eV (or redshifts around 10^6). This bound is saturated along the “delayed production” contour in Fig. 10, and a signal near this boundary would indicate extremely delayed production, potentially leaving a signatures in the CMB at small angular scales.

In practice, however, mechanizing such delayed production is nontrivial, as demonstrated in the case of resonant production of dark photons from axion oscillations [56, 160–162] discussed in Sec. IIC. Kinematic requirements (for efficient parametric resonance) generally restrict production to early epochs when the Hubble rate exceeded the dark photon mass, setting the fiducial postinflationary benchmark with $H_\star \approx m_A$ in Fig. 10. A signal from experiments such as ALPHA [113], BREAD [114], Dark E-Field Radio [109], DM Radio [110], or MADMAX [113] could therefore point to production delayed beyond this minimal benchmark. In contrast, a signal from LAMPOST [116], SuperCDMS [117], or an extension of BREAD using a highly excited cyclotron [115] would be consistent with these standard postinflationary production scenarios.

In Sec. IV, we showed that a number of underappreciated regimes of axion production (see Fig. 5) are indeed viable in broader parameter space. The standard regime of broad tachyonic resonance requires dimensionless axion–dark-photon coupling $\beta \gtrsim 10$, which is parametrically larger than the typical expectation that $\beta \sim \alpha_D$. If axion oscillations are delayed by some means (such that $H_\star \ll m_a$), resonance becomes more efficient even at β much smaller than unity (see Sec. IVA and also Ref. [162]). This regime of narrow resonance thus both increases the efficiency of production and decreases the degree of backreaction on the dark Higgs. Conversely, in Sec. IVB we describe a

slow-roll regime at very large coupling ($\beta \gg 50$), which could delay production until $H_\star \sim m_A/\beta$ independent of the axion mass. Although these dynamics ultimately must be corroborated with numerical simulations (see Appendix D 2), it would offer a straightforward and predictive production mechanism for dark photons at parametrically late times. We also raised the possibility that if the axion couples to the dark photon in the magnetic basis, then the axion–dark-photon coupling may naturally be $\beta \sim \alpha_D^{-1} \gg 1$ [169, 178, 230], correlating the timing of production with the coupling strength: $H_\star \sim m_A \alpha_D$ (see Fig. 10). Although this scenario is rather speculative due to the theoretical difficulties outlined in Sec. IV B, its potential simplicity and near-term detectability make it a compelling avenue for further study.

Finally, a scalar field responsible for the cosmological variation of the Abelian-Higgs parameters could directly produce dark photons. We considered two explicit scenarios: a rapidly varying dark gauge coupling driven by a runaway scalar [52] and narrow parametric resonance induced by an oscillating scalar [51]. Despite their distinct dynamics, both mechanisms can produce dark photons not just at early times when $H_\star \gtrsim m_A$ but also—at the cost of fine-tuning (see Fig. 8)—at much later times when $H_\star \ll m_A$. In the case of a rapidly varying dark gauge coupling (Sec. V C), the scalar not only sources a tachyonic resonance for the dark photon but also exponentially suppresses its bare mass, removing the kinematic barrier. The narrow-resonance case (Sec. V D), in contrast, relies on a unique instability that persists to arbitrarily late times provided that the dark-photon–scalar mass ratio is finely tuned to $1/2$.

While these scalar production scenarios must be tuned to provide an exception to the fiducial “postinflationary” line in Fig. 10, they both predict additional signatures that could test the models. Delayed production in both cases is accompanied by enhanced dark matter density perturbations on larger length scales, which could be probed by high-resolution CMB observations, the Lyman- α forest, line intensity mapping, and searches for dark matter substructure. Should vector dark matter be discovered at smaller masses and larger kinetic mixing, these complementary signatures could corroborate scalar couplings as the origin of the dark photon. The converse, however, does not hold: detecting small-scale structures or primordial gravitational waves (for dilaton-assisted inflationary production, discussed above) of a given size does not *require* the kinetic mixing to be as large as the corresponding defect formation bounds permit.

C. Model-angostic considerations

A model-independent bound on the kinetic mixing derives from the possibility that the hot Standard Model plasma restores symmetry to the dark Higgs at sufficiently high temperatures via the kinetic mixing portal (Sec. II B). If symmetry is restored, strings later form through the Kibble mechanism, precluding stable, cold dark photon dark matter at late times and leading to the bound of Eq. (2.18). Although this bound is much weaker than the postinflationary production bound [Eq. (2.8)] for the lowest possible reheating temperatures, it does imply that sufficiently light and strongly kinetically mixed dark photons (extending beyond the parameter space depicted in Fig. 10) are generically accompanied by a cosmic string network—a potential signature of an Abelian-Higgs dark sector that does not constitute the dark matter. Signals from dark matter detected by successors to SuperMAG [71], SNIPE [231], and AMAILS [232], which probe $\epsilon \gtrsim 10^{-8}$ at masses below 10^{-12} eV, would require some nondynamical explanation—specifically, a kinetic mixing that is parametrically larger than the dark gauge coupling.

One possible resolution to this issue lies in the mechanism that generates kinetic mixing. Section II assumed that kinetic mixing arises from the exchange of heavy fermions charged under both electromagnetism and the dark gauge group, as originally proposed in Ref. [59]. Modifications to this scenario that allow the kinetic mixing to be parametrically larger than the dark gauge

coupling could, in principle, circumvent the bounds discussed in Sec. II. Abelian clockwork is a well-established candidate mechanism to generate such a hierarchy [60]. In Sec. III, we assessed whether the additional degrees of freedom (i.e., Higgses) introduced by clockwork would impose additional constraints on the grounds of backreaction and defect formation [48]. Our analysis indicates that clockwork indeed provides a consistent means to boost kinetic mixing: as shown in Sec. III A, the dark photon’s mixing with the added clockwork fields is suppressed by the already-small dark gauge coupling, so it couples no more strongly to any clockwork Higgs. Section III B also indicates that any production of the clockwork gauge fields induced by production of the dark photon itself imposes no stronger backreaction bounds.

While the clockwork mechanism does, in principle, provide an explanation for kinetic mixing larger than expected on backreaction grounds, such a proposal is rather *ad hoc* since the added field content plays no role in the origin of the dark matter other than to make it arbitrarily detectable. Dark photon production from axions is an exception: clockwork can simultaneously enhance the axion–dark-photon coupling and the kinetic mixing and indeed is likely required to ensure the former is large enough for production to occur at all.

Finally, the dark photon’s mass could originate from the Stückelberg mechanism rather than the Higgs mechanism we focus on. Like a Higgs mass, a Stückelberg mass in known examples from string theory entails both radial and angular scalar degrees of freedom [54]. The angular field is absorbed by the dark photon, while the radial mode remains as a physical degree of freedom with a mass constrained similar to the dark Higgs, i.e., smaller than about $4\pi m_A/g_D$. The phase of the Stückelberg field can also wind and form strings; in contrast to the Higgs case, the symmetric point where the dark photon mass vanishes lies infinitely far away in field space [54]. Even if defects do not form, backreaction onto radial Stückelberg modes presumably occurs at the same parametric threshold as in the Higgs case, suggesting that the low-energy Proca theory breaks down in similar parameter space. In this case, the excluded parameter space we report for the Abelian-Higgs case corresponds to the regime in which the viability of dark photon production with Stückelberg masses has not been established. We leave a dedicated study of dark photon dark matter with Stückelberg masses to future work.

VII. CONCLUSION

The direct-detection parameter space for kinetically mixed dark photons has long been treated with a tacit assumption that there exists a consistent cosmology for dark photons of any mass and kinetic mixing—one that breaks down catastrophically for dark photons that acquire their mass through a (dark) Higgs mechanism. In such minimal scenarios, the magnitude of the kinetic mixing is determined by the dark gauge coupling, which also sets the regime of validity for the low-energy effective theory of a massive vector field. Breaching this threshold nucleates a string network that precludes cold dark photon dark matter [48]. In exploring the implications of these constraints, one perspective is to identify the most well-motivated regions of parameter space by examining concrete, minimal models of dark photon production. While the model that requires the fewest new degrees of freedom—gravitational production during inflation—is entirely undetectable, we showed that simple, UV-inspired physics can extend its parameter space to the reach of future electron recoil and noble gas detectors. Additional degrees of freedom, like rolling scalars, can also resonantly produce dark photons after inflation in parameter space that is broader but still inaccessible to most future haloscope experiments. We proposed a number of extensions thereof that, at the cost of some form of tuning, realize consistent dark photon production in all of the parameter space in reach of these searches.

An alternative approach studies the general implications of direct detection by any particular

upcoming experiment, whose search space is already determined by its design. Many of these dark photon searches are simply byproducts of experiments specifically designed to search for axions; much kinetic mixing parameter space will therefore be probed at little added cost, regardless of theoretical motivation. Our analysis demonstrates that the full dark photon parameter space can indeed be made viable, either through dynamical mechanisms or more *ad hoc* model building such as clockwork. The reach of modified production dynamics, however, is limited by the requirement that dark photons behave like cold dark matter at observed cosmological epochs, imposing a model-independent threshold beyond which mechanisms like clockwork are required. Notably, this regime encompasses almost all existing cosmological constraints, exemplifying the importance of theoretical input to infer the nature of the dark sector from direct-detection searches.

One motif of the various nonminimal models of dark photon production we studied is a correlation between laboratory measurements and cosmological and astrophysical signatures. Namely, the dynamics that allow for experimentally detectable kinetic mixing also predict unique phenomenology that could be probed by, for instance, future observations of the cosmic microwave background or searches for dark matter substructure. Ultralight dark photon dark matter scenarios also place strong requirements on cosmology more broadly. For the dilaton assist model discussed in Sec. VB, the dark photon’s kinetic mixing is only detectable if the energy scale of inflation is large enough to be observed via gravitational waves in the CMB. On the other hand, even if dark photon dark matter originates by some other mechanism—as it must if lighter than an meV, regardless of its kinetic mixing—avoiding the nucleation of defects during inflation places a strong bound on its energy scale [Eq. (2.12)]. Detectable, postinflationary production scenarios therefore generally require the energy scale of inflation be too low to be observed by future CMB experiments. By contrapositive, a detection thereof would place stringent limits on viable dark photon dark matter scenarios. The reheating temperature also cannot be too high, lest the Standard Model plasma restore the dark U(1) symmetry, seeding a string network via the Kibble mechanism.

Among the nonminimal models we studied, the scenarios with the most promising detection prospects frequently require some degree of parameter tuning. Nevertheless, the dynamical mechanisms we exploit—and our more model-agnostic analyses—provide a blueprint for pursuing viable constructions that may be more elegant or motivated. The potential for additional unique signatures, moreover, offers an avenue to falsify models or identify the physics underlying the dark sector. Then again, another reasonable response to the challenges in constructing dark photon models with large kinetic mixing is to pursue purely gravitational signatures of vector dark matter as a means of detection [233–244]. A deeper, synergistic understanding of the interplay between particle models and cosmological dynamics stands to further advance the theoretical status of detectable dark photon dark matter.

ACKNOWLEDGMENTS

We are grateful to Peter Adshead, Isabel Garcia Garcia, Anson Hook, Justin Kaidi, Andrew Long, Matthew Reece, Katelin Schutz, Olivier Simon, Lorenzo Sorbo, and especially Masha Baryakhtar and Junwu Huang for discussions that have been invaluable in the preparation of this manuscript. D.C. is supported through the Department of Physics and College of Arts and Science at the University of Washington and by the U.S. Department of Energy Office of Science under Award No. DE-SC0024375. Z.J.W. is supported in part by the Department of Physics and College of Arts and Science at the University of Washington and the Dr. Ann Nelson Endowed Professorship. D.C. is grateful for the hospitality of Perimeter Institute where part of this work was carried out. Research at Perimeter Institute is supported in part by the Government of Canada through the Department of Innovation, Science and Economic Development Canada and by the Province of Ontario through

the Ministry of Colleges and Universities. This material is partially supported by a grant from the Simons Foundation and the hospitality of the Aspen Center for Physics. This research was supported in part by Grant No. NSF PHY-2309135 to the Kavli Institute for Theoretical Physics (KITP). Dark photon parameter space limits and projections are compiled in Ref. [47, 245].

Appendix A: Scalar–Abelian-Higgs model

We first review the standard formulation of the spontaneously broken Abelian-Higgs model, extended to include arbitrary couplings to a scalar field. The classical Lagrangian describing a scalar–Abelian-Higgs theory is Eq. (5.1), quoted here:

$$\mathcal{L}_{\text{SAH}} = \frac{1}{2} \partial_\mu \phi \partial^\mu \phi - V(\phi) - \frac{W(\phi)}{4} F_{\mu\nu} F^{\mu\nu} + \frac{X(\phi)}{2} D_\mu \Phi (D^\mu \Phi)^* - \frac{\lambda Y(\phi)}{4} (|\Phi|^2 - v^2)^2. \quad (\text{A1})$$

The Higgs Φ is a complex scalar that we decompose into a phase and radial displacement from its vacuum expectation value, $\Phi = (v + h) e^{i\Pi/v}$. The covariant derivative is $D_\mu \Phi = \partial_\mu \Phi - i q_\Phi g_D A_\mu \Phi$, with g_D the dark gauge coupling and q_Φ the (integer-valued) Higgs charge. In the broken phase and written in terms of radial fluctuations h about the VEV and the Goldstone boson Π , Eq. (A1) expands to

$$\begin{aligned} \mathcal{L}_{\text{SAH}} = & \frac{1}{2} \partial_\mu \phi \partial^\mu \phi - V(\phi) - \frac{W(\phi)}{4} F_{\mu\nu} F^{\mu\nu} + \frac{X(\phi)}{2} m_A^2 A_\mu A^\mu \\ & + \frac{X(\phi)}{2} \partial_\mu h \partial^\mu h - Y(\phi) \left(\frac{\lambda}{4} h^4 + \lambda v h^3 + \frac{1}{2} m_h^2 h^2 \right) \\ & + \frac{X(\phi)}{2} \partial_\mu \Pi \partial^\mu \Pi + \frac{X(\phi)}{2} \left(\frac{h^2}{v^2} + \frac{2h}{v} \right) (\partial_\mu \Pi - m_A A_\mu) (\partial^\mu \Pi - m_A A^\mu), \end{aligned} \quad (\text{A2})$$

where $m_A = q_\Phi g_D v$ and $m_h = \sqrt{2\lambda}v$.

We fix unitary gauge, in which $\Pi = 0$. In a general spacetime, the Euler-Lagrange equation for the vector is

$$-\nabla_\mu [W(\phi) F^{\mu\nu}] = X(\phi) (1 + h/v)^2 m_A^2 A^\nu \equiv \mathcal{X}(\phi, h) m_A^2 A^\nu. \quad (\text{A3})$$

The covariant divergence thereof sets

$$0 = \nabla^\alpha [\mathcal{X}(\phi, h) A_\alpha], \quad (\text{A4})$$

which for $\mathcal{X}(\phi, h) = 1$ reduces to the Lorenz “gauge” condition $\nabla^\alpha A_\alpha = 0$ as applicable for massive vectors (i.e., Proca fields). The equations of motion are therefore

$$\begin{aligned} 0 = & \nabla_\mu \nabla^\mu \phi + V'(\phi) + \frac{W'(\phi)}{4} F_{\mu\nu} F^{\mu\nu} - \frac{X'(\phi)}{2} m_A^2 A_\mu A^\mu \\ & - \frac{X'(\phi)}{2} \nabla_\mu h \nabla^\mu h + \frac{\lambda Y'(\phi)}{4} (h^2 + 2hv)^2 \end{aligned} \quad (\text{A5a})$$

$$0 = \nabla_\mu \nabla^\mu h + \frac{X'(\phi)}{X(\phi)} \nabla_\mu \phi \nabla^\mu h + \frac{Y(\phi)}{X(\phi)} [\lambda h^3 + 3\lambda v h^2 + m_h^2 h] + (1 + h/v) m_A^2 A_\mu A^\mu / v \quad (\text{A5b})$$

$$0 = \nabla^\alpha \nabla_\alpha A_\beta - R_{\sigma\beta} A^\sigma + \nabla_\nu [A_\mu \nabla^\mu \ln \mathcal{X}(\phi, h)] + \frac{\nabla^\alpha W(\phi)}{W(\phi)} F_{\alpha\beta} + \frac{\mathcal{X}(\phi, h)}{W(\phi)} m_A^2 A_\beta, \quad (\text{A5c})$$

where $R_{\sigma\beta}$ is the Ricci tensor and the Higgs mass is $m_h = \sqrt{2\lambda}v$.

As in the main text, we restrict our discussion to the FLRW spacetime with metric

$$ds^2 = dt^2 - a(t)^2 \delta_{ij} dx^i dx^j \quad (\text{A6})$$

and take the scalar to be homogeneous: $\phi(t, \mathbf{x}) = \bar{\phi}(t)$. The form of Eq. (A5) motivates absorbing the $\bar{\phi}$ dependence of the theory into its fundamental parameters as in Eq. (5.5). We expand the Higgs and vector components in Fourier space as

$$h(t, \mathbf{x}) = \bar{h}(t) + \int \frac{d^3 k}{(2\pi)^3} \delta h(t, \mathbf{k}) e^{i\mathbf{k} \cdot \mathbf{x}} \quad (\text{A7a})$$

$$A_0(t, \mathbf{x}) = \int \frac{d^3 k}{(2\pi)^3} A_0(t, \mathbf{k}) e^{i\mathbf{k} \cdot \mathbf{x}} \quad (\text{A7b})$$

$$A_i(t, \mathbf{x}) = \sum_{\lambda}^{\{\pm, \parallel\}} \int \frac{d^3 k}{(2\pi)^3} A_{\lambda}(t, \mathbf{k}) \varepsilon_i^{\lambda}(\mathbf{k}) e^{i\mathbf{k} \cdot \mathbf{x}}, \quad (\text{A7c})$$

where the polarization vectors $\varepsilon^{\pm}(\mathbf{k})$ and $\varepsilon^{\parallel}(\mathbf{k})$ form an orthogonal basis of polarizations [i.e., $\varepsilon_m^{\lambda}(\mathbf{k}) \varepsilon_m^{\lambda'}(\mathbf{k})^* = \delta^{\lambda\lambda'}$] that are respectively transverse [$k_m \varepsilon_m^{\pm}(\mathbf{k}) = 0$] and longitudinal [$ik_m \varepsilon_m^{\parallel}(\mathbf{k}) = k$] to the wave number \mathbf{k} . They are Hermitian [$\varepsilon_m^{\lambda}(-\mathbf{k}) = \varepsilon_m^{\lambda}(\mathbf{k})^*$] and the circular polarization vectors satisfy $\varepsilon_m^{\pm}(\mathbf{k})^* = \varepsilon_m^{\mp}(\mathbf{k})$. The linearized equations of motion decomposed onto this basis (and written in terms of the $\bar{\phi}$ -dependent parameters) evaluate to

$$0 = \ddot{\bar{\phi}} + 3H\dot{\bar{\phi}} + V'(\bar{\phi}) \quad (\text{A8a})$$

$$0 = \ddot{\bar{h}} + \left[3H + \frac{\partial_t X(\bar{\phi})}{X(\bar{\phi})} \right] \dot{\bar{h}} + \left[X(\bar{\phi}) \lambda(\bar{\phi}) \bar{h}^2 + 3\sqrt{X(\bar{\phi})} \lambda(\bar{\phi}) v(\bar{\phi}) \bar{h} + m_h(\bar{\phi})^2 \right] \bar{h} \quad (\text{A8b})$$

$$0 = \delta \ddot{h} + \left[3H + \frac{\partial_t X(\bar{\phi})}{X(\bar{\phi})} \right] \delta \dot{h} + \left[\frac{k^2}{a^2} + 3X(\bar{\phi}) \lambda(\bar{\phi}) \bar{h}^2 + 6\sqrt{X(\bar{\phi})} \lambda(\bar{\phi}) v(\bar{\phi}) \bar{h} + m_h(\bar{\phi})^2 \right] \delta h \quad (\text{A8c})$$

$$0 = \ddot{A}_{\pm} + \left[H + \frac{\partial_t W(\bar{\phi})}{W(\bar{\phi})} \right] \dot{A}_{\pm} + \left[\frac{k^2}{a^2} + m_A(\bar{\phi}, \bar{h})^2 \right] A_{\pm} \quad (\text{A8d})$$

$$0 = \ddot{A}_{\parallel} + \left[H + \frac{\partial_t W(\bar{\phi})}{W(\bar{\phi})} \right] \dot{A}_{\parallel} + \left[\frac{k^2}{a^2} + m_A(\bar{\phi}, \bar{h})^2 \right] A_{\parallel} - \left[2H + \frac{\partial_t \mathcal{X}(\bar{\phi}, \bar{h})}{\mathcal{X}(\bar{\phi}, \bar{h})} - \frac{\partial_t W(\bar{\phi})}{W(\bar{\phi})} \right] k A_0. \quad (\text{A8e})$$

Here we use the shorthand $m_A(\phi, h) = m_A(\phi)(1 + h/v)^2$. In addition, Eq. (A4) reduces to

$$0 = -\dot{A}_0 - \left(3H + \frac{\partial_t \mathcal{X}(\bar{\phi}, \bar{h})}{\mathcal{X}(\bar{\phi}, \bar{h})} \right) A_0 + \frac{\partial_i A_i}{a^2} \quad (\text{A9})$$

and the $\nu = 0$ component of Eq. (A3) (i.e., Gauss's law) reads

$$0 = k \dot{A}_{\parallel} + [k^2 + a^2 m_A(\bar{\phi}, \bar{h})] A_0; \quad (\text{A10})$$

solving Eq. (A10) for A_0 and substituting into Eq. (A8e) yields

$$0 = \ddot{A}_{\parallel} + \frac{[3H + \partial_t \ln \mathcal{X}(\bar{\phi}, \bar{h})] k^2 + [H + \partial_t \ln W(\bar{\phi})] a^2 m_A(\bar{\phi}, \bar{h})^2}{k^2 + a^2 m_A(\bar{\phi}, \bar{h})^2} \dot{A}_{\parallel} + \left[\frac{k^2}{a^2} + m_A(\bar{\phi}, \bar{h})^2 \right] A_{\parallel}. \quad (\text{A11})$$

For the rescaled fields $\mathfrak{h} = \sqrt{X(\bar{\phi})}h$ and $\mathcal{A}_\pm = \sqrt{W(\bar{\phi})}A_\pm$, the equations of motion reduce to

$$0 = \ddot{\mathfrak{h}} + 3H\dot{\mathfrak{h}} + \left[\lambda(\bar{\phi})\bar{\mathfrak{h}}^2 + 3\lambda(\bar{\phi})v(\bar{\phi})\bar{\mathfrak{h}} + m_h(\bar{\phi})^2 - \frac{3H}{2} \frac{\partial_t X(\bar{\phi})}{X(\bar{\phi})} - \frac{\partial_t^2 \sqrt{X(\bar{\phi})}}{\sqrt{X(\bar{\phi})}} \right] \bar{\mathfrak{h}} \quad (\text{A12})$$

$$0 = \delta\ddot{\mathfrak{h}} + 3H\delta\dot{\mathfrak{h}} + \left[\frac{k^2}{a^2} + 3\lambda(\bar{\phi})\bar{\mathfrak{h}}^2 + 6\lambda(\bar{\phi})v(\bar{\phi})\bar{\mathfrak{h}} + m_h(\bar{\phi})^2 - \frac{3H}{2} \frac{\partial_t X(\bar{\phi})}{X(\bar{\phi})} - \frac{\partial_t^2 \sqrt{X(\bar{\phi})}}{\sqrt{X(\bar{\phi})}} \right] \delta\mathfrak{h} \quad (\text{A13})$$

$$0 = \ddot{\mathcal{A}}_\pm + H\dot{\mathcal{A}}_\pm + \left[\frac{k^2}{a^2} + m_A(\bar{\phi}, \bar{h})^2 - \frac{H}{2} \frac{\partial_t W(\bar{\phi})}{W(\bar{\phi})} - \frac{\partial_t^2 \sqrt{W(\bar{\phi})}}{\sqrt{W(\bar{\phi})}} \right] \mathcal{A}_\pm. \quad (\text{A14})$$

Observe that the only couplings to $\bar{\phi}$ not embedded in the parameters defined in Eq. (5.5) are derivative couplings.

The stress-energy tensor for Eq. (A2) (in unitary gauge) is

$$\begin{aligned} T^\mu{}_\nu = W(\phi) & \left[F^{\mu\alpha} F_{\nu\alpha} - m_A(\phi, h)^2 A^\mu A_\nu + \delta^\mu{}_\nu \left(-\frac{1}{4} F_{\alpha\beta} F^{\alpha\beta} + \frac{1}{2} m_A(\phi, h)^2 A_\alpha A^\alpha \right) \right] \\ & + X(\phi) \left[-\partial^\mu h \partial_\nu h + \delta^\mu{}_\nu \left(\frac{1}{2} \partial_\alpha h \partial^\alpha h - \frac{Y(\phi)}{X(\phi)} \left[\frac{\lambda}{4} h^4 + \lambda v h^3 + \frac{1}{2} m_h^2 h^2 \right] \right) \right] \\ & - \partial^\mu \phi \partial_\nu \phi + \delta^\mu{}_\nu \left(\frac{1}{2} \partial^\alpha \phi \partial_\alpha \phi - V(\phi) \right). \end{aligned} \quad (\text{A15})$$

Using Eq. (A10) to solve for A_0 , we may express the dark photon's average energy density $\bar{\rho}_A$ and pressure \bar{P}_A in terms of the polarization decomposition Eq. (A7c). To the same level of approximation as Eq. (A8) (and assuming isotropic initial conditions), the contributions from the transverse and longitudinal components to the energy density $\bar{\rho}_A$ are respectively

$$\bar{\rho}_\pm(t) = \frac{W(\bar{\phi})}{4\pi^2 a^2} \int dk k^2 \left[|\dot{A}_\pm|^2 + \frac{k^2}{a^2} |A_\pm|^2 + m_A(\bar{\phi}, \bar{h})^2 |A_\pm|^2 \right] \quad (\text{A16a})$$

and

$$\bar{\rho}_\parallel(t) = \frac{W(\bar{\phi}) m_A(\bar{\phi}, \bar{h})^2}{4\pi^2 a^2} \int dk k^2 \left[\frac{1}{k^2 + a^2 m_A(\bar{\phi}, \bar{h})^2} |a\dot{A}_\parallel|^2 + |A_\parallel|^2 \right], \quad (\text{A16b})$$

and those to the pressure P_A are

$$\bar{P}_\pm(t) = \frac{W(\bar{\phi})}{12\pi^2 a^2} \int dk k^2 \left[|\dot{A}_\pm(\tau, k)|^2 + \frac{k^2}{a^2} |A_\pm(\tau, k)|^2 - m_A(\bar{\phi}, \bar{h})^2 |A_\pm(\tau, k)|^2 \right] \quad (\text{A17a})$$

and

$$\bar{P}_\parallel(t) = \frac{W(\bar{\phi}) m_A(\bar{\phi}, \bar{h})^2}{12\pi^2 a^2} \int dk k^2 \left[\frac{3k^2 + a^2 m_A(\bar{\phi}, \bar{h})^2}{[k^2 + a^2 m_A(\bar{\phi}, \bar{h})^2]^2} |a\dot{A}_\parallel(\tau, k)|^2 - |A_\parallel(\tau, k)|^2 \right]. \quad (\text{A17b})$$

Appendix B: Quantum corrections

We seek to compute the one-loop quantum corrections to the theory of a scalar coupled to the standard Abelian-Higgs model, Eq. (5.1). The quantization of theories with noncanonical kinetic terms entails subtleties whose neglect leads to incorrect scattering amplitudes and can, in our

case, severely alter the ultraviolet (UV) divergences of radiative corrections. We first review the appropriate formulation before proceeding to compute one-loop effects in the scalar–Abelian-Higgs model.

1. Quantization of noncanonical field theories

To compute quantum corrections, we require the Hamiltonian \mathcal{H} (specifically as a functional of fields and their four-gradients and *not* the conjugate momenta as well) corresponding to Eq. (A2), which generates the time evolution and interactions of the theory. In classical field theory, the Hamiltonian and Lagrangian are related by a Legendre transform, and the only complication in theories with noncanonical kinetic terms is that fields’ conjugate momenta are not trivially related to their time derivatives. In quantum field theory, the appropriate Hamiltonian coincides with the Legendre transform of the Lagrangian *only* if the kinetic terms are canonical.

Deriving the effect of kinetic couplings is most straightforward in the path-integral formalism (see Ref. [246] section 9.3, whose notation we partly adopt below), in which the generating functional for a general multiplet of bosons ϕ_a with conjugate momenta π_a is

$$\mathcal{Z} = \int \prod_a \left[\mathcal{D}\phi_a \frac{\mathcal{D}\pi_a}{2\pi} \right] \exp \left\{ \frac{i}{\hbar} \int d^4x \left[\sum_a \dot{\phi}_a(x) \pi_a(x) - \mathcal{H}[\phi_a(x), \pi_a(x)] \right] \right\}. \quad (\text{B1})$$

For ease of illustration and generality, parametrize the Hamiltonian as

$$\mathcal{H}[\phi_a, \pi_a] = \frac{1}{2} \sum_{a,b} \pi_a A_{ab}[\phi] \pi_b + \sum_a B_a[\phi] \pi_a + C[\phi]. \quad (\text{B2})$$

In a canonical theory, $A_{ab}[\phi] = \delta_{ab}$. The functional $C[\phi]$ includes (spatial) gradient and potential terms for a scalar theory and mass, current-coupling, and magnetic-field terms for a gauge theory. The salient effects we aim to illustrate depend only on $A_{ab}[\phi]$; we retain a general parametrization for succinctness and provide an explicit mapping of Eq. (B2) to the scalar–Abelian-Higgs theory later on.

Because the kinetic term in Eq. (B2) is still quadratic in the conjugate momenta, the path integral over π_a may be computed exactly. The argument of the exponential in the path integral indeed coincides with the (inverse) Legendre transform of the Hamiltonian Eq. (B2), as a consequence of the integration over π_a instead of Hamilton’s equations [246]:

$$\mathcal{Z} = \int \prod_a [\mathcal{D}\phi_a] \det(2\pi i A[\phi]/\hbar)^{-1/2} \exp \left\{ \frac{i}{\hbar} \int d^4x \mathcal{L}[\phi, \dot{\phi}] \right\}, \quad (\text{B3})$$

where

$$\mathcal{L}[\phi_a, \dot{\phi}_a] = \sum_{a,b} \left[\frac{1}{2} \dot{\phi}_a A[\phi]_{ab}^{-1} \dot{\phi}_b + \frac{1}{2} B_a[\phi] A[\phi]_{ab}^{-1} B_b[\phi] - B_a[\phi] A[\phi]_{ab}^{-1} \dot{\phi}_b \right] - C[\phi]. \quad (\text{B4})$$

While Eq. (B4) is superficially identical to the corresponding classical result, any field dependence in the determinant factor of Eq. (B3) (via the kinetic term in $A[\phi]$) *does* modify the path integral, effectively introducing to the Lagrangian an additional term

$$\Delta\mathcal{L} = \frac{i\hbar}{2} \int \frac{d^4k}{(2\pi)^4} \text{tr} \ln A[\phi]. \quad (\text{B5})$$

Instead of performing the path integral over π_a , we could shift the conjugate momentum to

$$\pi'_a = \pi_a - A[\phi]_{ab}^{-1} (B_b[\phi] - \dot{\phi}_b) \quad (\text{B6})$$

and retain it as an auxiliary degree of freedom in the Lagrangian that interacts with ϕ :

$$\mathcal{L}[\phi_a, \dot{\phi}_a, \pi'_a] = -\frac{1}{2} \sum_{a,b} A_{ab}[\phi] \pi'_a \pi'_b + \mathcal{L}[\phi_a, \dot{\phi}_a]. \quad (\text{B7})$$

Though π'_a is nonpropagating, it modifies correlation functions of ϕ_a through loops. That the leading contributions from the new terms in the Lagrangian should be counted at one-loop level is less obvious in the form Eq. (B5), but is affirmed by the relative factor of \hbar acquired by $\Delta\mathcal{L}$ when the determinant factor is reabsorbed into the Lagrangian.¹⁸

We now map the preceding general results to a massive vector field kinetically coupled to a scalar field. We replace $\phi_a \rightarrow A_i$ and $\pi_a \rightarrow E_i$. Recovering the covariant Lagrangian

$$\mathcal{L} = -\frac{W}{4} F_{\mu\nu} F^{\mu\nu} + \frac{1}{2} m_A^2 A_\mu A^\mu + J_\mu A^\mu \quad (\text{B8})$$

(with J_μ standing in for the Higgs interactions) requires choosing

$$A_{ij} = W^{-1} \delta_{ij} \quad (\text{B9a})$$

$$B_i = \partial_i A_0 \quad (\text{B9b})$$

$$C = \frac{1}{2} m_A^2 (A_i)^2 + \frac{W}{2} \left(\epsilon^{ijk} \partial_j A_k \right)^2 + J_i A_i \quad (\text{B9c})$$

in Eq. (B2) and, just as for a canonical vector field, introducing A_0 as an auxiliary field (also integrated over in \mathcal{Z}) and adding to the Hamiltonian

$$\Delta\mathcal{H} = -\frac{1}{2} m_A^2 \left(A_0 - \frac{\partial_i E_i - J_0}{m_A^2} \right)^2. \quad (\text{B10})$$

The Higgs and the Goldstone, whose kinetic terms in the Lagrangian are multiplied by X , each contribute a copy of Eq. (B5) with A set to X^{-1} . The effective Lagrangian therefore includes the contribution

$$\Delta\mathcal{L} = -\frac{3i\hbar}{2} \int \frac{d^4 k}{(2\pi)^4} \ln W - i\hbar \int \frac{d^4 k}{(2\pi)^4} \ln X \quad (\text{B11})$$

in addition to the classical Lagrangian.

2. Background-field expansion

With the full quantum theory in tow, we may compute radiative corrections. We regulate with a finite momentum cutoff Λ under the usual interpretation that it corresponds to the scale of new physics in a given UV completion of the effective theory described by Eq. (A2). We seek to assess what limitations on Λ are imposed to ensure consistency of the scalar production scenario—principally, avoiding large corrections to the scalar's classical potential. Since we consider scalar field

¹⁸ Related observations were made in previous studies of noncanonical field theories: the first exposition on the additional interactions arising in noncanonical field theories [247] found in chiral perturbation theory that their contribution to the pion propagator appears at next-to-leading order in the pion decay constant, and when considering loop corrections during inflation their contribution is suppressed in the slow-roll expansion [248, 249].

configurations with classical homogeneous components, we perform a standard background-field expansion to compute the effective potential due to quantum fluctuations.

We first expand $\phi \rightarrow f\varphi_b + \phi$ in Eq. (A2), where $\varphi_b = \phi_b/f$ is treated as a spacetime constant. We then drop constant terms and tadpoles (i.e., terms with fewer than two powers of the fluctuating fields). We gauge fix according to the standard Faddeev-Popov procedure, choosing the gauge fixing functional

$$G(A_\mu, \Pi) = \sqrt{X(\phi)} (\partial_\mu A^\mu - \xi m_A \Pi); \quad (\text{B12})$$

the factor of $\sqrt{X(\phi)}$ introduced relative to the textbook choice ensures that terms that mix A_μ and Π in the quadratic action still cancel when $-G(A_\mu, \Pi)^2/2\xi$ is added to the action. The Faddeev-Popov determinant also picks up this factor of $\sqrt{X(\phi)}$, which we account for by including it in the action for the ghosts c and \bar{c} . Gauge fixing then adds to the Lagrangian

$$\mathcal{L}_{\text{FP}} = -\frac{X(\phi)}{2\xi} (\partial_\mu A^\mu - \xi m_A \Pi)^2 + \sqrt{X(\phi)} (\partial_\mu \bar{c} \partial^\mu c - \xi m_A^2 c \bar{c}). \quad (\text{B13})$$

Finally, we canonically normalize¹⁹ fields by replacing A_μ with $A_\mu/\sqrt{W(\varphi_b)}$, h with $h/\sqrt{X(\varphi_b)}$, Π with $\Pi/\sqrt{X(\varphi_b)}$, and c with $c/\sqrt[4]{X(\varphi_b)}$. To compute the effective potential we require only the quadratic action (including background-field dependence in effective masses). The part of $\mathcal{L}_{\text{SAH}} + \mathcal{L}_{\text{FP}}$ quadratic in fields is

$$\mathcal{L}_{(2)} = -\frac{1}{4} F_{\mu\nu} F^{\mu\nu} - \frac{1}{2\xi(\varphi_b)} (\partial_\mu A^\mu)^2 + \frac{1}{2} m_A(\varphi_b)^2 A_\mu A^\mu + \frac{1}{2} \partial_\mu \phi \partial^\mu \phi - \frac{1}{2} m(\varphi_b)^2 \phi^2 \quad (\text{B14})$$

$$+ \frac{1}{2} \partial_\mu h \partial^\mu h - \frac{1}{2} m_h(\varphi_b)^2 h^2 + \frac{1}{2} \partial_\mu \Pi \partial^\mu \Pi - \frac{\xi m_A^2}{2} \Pi^2 + \partial_\mu \bar{c} \partial^\mu c - \xi m_A^2 c \bar{c}, \quad (\text{B15})$$

where $m_A(\varphi_b)$ and $m_h(\varphi_b)$ are defined in analogy to Eq. (5.5) and

$$m(\varphi_b)^2 \equiv V''(f\varphi_b)/f^2 \quad (\text{B16})$$

$$\xi(\varphi_b) \equiv \xi W(\varphi_b)/X(\varphi_b). \quad (\text{B17})$$

For completeness, we also report the interaction Lagrangian (in unitary gauge, $\xi \rightarrow \infty$, so that we can neglect the Goldstone boson and ghosts), as would be needed to compute radiative corrections:

$$\begin{aligned} \mathcal{L}_{\text{int}} = & -\frac{1}{4} F_{\mu\nu} F^{\mu\nu} \sum_{n=1}^{\infty} \frac{1}{n!} \frac{W^{(n)}(\varphi_b)}{W(\varphi_b)} \frac{\phi^n}{f^n} + \left[\frac{1}{2} \partial_\mu h \partial^\mu h + \frac{1}{2} m_A(\varphi_b)^2 A_\mu A^\mu \right] \sum_{n=1}^{\infty} \frac{1}{n!} \frac{X^{(n)}(\varphi_b)}{X(\varphi_b)} \frac{\phi^n}{f^n} \\ & + m_A(\varphi_b)^2 \left(\frac{h}{v(\varphi_b)} + \frac{h^2}{2v(\varphi_b)^2} \right) A_\mu A^\mu \sum_{n=0}^{\infty} \frac{1}{n!} \frac{X^{(n)}(\varphi_b)}{X(\varphi_b)} \frac{\phi^n}{f^n} - \sum_{n=3}^{\infty} \frac{\tilde{V}^{(n)}(\varphi_b)}{n! f^n} \phi^n \\ & - \frac{1}{2} m_h(\varphi_b)^2 h^2 \sum_{n=1}^{\infty} \frac{1}{n!} \frac{Y^{(n)}(\varphi_b)}{Y(\varphi_b)} \frac{\phi^n}{f^n} - \left[\frac{\lambda(\varphi_b)}{4} h^4 + \lambda(\varphi_b) v(\varphi_b) h^3 \right] \sum_{n=0}^{\infty} \frac{1}{n!} \frac{Y^{(n)}(\varphi_b)}{Y(\varphi_b)} \frac{\phi^n}{f^n}. \end{aligned} \quad (\text{B18})$$

The additional interactions incurred in the quantum theory [Eq. (B11)] expand to

$$\Delta\mathcal{L} = -\frac{i}{2} \int \frac{d^4k}{(2\pi)^4} \sum_{n=0}^{\infty} \frac{1}{n!} \left(\frac{\phi}{f} \right)^n \left[3 \frac{\partial^n \ln W(\varphi)}{\partial \varphi^n} + 2 \frac{\partial^n \ln X(\varphi)}{\partial \varphi^n} \right]_{\varphi=\varphi_b}. \quad (\text{B19})$$

¹⁹ “Canonically normalize” in the sense that propagators take their standard form—no interactions are altered by doing so, only the point at which we rearrange factors of $W(\varphi_b)$ and $X(\varphi_b)$ to write results in canonical form.

Both the ϕ -independent term and the quadratic term are required explicitly for our purposes; they are

$$\Delta\mathcal{L}_{(0)} = -\frac{i}{2} \int \frac{d^4k}{(2\pi)^4} [3 \ln W(\varphi_b) + 2 \ln X(\varphi_b)] \quad (\text{B20})$$

$$\begin{aligned} \Delta\mathcal{L}_{(2)} = & -\frac{3i}{4f^2} \int \frac{d^4k}{(2\pi)^4} \left[\frac{W^{(2)}(\varphi_b)}{W(\varphi_b)} - \left(\frac{W^{(1)}(\varphi_b)}{W(\varphi_b)} \right)^2 \right] \phi^2 \\ & -\frac{i}{2f^2} \int \frac{d^4k}{(2\pi)^4} \left[\frac{X^{(2)}(\varphi_b)}{X(\varphi_b)} - \left(\frac{X^{(1)}(\varphi_b)}{X(\varphi_b)} \right)^2 \right] \phi^2. \end{aligned} \quad (\text{B21})$$

The coefficient of $-\phi^2/2$ is an effective one-loop contribution to the scalar's squared mass. In practice, Eqs. (B20) and (B21) act like counterterms to photon and Higgs loops and cancel leading divergences.

3. Effective potential

The one-loop effective potential may be computed by integrating the quadratic action over the fields, Eq. (B15) [250]. The contribution from scalar fluctuations is

$$e^{i\Delta\Gamma[\phi_b]^{(1),\phi}} = \int \mathcal{D}\phi \exp \left\{ i \int d^4x \left[\frac{1}{2} \partial_\mu \phi \partial^\mu \phi - \frac{1}{2} m(\varphi_b)^2 \phi^2 \right] \right\}, \quad (\text{B22})$$

which, integrated over ϕ , adds to the effective action

$$i\Delta\Gamma[\phi_b]^{(1),\phi} = -\frac{1}{2} \int d^4x \int \frac{d^4k}{(2\pi)^4} \ln \left(1 - \frac{m(\varphi_b)^2}{k^2} \right). \quad (\text{B23})$$

At next-to-leading order in $\Lambda \gg m(\varphi_b)$, the resulting effective potential is

$$\Delta V[\phi_b]^{(1),\phi} = \frac{\Lambda^2 m(\varphi_b)^2}{2(4\pi)^2} - \frac{m(\varphi_b)^4}{8(4\pi)^2} \left[1 + 2 \ln \left(1 + \frac{\Lambda^2}{m(\varphi_b)^2} \right) \right], \quad (\text{B24})$$

which is subdominant to the bare potential when $\Lambda^2/2(4\pi f)^2 < 1$. In the special case that $V(\varphi_b)$ is a pure exponential function, the quantum corrections to the scalar effective potential arising from scalar loops organize into an expansion in the number of vertices [200]. At one-vertex level, the corrections are directly proportional to $V(\varphi_b)$ and can therefore be absorbed into the overall normalization of the potential.

The Higgs contribution is

$$e^{i\Delta\Gamma[\phi_b]^{(1),h}} = \int \frac{\mathcal{D}h}{\sqrt{X(\varphi_b)}} \exp \left\{ i \int d^4x \left[\frac{1}{2} \partial_\mu h \partial^\mu h - \frac{1}{2} m_h(\varphi_b)^2 h^2 \right] \right\} \quad (\text{B25})$$

Observe that the measure is rescaled in accordance with the field redefinition made previously. The resulting effective potential contribution is

$$\Delta V[\phi_b]^{(1),h} = -\frac{i}{2} \int \frac{d^4k}{(2\pi)^4} \left[\ln X(\varphi_b) + \ln \left(1 - \frac{m_h(\varphi_b)^2}{k^2} \right) \right]. \quad (\text{B26})$$

The calculation for the Goldstone proceeds identically:

$$\Delta V[\phi_b]^{(1),\Pi} = -\frac{i}{2} \int \frac{d^4 k}{(2\pi)^4} \left[\ln X(\varphi_b) + \ln \left(1 - \frac{\xi m_A^2}{k^2} \right) \right]. \quad (\text{B27})$$

Recall that the ghosts were rescaled by a factor of $\sqrt[4]{X(\varphi_b)}$; however, as Grassmann numbers their measure changes by the inverse of the applied scaling transformation. Therefore,

$$e^{i\Delta\Gamma[\phi_b]^{(1),c}} = \int \mathcal{D}c \mathcal{D}\bar{c} \sqrt{X(\varphi_b)} \exp \left\{ i \int d^4 x \left(\partial_\mu \bar{c} \partial^\mu c - \xi m_A^2 c \bar{c} \right) \right\}, \quad (\text{B28})$$

so

$$\Delta V[\phi_b]^{(1),c} = \frac{i}{2} \int \frac{d^4 k}{(2\pi)^4} \left[\ln X(\varphi_b) + 2 \ln \left(1 - \frac{\xi m_A^2}{k^2} \right) \right]. \quad (\text{B29})$$

Finally, the quadratic action for the photon may be written as

$$e^{i\Delta\Gamma[\phi_b]^{(1),A}} = \int \frac{\mathcal{D}A_\mu}{W(\varphi_b)^2} \exp \left\{ -\frac{i}{2} \int d^4 x A^\mu \Delta_{A,\mu\nu}^{-1} A^\nu \right\} = W(\varphi_b)^{-2} \det [\Delta_A^{-1}]^{-1/2} \quad (\text{B30})$$

where

$$\Delta_{A,\mu\nu}^{-1} \equiv -g^{\mu\nu} [\partial_\alpha \partial^\alpha + m_A(\varphi_b)^2] + \left(1 - \frac{1}{\xi(\varphi_b)} \right) \partial^\mu \partial^\nu. \quad (\text{B31})$$

The functional determinant may be computed in Euclidean time ($\tau = t/i$) as an integral over its (Fourier-space) eigenvalues,

$$\ln \det \Delta_{A,\mu\nu}^{-1} = i \int \frac{d^4 k_E}{(2\pi)^4} \text{tr} \ln \left\{ [-k_E^2 - m_A(\varphi_b)^2] \left[-\delta^{\mu\nu} + \left(1 - \frac{1}{\xi(\varphi_b)} \right) \frac{k_E^\mu k_E^\nu}{k_E^2 + m_A(\varphi_b)^2} \right] \right\}. \quad (\text{B32})$$

Series expanding the matrix logarithm, simplifying each term, resumming, and shuffling constant factors (which are dropped from the effective potential) yields

$$\ln \det \Delta_{A,\mu\nu}^{-1} = i \int \frac{d^4 k_E}{(2\pi)^4} \left\{ 3 \ln \left(1 + \frac{m_A(\varphi_b)^2}{k_E^2} \right) + \ln \left(1 + \frac{\xi m_A^2}{k_E^2} \right) - \ln \xi(\varphi_b) \right\}. \quad (\text{B33})$$

The first term is the contribution from the three physical dark photon polarizations. Substituting Eq. (B17) to compute $\Delta V[\phi_b]^{(1),A}$ via Eq. (B30) and summing with Eqs. (B26), (B27), and (B29) yields a net contribution from the Abelian-Higgs sector of

$$\Delta V[\phi_b]^{(1)} = \frac{1}{2} \int \frac{d^4 k_E}{(2\pi)^4} \left[3 \ln \left(1 + \frac{m_A(\varphi_b)^2}{k_E^2} \right) + \ln \left(1 + \frac{m_h(\varphi_b)^2}{k_E^2} \right) + 3 \ln W(\varphi_b) + 2 \ln X(\varphi_b) \right]. \quad (\text{B34})$$

Observe that the latter two terms, which diverge quartically, precisely cancel the contributions incurred from quantizing the theory, $\Delta\mathcal{L}_{(0)}$ [Eq. (B20)], once Eq. (B34) is subtracted from the Lagrangian. (In addition, the ξ -dependent contributions from the Goldstone, ghosts, and photon all cancel, though they are independent of the background field anyway.) Absorbing $\Delta\mathcal{L}_{(0)}$ into the

effective potential, at next-to-leading order in large Λ we have

$$\Delta V[\phi_b]^{(1)} = \frac{3\Lambda^2 m_A(\varphi_b)^2}{2(4\pi)^2} - \frac{3m_A(\varphi_b)^4}{8(4\pi)^2} \left[1 + 2 \ln \left(1 + \frac{\Lambda^2}{m_A(\varphi_b)^2} \right) \right] \\ + \frac{\Lambda^2 m_h(\varphi_b)^2}{2(4\pi)^2} - \frac{m_h(\varphi_b)^4}{8(4\pi)^2} \left[1 + 2 \ln \left(1 + \frac{\Lambda^2}{m_h(\varphi_b)^2} \right) \right]. \quad (\text{B35})$$

Since we expect Λ to be much larger than any mass scale in the problem, the one-loop contributions to the effective potential are subdominant to the classical potential when

$$\frac{\Lambda^2}{(4\pi f)^2} \lesssim \frac{m(\varphi_b)^2}{\max[m(\varphi_b)^2, m_A(\varphi_b)^2, m_h(\varphi_b)^2]}. \quad (\text{B36})$$

If coupling functions are chosen such that any of the fields' masses are *not* dependent on φ_b , then they do not contribute to the one-loop effective potential and are not considered in Eq. (B36).

At two-loop order, it is unclear whether quartic divergences cancel in a manner similar to those that arise at one loop [via Eq. (B21)]. Though addressing this question is important to assess the naturalness of coupled scalar theories in general, the two-loop calculations are substantially more involved and we leave them to future work.

Appendix C: Axion to dark photon conversion at large coupling

In this section, we detail the dynamics of dark photon production from axions in the large- β regime up until perturbation theory breaks down. We show that the breakdown of perturbation theory coincides with the time when friction sourced by the dark photon becomes important. As a result, the full study of this production mechanism ultimately requires nonlinear simulations.

The equations of motion that we consider are Eq. (2.21b) for the dark photon and

$$0 = \ddot{\phi} + 3H\dot{\phi} + \left(\frac{k^2}{a^2} + m_a^2 \right) \phi - \frac{\beta}{f_a} [\mathbf{E} \cdot \mathbf{B}](k) \quad (\text{C1})$$

for the axion, neglecting possible higher-order self-interactions in the axion potential. The backreaction of the dark photon onto the axion's equation of motion is given by (see, e.g., Ref. [251])

$$\langle \mathbf{E} \cdot \mathbf{B} \rangle = -\frac{1}{2a^3} \sum_{\lambda=\pm} \lambda \int \frac{d^3k}{(2\pi)^3} \frac{d}{dt} |A_\lambda|^2 \quad (\text{C2})$$

at the background level. We also require

$$\langle \{ [\mathbf{E} \cdot \mathbf{B}](\xi_1, \mathbf{k}) - \langle \mathbf{E} \cdot \mathbf{B} \rangle(\xi_1) \} \{ [\mathbf{E} \cdot \mathbf{B}](\xi_2, \mathbf{0}) - \langle \mathbf{E} \cdot \mathbf{B} \rangle(\xi_2) \} \rangle \\ = \frac{1}{a^3(\xi_1)a^3(\xi_2)} \int \frac{d^3p}{(2\pi)^3} |\mathbf{p}| |\boldsymbol{\varepsilon}^+(\mathbf{p})^* \cdot \boldsymbol{\varepsilon}^+(\mathbf{p} + \mathbf{k})|^2 \\ \times \left[|\mathbf{p} + \mathbf{k}| \dot{A}_+(\xi_1, \mathbf{p}) A_+(\xi_1, \mathbf{p} + \mathbf{k})^* \dot{A}_+(\xi_2, \mathbf{p} + \mathbf{k})^* A_+(\xi_2, \mathbf{p}) \right. \\ \left. + |\mathbf{p}| \dot{A}_+(\xi_1, \mathbf{p} + \mathbf{k}) A_+(\xi_1, \mathbf{p})^* \dot{A}_+(\xi_2, \mathbf{p} + \mathbf{k})^* A_+(\xi_2, \mathbf{p}) \right]. \quad (\text{C3})$$

where the polarization vectors are defined below Eq. (A7), ξ_1 and ξ_2 denote two different times,

and we keep only the + polarization in the four-point function for simplicity. Note the identity

$$\boldsymbol{\varepsilon}^\lambda(\mathbf{p})^* \cdot \boldsymbol{\varepsilon}^{\lambda'}(\mathbf{p} + \mathbf{k}) = \frac{1}{2} + \frac{\lambda\lambda'}{2} \frac{|\mathbf{p} \cdot (\mathbf{p} + \mathbf{k})|}{|\mathbf{p}| |\mathbf{p} + \mathbf{k}|}. \quad (\text{C4})$$

The initial condition of the dark photon is set by the Bunch-Davies vacuum:

$$A_\lambda(\mathbf{k}) = \frac{1}{\sqrt{2}^4 \sqrt{k^2 + a^2 m_A^2}} \quad (\text{C5a})$$

$$\dot{A}_\lambda(\mathbf{k}) = i \frac{k}{a} A_\lambda(\mathbf{k}). \quad (\text{C5b})$$

We decompose the axion into a homogeneous part $\bar{\phi}(t)$ and a perturbation $\delta\phi(t, \mathbf{k})$ which satisfy

$$\frac{\beta}{f_a} \langle \mathbf{E} \cdot \mathbf{B} \rangle = \ddot{\bar{\phi}} + 3H\dot{\bar{\phi}} + m_a^2 \bar{\phi}, \quad (\text{C6})$$

$$\frac{\beta}{f_a} (\mathbf{E} \cdot \mathbf{B} - \langle \mathbf{E} \cdot \mathbf{B} \rangle) = \delta\ddot{\phi} + 3H\delta\dot{\phi} + \left(\frac{k^2}{a^2} + m_a^2 \right) \delta\phi. \quad (\text{C7})$$

We take a homogeneous initial condition for the axion,

$$\delta\phi = \delta\dot{\phi} = 0. \quad (\text{C8})$$

Finally, we enumerate a number of useful identities. If

$$A(t) = A_0 \bar{A}(t) \exp \left\{ -\frac{1}{2} \left(\frac{k - k_0(t)}{a(t)\epsilon(t)} \right)^2 \right\}, \quad (\text{C9})$$

then

$$A(t)A(t') \xrightarrow{\epsilon \rightarrow 0} A_0^2 \bar{A}^2(t) \pi^{3/4} 2^{1/4} [a(t)\epsilon(t)]^{3/2} \delta(k - k_0(t)) \sqrt{\delta(k_0(t) - k_0(t'))}. \quad (\text{C10})$$

Note that we have represented the temporal delta function inside a square root, anticipating the appearance of another factor of the delta function coming from the other pair of A s. One can solve Eq. (C7) for the variance of the axion field in terms of the dark photon as

$$\begin{aligned} \langle \delta\phi^2 \rangle &= \frac{\beta^2}{f_a^2} \int_0^t d\xi_1 d\xi_2 \int \frac{d^3k}{(2\pi)^3} G_k(t, \xi_1) G_k(t, \xi_2) \\ &\quad \times \langle \{[\mathbf{E} \cdot \mathbf{B}](\xi_1, \mathbf{k}) - \langle \mathbf{E} \cdot \mathbf{B} \rangle(\xi_1)\} \{[\mathbf{E} \cdot \mathbf{B}](\xi_2, \mathbf{0}) - \langle \mathbf{E} \cdot \mathbf{B} \rangle(\xi_2)\} \rangle. \end{aligned} \quad (\text{C11})$$

If we assume that time derivatives can be replaced a factor of some scale Γ and that $A_{\mathbf{k}}(\xi)$ is of the form Eq. (C10) with $A_0 = 1/\sqrt{k}$, then

$$\langle \delta\phi^2 \rangle = \frac{1}{2^{7/2} \pi^{5/2}} \frac{\beta^2 m_A^4}{f_a^2} \int_0^\tau \frac{d\xi}{\xi^{3/2}} \left| \frac{d\kappa_0}{d\xi} \right|^{-1} \kappa_0^2 \Gamma^2 \bar{A}^4 \epsilon^3 \int_0^{2\kappa_0} \kappa d\kappa G_\kappa^2(\xi, \tau) \left(1 - \left(\frac{\kappa}{2\kappa_0} \right)^2 \right)^2 \quad (\text{C12})$$

with $t = \tau/m_A$, $a = a_0 \sqrt{\tau}$ and $\kappa = a_0 m_A \tau$, with all other quantities implicitly rewritten in units of m_A .

Having enumerated the important formulas, we now discuss the dynamics. The dark photon is

not produced so long as $\dot{\bar{\phi}}$ remains below the production threshold velocity $\dot{\bar{\phi}}_P$, during which time the axion evolves as an entirely free field:

$$\bar{\phi} = \bar{\phi}(0) \left(1 - \frac{1}{5}(m_a t)^2 \right) \quad (\text{C13})$$

and $\delta\phi = 0$. The threshold velocity $\dot{\bar{\phi}}_P$ is the velocity beyond which at least one dark photon mode becomes tachyonic, i.e.,

$$\frac{k_P^2}{a^2} + \frac{\beta}{f_a} \dot{\bar{\phi}}_P \frac{k_P}{a} + m_A^2 = 0, \quad (\text{C14})$$

which picks out the velocity

$$\dot{\bar{\phi}}_P = -\frac{2m_A f_a}{\beta} \quad (\text{C15})$$

and wave number $k_P/a = m_A$. Once the velocity of the axion exceeds this threshold one of the dark photon polarizations (in our convention, the + polarization) undergoes a tachyonic resonance. The characteristic dark photon wave number produced is roughly $k/a \sim \beta \dot{\bar{\phi}}/f_a$, so very shortly after resonance starts we may neglect the dark photon's mass. In order to simplify our discussion, we introduce the following set of variables:

$$a = a_0 \tau^{1/2}, \quad t = \tau/m_A, \quad k = m_A a_0 \kappa, \quad \theta_0 \beta = \frac{m_A^2}{m_a^2} B. \quad (\text{C16})$$

and the dimensionless initial axion displacement is $\theta_0 \equiv \bar{\phi}(0)/f_a$. In terms of these dimensionless variables, the dark photon equation of motion becomes

$$0 = \frac{1}{\tau^{1/4}} \frac{d^2}{d\tau^2} (\tau^{1/4} A) + \left(\frac{\kappa^2}{\tau} + 1 + \frac{3}{16\tau^2} - \frac{2}{5} B \kappa \tau^{1/2} \right) A. \quad (\text{C17})$$

We may solve this equation in the WKB approximation to find

$$A^+ \approx A^+(0) \left[\frac{\tau_P}{\tau} \right]^{1/4} \exp \left[\int_{\tau_P}^{\tau} d\tau' \sqrt{\frac{2}{5} B \kappa \tau'^{1/2} - \frac{\kappa^2}{\tau'} - 1 - \frac{3}{16\tau'^2}} \right], \quad (\text{C18})$$

where τ_P is the dimensionless time at which the exponent becomes real. For modes that start growing some time after τ_P , it is a decent approximation to drop both the third and fourth terms (bare mass and Hubble respectively). In this approximation, we have

$$\tau_P = \left(\frac{5\kappa}{2B} \right)^{2/3}, \quad (\text{C19})$$

and the integral reduces to

$$A^+ \approx A_0 \left[\frac{\tau_P}{\tau} \right]^{1/4} \exp \left[\frac{\kappa^{4/3}}{B^{1/3}} \int_{(5/2)^{2/3}}^{\tau(B/\kappa)^{2/3}} dx \sqrt{\frac{2}{5} x^{1/2} - \frac{1}{x}} \right], \quad (\text{C20})$$

which may be expressed in terms of a Gaussian hypergeometric function. However, we simply approximate A^+ by a Gaussian centered on its local maximum—an excellent approximation because the dark photon transfer function is sharply peaked.

The local maximum of the argument of the exponent in Eq. (C20) is located at

$$\kappa = \kappa_0 \equiv C_0 B \tau^{3/2} \quad (\text{C21})$$

with $C_0 = 0.077082$ and is locally approximated by a parabola

$$C_1 B \tau^2 \left(1 - C_2 \left(\frac{\kappa}{\kappa_0} - 1 \right)^2 \right) \quad (\text{C22})$$

with $C_1 = 0.0788847$ and $C_2 = 0.253765$. With this approximation, it is straightforward to calculate

$$\langle \mathbf{E} \cdot \mathbf{B} \rangle = -\frac{m_A^5 a_0}{2\tau^{3/2}} \int \frac{d^3 \kappa}{(2\pi)^3} \kappa \frac{d}{d\tau} |A|^2 \quad (\text{C23})$$

$$\approx -\frac{m_A^4}{(2\pi)^2} \sqrt{\frac{2\pi C_1 B}{C_2}} e^{2C_1 B \tau^2} \left(\frac{5\kappa_0}{2B} \right)^{1/3} \frac{\kappa_0^3}{\tau^2}, \quad (\text{C24})$$

where we have approximated the Gaussian by a δ -function

$$e^{-2C_1 B \tau^2 C_2 \left[\frac{\kappa}{\kappa_0} - 1 \right]^2} \approx \sqrt{\frac{\pi}{2C_1 C_2 B \tau^2}} \delta \left(\frac{\kappa}{\kappa_0} - 1 \right). \quad (\text{C25})$$

Using this estimate for $\langle \mathbf{E} \cdot \mathbf{B} \rangle$, we can compute the backreaction onto the homogeneous mode $\bar{\phi}$ using the Green's function for Eq. (C6) with appropriate boundary conditions:

$$G(t, \xi) = \frac{\pi}{2^{1/2}} \frac{\xi^{5/4}}{t^{1/4}} \left(J_{-\frac{1}{4}}(m_a \xi) J_{\frac{1}{4}}(m_a t) - J_{\frac{1}{4}}(m_a \xi) J_{-\frac{1}{4}}(m_a t) \right). \quad (\text{C26})$$

We note that for large β , backreaction kicks in well before $H = m_a$, and therefore the axion may be approximated as massless [or equivalently, we may take the small t, ξ limit of Eq. (C26)], and so we may approximate

$$G(t, \xi) \approx 2\xi \left(1 - \sqrt{\frac{\xi}{t}} \right). \quad (\text{C27})$$

Thus, we find

$$\bar{\phi} = \bar{\phi}(0) \left(1 - \frac{1}{5} (m_a t)^2 \right) + \frac{\beta}{f_a} \int_0^t d\xi G(t, \xi) \langle \mathbf{E} \cdot \mathbf{B} \rangle \quad (\text{C28})$$

$$\approx f_a \theta_0 \left(1 - \frac{1}{5} (m_a t)^2 \right) + \frac{\beta}{f_a} N_{\text{FR},0} m_a^2 (\beta \theta_0)^{3/2} (m_a t) e^{2C_1 \beta \theta_0 (m_a t)^2}, \quad (\text{C29})$$

where the numerical factor is

$$N_{\text{FR},0} = \sqrt{\frac{C_1}{(2\pi)^3 C_2}} \frac{5^{1/3}}{2^{1/3}} \frac{C_0^{10/3}}{16 C_1^2} = 9.4058 \times 10^{-5}. \quad (\text{C30})$$

The time of backreaction is roughly determined by $\dot{\bar{\phi}} = 0$, which occurs at

$$t_{\text{BR}} = \frac{1}{m_a} \sqrt{\frac{1}{4C_1 \beta \theta_0} W \left[\frac{f_a^4}{25 C_1 N_{\text{FR},0}^2 m_a^4 \beta^6 \theta_0^2} \right]}, \quad (\text{C31})$$

where W is the Lambert W function evaluated on its principal branch. At this time, the energy density stored in the dark photon is approximately $\rho_A \sim \rho_a/\beta$.

Now that we have determined the evolution of the homogeneous mode, we compute the perturbations to the axion to determine whether they become large prior to t_{BR} . We apply Eq. (C11), where G_k is the Green's function of the Klein-Gordon equation with appropriate boundary conditions [Eq. (C8)],

$$G_k(t, \xi) = 2\xi e^{-im_a(\xi+t)} \left[{}_1F_1\left(\frac{ik^2t}{2m_a a^2} + \frac{1}{4}; \frac{1}{2}; 2im_a \xi\right) {}_1F_1\left(\frac{ik^2t}{2m_a a^2} + \frac{3}{4}; \frac{3}{2}; 2im_a t\right) \right. \quad (\text{C32})$$

$$\left. -\sqrt{\frac{\xi}{t}} {}_1F_1\left(\frac{ik^2t}{2m_a a^2} + \frac{3}{4}; \frac{3}{2}; 2im_a \xi\right) {}_1F_1\left(\frac{ik^2t}{2m_a a^2} + \frac{1}{4}; \frac{1}{2}; 2im_a t\right) \right]. \quad (\text{C33})$$

In order to evaluate the integral in Eq. (C11), we make use of the δ -function approximation for A . In this case, we are dealing with the product of two A s evaluated at different momenta. Since each A on its own is essentially a δ -function, the product of four A 's of different arguments imposes an additional condition: not only must k and $k+p$ match $m_A a_0 \kappa_0$, but we must also have $\xi_1 = \xi_2$ because κ_0 is a function of ξ_1 or ξ_2 . To see this explicitly, we complete the square as in Eq. (C10), with

$$A = A_0 \left[\frac{\tau_P}{\tau_\xi} \right]^{1/4} e^{C_1 B \tau_\xi^2} \exp \left\{ -\frac{1}{2} \left(\frac{\kappa - \kappa_0}{\kappa_0 / \sqrt{2C_1 C_2 B \tau_\xi^2}} \right)^2 \right\} \quad (\text{C34})$$

where τ_ξ is τ in Eq. (C16) evaluated at $t = \xi$. Upon multiplying $A(\tau_{\xi_1})A(\tau_{\xi_2})$, we find a pair of Gaussians, one of which imposes $\kappa = \kappa_0$, and the other which imposes $\tau_{\xi_1} = \tau_{\xi_2}$. This is the simplification that allows us to reduce Eq. (C11) to Eq. (C12).

To further simplify the integral, we can approximate the Green's function Eq. (C32) in precisely the same way as we approximated it for the homogeneous mode, i.e., by dropping the axion's bare mass, leading to

$$G_k(t, \xi) \approx \frac{\tau_\xi}{m_A \kappa \sqrt{\tau}} \sin \left[2\kappa (\sqrt{\tau} - \sqrt{\tau_\xi}) \right]. \quad (\text{C35})$$

Further, it turns out that the dominant contribution to the integral comes from κ and τ_ξ such that the argument of sin is small, so Eq. (C27) is an excellent approximation to Eq. (C35) when evaluating Eq. (C12). Finally, we replace time derivatives of A with $\Gamma = 2C_1 B \tau$, which is valid once modes start growing rapidly, i.e. $C_1 B \tau^2 \gg 1$. With these approximations, evaluating $\langle \delta\phi^2 \rangle$ becomes trivial. We apply Eq. (C12) with

$$\begin{aligned} \kappa_0 &= C_0 B \tau^{3/2}, \quad \epsilon = \frac{\kappa_0}{\sqrt{2C_1 C_2 B \tau^3}}, \quad \Gamma = 2C_1 B \tau, \quad \left| \frac{d\kappa_0}{d\tau} \right|^{-1} = \frac{2}{3C_0 B \tau^{1/2}}, \\ G_\kappa &= 2\xi \left(1 - \sqrt{\frac{\xi}{\tau}} \right), \quad \bar{A}^2 = \left(\frac{\tau_P}{\tau} \right)^{1/2} e^{2C_1 B \tau^2}, \quad \text{and } \tau_P = \left(\frac{5\kappa_0}{2B} \right)^{2/3}, \end{aligned} \quad (\text{C36})$$

yielding

$$\langle \delta\phi^2 \rangle \approx N_{\text{FR},1} \frac{m_a^4 \beta^2}{f_a^2} (\beta\theta_0)^{7/2} (m_a t)^3 e^{4C_1 \beta \theta_0 (m_a t)^2}, \quad (\text{C37})$$

where

$$N_{\text{FR},1} = \frac{5^{2/3} C_0^{20/3}}{2^{2/3} \pi^{5/2} 4608 C_1^{5/2} C_2^{3/2}} = 3.88565 \times 10^{-9}. \quad (\text{C38})$$

Having computed the perturbations, we may now compare them to the backreaction onto the homogeneous mode

$$\frac{\langle \delta \phi^2 \rangle}{[\bar{\phi}(t) - \bar{\phi}(0) (1 - \frac{1}{5}(m_a t)^2)]^2} \approx 0.43921 \sqrt{\beta \theta_0} m_a t. \quad (\text{C39})$$

Evaluating this ratio at $t = t_{\text{BR}}$, we find that the perturbations become order 1 at roughly the same time backreaction becomes important. This coincidence could have been anticipated, given that it is a common process $\mathbf{E} \cdot \mathbf{B}$ that drives both perturbations and backreaction.

Appendix D: Delayed axion oscillations

1. Efficient growth condition

As discussed in [IV A](#), dark photon production from axions can be efficient with $\beta \theta_0 \ll 1$ if oscillations are substantially delayed relative to the standard time, $H \sim m_a$. In this appendix, we derive the modified condition for efficient resonance, Eq. [\(4.1\)](#).

The growth rate of the transverse modes may be calculated from the equation of motion Eq. [\(2.21b\)](#) by mapping it onto an equivalent Mathieu-type equation,

$$0 = A''(\tau) + (a + 2q \cos 2\tau) A(\tau), \quad (\text{D1})$$

with $2\tau = m_a t$, primes representing τ derivatives, and

$$\tilde{a} = 4 \left(\frac{k^2}{a^2 m_a^2} + \frac{m_A^2}{m_a^2} \right) \quad (\text{D2})$$

$$\tilde{q} = \frac{2k\beta\theta_0}{am_a} (2H_{\text{osc}t})^{-3/4}. \quad (\text{D3})$$

Equation [\(D1\)](#) is not technically a Mathieu-type equation since the coefficients \tilde{a} and \tilde{q} depend on t . However, so long as $m_a t \gg 1$, this time dependence is slow and can be treated adiabatically. The instantaneous growth rate for the transverse dark photon modes is therefore

$$\Gamma = \pm \frac{m_a}{4} \sqrt{\tilde{q}^2 - (1 - \tilde{a})^2}. \quad (\text{D4})$$

The total growth of a given mode is then

$$A(t)/A(0) \approx \exp \left\{ \int_{1/2H_{\text{osc}}}^t dt' \Re[\Gamma] \right\}. \quad (\text{D5})$$

Efficient production requires growth rates exceeding H . Near threshold, the resonance takes place almost entirely at a single wave number; as long as this single wave number remains inside the

resonance band (i.e., has not redshifted out of it), the energy density growth is approximated by²⁰

$$\frac{\dot{\rho}_A}{\rho_A} \approx \max_k 2\Gamma(k) = \frac{1}{2}\beta\theta_0 m_a \sqrt{\left(1 - \frac{4m_A^2}{m_a^2}\right) \left(\frac{H}{H_{\text{osc}}}\right)^{3/2} + \frac{1}{4}\beta^2\theta_0^2 \left(\frac{H}{H_{\text{osc}}}\right)^3}. \quad (\text{D6})$$

There are two limits of this equation to consider. First, if $m_a \leq 2m_A$, then the first term inside the root is negative, and must be compensated for by the second term, requiring $\beta\theta_0 \gg 1$. In this case, resonance starts almost immediately and quickly becomes nonperturbative (corresponding to the case discussed in Appendix C). On the other hand, if $\beta\theta_0$ is small, then resonance requires $m_a \geq 2m_A$. In this limit, modes redshift from one edge of the resonance band to the other in a time interval

$$\Delta t = \frac{\beta\theta_0}{H_{\text{osc}}}, \quad (\text{D7})$$

where we have taken the $2m_A \ll m_a$, $t \sim 1/2H_{\text{osc}}$, and $\beta\theta_0 \ll 1$ limits. The resulting total growth is

$$\rho_A ([2H_{\text{osc}}]^{-1} + \Delta t) \sim \rho_A ([2H_{\text{osc}}]^{-1}) \exp \left\{ \frac{m_a}{2H_{\text{osc}}} \beta^2 \theta_0^2 \right\}. \quad (\text{D8})$$

Thus, we arrive at the efficient resonance condition Eq. (4.1),

$$\beta\theta_0 \sqrt{\frac{m_a}{2H_{\text{osc}}}} \gg 1. \quad (\text{D9})$$

2. Axion fragmentation time

As discussed in Sec. IV A, attractive self-interactions can fragment the axion before it transfers all of its energy to the dark photon. For a general axion potential approximated as

$$V(\phi_a) = m_a^2 f_a^2 \left[\frac{1}{2} \left(\frac{\phi_a}{f_a} \right)^2 + \frac{1}{3!} A \left(\frac{\phi_a}{f_a} \right)^3 + \frac{1}{4!} B \left(\frac{\phi_a}{f_a} \right)^4 \right], \quad (\text{D10})$$

the growth rate of axion perturbations (derived in Appendix C of Ref. [173]) is

$$\Gamma = |\delta\omega| \Re \sqrt{1 - \left(1 + \frac{k^2}{2m_a \delta\omega a^2} \right)^2}, \quad (\text{D11})$$

where $\delta\omega$ is the change in the oscillation frequency of the axion relative to its bare mass. At leading order in self-interactions,

$$\delta\omega = m_a \frac{3B - 5A^2}{24} \langle \Theta^2 \rangle. \quad (\text{D12})$$

We compare this to the expression Eq. (D6) in the limit $m_A \rightarrow 0$, $t \sim 1/2H_{\text{osc}}$, and $\beta\theta_0 \ll 1$: the dark photon mode growth rate is $\Gamma = m_a \beta\theta_0/4$. Thus, the axion fragments before the dark photon

²⁰ Once this mode has redshifted outside of the resonance band, the energy density growth is linear instead of exponential.

absorbs $\mathcal{O}(1)$ of the axion energy density unless

$$|m_a \beta \theta_0 / 4| > -\delta\omega. \quad (\text{D13})$$

Implicit in this inequality is the statement that if axion self-interactions are repulsive then the axion perturbations do not grow. To achieve efficient resonance at the natural expectation $\beta\theta_0 \sim \alpha_D$ without backreaction, attractive self-interactions are practically excluded.

In summary, though delayed axion oscillations can significantly reduce the requisite dimensionless axion–dark-photon coupling, even very weak attractive self-interactions cause the axion to fragment before all the dark photon dark matter is produced. Viable dark photon production essentially requires repulsive self-interactions. As the axion is a periodic field, oscillations of large enough amplitude are guaranteed to induce attractive self-interactions. Mechanizing repulsive self-interactions requires quite a bit of machinery (see the extensive discussion in Ref. [175]), which even then only extend over a limited field range.

“Axion friendship” [173, 174] is a phenomenon whereby pairs of axions with nearby masses exchange energy through nonlinear autoresonance [252–256]. If the axions in the friendly pair have hierarchical decay constants $f_{j+1}/f_j = \mathcal{F} \gg 1$, the axion with the smaller decay constant can siphon nearly all the energy from its friend, parametrically delaying the onset of decaying oscillations to $H_{\text{osc}} \sim m_a \mathcal{F}^{4/3}$. Although the requirement of nearby masses constitutes a coincidence, such pairs may be common in axiverse-type scenarios [43]. In fact, it has been found that in realistic string compactifications the friendship parameter $\mu \equiv m_j/m_{j+1}$, which measures the ratio of neighboring axion masses, lies in the requisite range $\mu \in [0.75, 1]$ for a growing fraction of pairs as the number of axions increases [176].²¹

Appendix E: Plasma dynamics

Between electron-positron annihilation and recombination, the SM plasma comprises photons, nonrelativistic electrons, and nonrelativistic nuclei. The Universe is charge neutral, so the electron and proton number densities are both

$$n_e = \eta_B \frac{2\zeta(3)}{\pi^2} T^3, \quad (\text{E1})$$

where $\eta_B \approx 6 \times 10^{-10}$ is the baryon-to-photon ratio and T the plasma temperature. The rate of Thomson scattering between photons and electrons and of Coulomb scattering between electrons and protons are respectively $\dot{\kappa}_T = n_e \sigma_T$ and $\dot{\kappa}_C = n_e \sigma_C$, where the corresponding cross sections are [64]

$$\sigma_T = \frac{8\pi\alpha^2}{3m_e^2} \quad (\text{E2})$$

$$\sigma_C = \frac{4\sqrt{2}\pi\alpha^2}{3\sqrt{m_e T^3}} \ln \left(\frac{4\pi T^3}{\alpha^3 n_e} \right), \quad (\text{E3})$$

In terms of the proton-to-electron mass ratio $\mu_p \equiv m_p/m_e$, the Thomson cross section for protons is $\mu_p^{-2} \sigma_T$. In the epoch of interest, the Thomson and Coulomb rates are quite rapid relative to the

²¹ The range $\mu \in [0.75, 1]$ is for a cosine potential which has attractive self-interactions. In the case of repulsive self-interactions the range switches to $\mu \in [1, 1.25]$ or so.

Hubble rate:

$$\frac{\dot{\kappa}_T}{H} \approx 10^3 \frac{T}{\text{eV}} \frac{\eta_B}{6 \times 10^{-10}} \quad (\text{E4a})$$

$$\frac{\dot{\kappa}_C}{H} \approx 5.8 \times 10^{12} \left(\frac{T}{\text{eV}} \right)^{1/2} \frac{\eta_B}{6 \times 10^{-10}} \quad (\text{E4b})$$

taking $H^2 = g_* \pi^2 T^4 / 90 M_{\text{pl}}^2$ where $g_* \approx 3.38$. Treating the plasma as three coupled, perfect fluids that jointly satisfy the energy-momentum conservation equations is therefore an excellent approximation. For simplicity of exposition, we ignore the fact that about a quarter of the protons are bound in helium nuclei, considering a single fluid of protons. Strictly speaking, this description is only applicable after electron-positron annihilation completes, which occurs around a temperature of $T \approx 20$ keV [257]; at higher temperatures the positrons and electrons are equally abundant, and e^+e^- scattering processes are also important.

Large-scale photons (i.e., with wave number much smaller than the plasma temperature) couple to the bulk motion of the fluid via Lorentz forces. Longitudinal modes (or scalar degrees of freedom in cosmological perturbation theory) couple to density perturbations and gravitational potentials, making for a large, complex set of coupled differential equations. Transverse photon modes, on the other hand, induce vorticity in the plasma. Vector perturbations of the metric, however, do not appear explicitly in the momentum conservation equations and in fact do not couple directly to a fluid's velocity if that fluid supports no anisotropic stress [258]. As already argued, the photons, electrons, and protons interact rapidly enough to suppress any anisotropic stress in the epoch of interest. The equations of motion for the transverse (vortical) modes [decomposed onto the same basis as Eq. (A7c)] in the plasma are

$$\dot{u}_{\gamma,\pm} = \dot{\kappa}_T (u_{e,\pm} - u_{\gamma,\pm}) + \mu_p^{-2} \dot{\kappa}_T (u_{p,\pm} - u_{\gamma,\pm}) \quad (\text{E5a})$$

$$\dot{u}_{e,\pm} = -H u_{e,\pm} + R_e \dot{\kappa}_T (u_{\gamma,\pm} - u_{e,\pm}) + \dot{\kappa}_C (u_{p,\pm} - u_{e,\pm}) - \frac{e}{m_e} \dot{A}_\pm \quad (\text{E5b})$$

$$\dot{u}_{p,\pm} = -H u_{p,\pm} + R_e \mu_p^{-3} \dot{\kappa}_T (u_{\gamma,\pm} - u_{p,\pm}) + \mu_p^{-1} \dot{\kappa}_C (u_{e,\pm} - u_{p,\pm}) + \frac{e}{m_p} \dot{A}_\pm. \quad (\text{E5c})$$

Here $u_{a,\pm}$ are the transverse polarizations of the fluid velocity for the photons, electrons, and protons ($a = \gamma, e$, and p , respectively). The photon-to-electron density ratio

$$R_e \equiv \frac{4\bar{\rho}_\gamma}{3\bar{\rho}_e} = 1.175 \times 10^4 \frac{T}{\text{eV}} \left(\frac{\eta_B}{6 \times 10^{-10}} \right)^{-1} \quad (\text{E6})$$

encodes the relative rate of momentum transfer for electrons and photons due to Thomson scattering.

The photon couples to the SM 3-current, which is given terms of the proton-electron slip by

$$J_\pm = n_e (u_{p,\pm} - u_{e,\pm}) \quad (\text{E7})$$

and, combining Eqs. (E5b) and (E5c), evolves according to

$$\begin{aligned} \dot{J}_\pm + [4H + (1 + \mu_p^{-1}) \dot{\kappa}_C] J_\pm = & -R_e \dot{\kappa}_T n_e [u_{\gamma,\pm} - u_{e,\pm} + \mu_p^{-3} (u_{\gamma,\pm} - u_{p,\pm})] \\ & + n_e \frac{e}{m_e} (1 + \mu_p^{-1}) \dot{A}_\pm. \end{aligned} \quad (\text{E8})$$

From here on out we drop the term arising from Thomson scattering of protons, $\mu_p^{-3} (u_{\gamma,\pm} - u_{p,\pm})$, and also neglect Hubble friction when it is directly added with $\dot{\kappa}_T$ or $\dot{\kappa}_C$. Taking a time derivative of Eq. (E8) and simplifying with Eq. (E5b), the current equation of motion may be written in the

form

$$\ddot{J}_\pm + \nu(t)\dot{J}_\pm + \omega(t)^2 J_\pm = -HR_e\dot{\kappa}_T n_e u_{e,\pm} + n_e \frac{e}{m_e} \ddot{A}_\pm + \gamma(t)n_e \frac{e}{m_e} \dot{A}_\pm \quad (\text{E9})$$

where

$$\nu(t) = \dot{\kappa}_C + (1 + R_e) \dot{\kappa}_T \quad (\text{E10a})$$

$$\omega(t)^2 = (1 + \mu_p^{-1} R_e) \dot{\kappa}_C \dot{\kappa}_T \quad (\text{E10b})$$

$$\gamma(t) = (1 + \mu_p^{-1} R_e) \dot{\kappa}_T. \quad (\text{E10c})$$

In Eqs. (E9) and (E10) we took $1 + \mu_p^{-1} \approx 1$, but $\mu_p^{-1} R_e$ is not necessarily small. However, consultation with Eqs. (E4) and (E6) shows that $\omega(t)$ and $\gamma(t)$ are always negligible relative to $\nu(t)$. On the same basis, the term proportional to the electron velocity in Eq. (E9) is also negligible unless the electron velocity is drastically larger than $u_{p,\pm} - u_{e,\pm}$. With these approximations, Eq. (E9) depends only \dot{J}_\pm , \ddot{J}_\pm , and \ddot{A}_\pm . Since all time-dependent coefficients vary only on the Hubble timescale, which we have already taken to be negligible, we may approximate

$$\dot{J}_\pm + \nu(t)J_\pm = \frac{\omega_p(t)^2}{e} \dot{A}_\pm \quad (\text{E11})$$

with the plasma damping rate $\nu(t)$ defined in Eq. (E10a) and the plasma frequency defined by

$$\omega_p^2 = \frac{e^2 n_e}{m_e} = \frac{2\zeta(3)e^2 \eta_B}{\pi^2} \frac{T^3}{m_e} = \left[5.121 \times 10^{-9} \text{ eV} \sqrt{\frac{\eta_B}{6 \times 10^{-10}}} \left(\frac{T}{\text{eV}} \right)^{3/2} \right]^2. \quad (\text{E12})$$

Relative to Ref. [64], which considered the coupling of kinetically mixed dark photons to the electron-ion plasma in the interstellar medium, the Thomson scattering of photons with electrons relevant at early times provides an additional resistance of the plasma to bulk charge separation. In fact, momentum transfer due to Thomson scattering becomes more important than that due to Coulomb scattering at temperatures above $T \sim 190$ eV, coincident with the time period of interest (redshifts $z \sim 10^6$).

Finally, the Thomson scattering and momentum exchange rates and the Coulomb rate relative to the plasma frequency are

$$\frac{R_e \dot{\kappa}_T}{\omega_p} = \frac{8\alpha^2 \sqrt{2\zeta(3)\eta_B}}{3e} \frac{2\pi^4}{45\zeta(3)\eta_B} \left(\frac{T}{m_e} \right)^{5/2} \approx 106.9 \left(\frac{T}{m_e} \right)^{5/2} \quad (\text{E13a})$$

$$\frac{\dot{\kappa}_C}{\omega_p} = \frac{4\sqrt{2\pi}\alpha^2 \sqrt{m_e n_e}}{3e\sqrt{m_e T_e^3}} \ln \Lambda_C = \frac{8\alpha^2 \sqrt{\zeta(3)\eta_B/\pi}}{3e} \ln \Lambda_C \approx 2.84 \times 10^{-7}. \quad (\text{E13b})$$

At temperatures $T \lesssim 10^{-2} m_e$ (but still before recombination), the resistivity of the plasma is therefore negligible compared to the plasma frequency.

-
- [1] G. Bertone, D. Hooper, and J. Silk, Particle dark matter: Evidence, candidates and constraints, *Phys. Rept.* **405**, 279 (2005), [arXiv:hep-ph/0404175](#).
 - [2] G. Bertone and D. Hooper, History of dark matter, *Rev. Mod. Phys.* **90**, 045002 (2018), [arXiv:1605.04909 \[astro-ph.CO\]](#).
 - [3] M. R. Buckley and A. H. G. Peter, Gravitational probes of dark matter physics, *Phys. Rept.* **761**, 1

- (2018), [arXiv:1712.06615 \[astro-ph.CO\]](#).
- [4] Y. B. Zel'dovich, Magnetic model of universe, *Zh. Eksp. Teor. Fiz* **48**, 986 (1965).
 - [5] Y. B. Zel'dovich, L. Okun, and S. Pikelner, Quarks: the astrophysical and physical-chemistry aspects (translation), *Usp. Fiz. Nauk* **84**, 113 (1965).
 - [6] H.-Y. Chiu, Symmetry between particle and anti-particle populations in the universe, *Phys. Rev. Lett.* **17**, 712 (1966).
 - [7] M. Viel, G. D. Becker, J. S. Bolton, and M. G. Haehnelt, Warm dark matter as a solution to the small scale crisis: New constraints from high redshift Lyman- α forest data, *Phys. Rev. D* **88**, 043502 (2013), [arXiv:1306.2314 \[astro-ph.CO\]](#).
 - [8] V. Iršič *et al.*, New Constraints on the free-streaming of warm dark matter from intermediate and small scale Lyman- α forest data, *Phys. Rev. D* **96**, 023522 (2017), [arXiv:1702.01764 \[astro-ph.CO\]](#).
 - [9] A. Garzilli, A. Magalich, O. Ruchayskiy, and A. Boyarsky, How to constrain warm dark matter with the Lyman- α forest, *Mon. Not. Roy. Astron. Soc.* **502**, 2356 (2021), [arXiv:1912.09397 \[astro-ph.CO\]](#).
 - [10] B. Villasenor, B. Robertson, P. Madau, and E. Schneider, New constraints on warm dark matter from the Lyman- α forest power spectrum, *Phys. Rev. D* **108**, 023502 (2023), [arXiv:2209.14220 \[astro-ph.CO\]](#).
 - [11] J.-W. Hsueh, W. Enzi, S. Vegetti, M. Auger, C. D. Fassnacht, G. Despali, L. V. E. Koopmans, and J. P. McKean, SHARP – VII. New constraints on the dark matter free-streaming properties and substructure abundance from gravitationally lensed quasars, *Mon. Not. Roy. Astron. Soc.* **492**, 3047 (2020), [arXiv:1905.04182 \[astro-ph.CO\]](#).
 - [12] D. Gilman, S. Birrer, A. Nierenberg, T. Treu, X. Du, and A. Benson, Warm dark matter chills out: constraints on the halo mass function and the free-streaming length of dark matter with eight quadruple-image strong gravitational lenses, *Mon. Not. Roy. Astron. Soc.* **491**, 6077 (2020), [arXiv:1908.06983 \[astro-ph.CO\]](#).
 - [13] W. Enzi *et al.*, Joint constraints on thermal relic dark matter from strong gravitational lensing, the Ly α forest, and Milky Way satellites, *Mon. Not. Roy. Astron. Soc.* **506**, 5848 (2021), [arXiv:2010.13802 \[astro-ph.CO\]](#).
 - [14] E. O. Nadler, S. Birrer, D. Gilman, R. H. Wechsler, X. Du, A. Benson, A. M. Nierenberg, and T. Treu, Dark Matter Constraints from a Unified Analysis of Strong Gravitational Lenses and Milky Way Satellite Galaxies, *Astrophys. J.* **917**, 7 (2021), [arXiv:2101.07810 \[astro-ph.CO\]](#).
 - [15] S. Tremaine and J. E. Gunn, Dynamical Role of Light Neutral Leptons in Cosmology, *Phys. Rev. Lett.* **42**, 407 (1979).
 - [16] A. Boyarsky, O. Ruchayskiy, and D. Iakubovskiy, A Lower bound on the mass of Dark Matter particles, *JCAP* **03**, 005, [arXiv:0808.3902 \[hep-ph\]](#).
 - [17] C. J. Hogan and J. J. Dalcanton, New dark matter physics: clues from halo structure, *Phys. Rev. D* **62**, 063511 (2000), [arXiv:astro-ph/0002330](#).
 - [18] J. J. Dalcanton and C. J. Hogan, Halo cores and phase space densities: Observational constraints on dark matter physics and structure formation, *Astrophys. J.* **561**, 35 (2001), [arXiv:astro-ph/0004381](#).
 - [19] D. Boyanovsky, H. J. de Vega, and N. Sanchez, Constraints on dark matter particles from theory, galaxy observations and N-body simulations, *Phys. Rev. D* **77**, 043518 (2008), [arXiv:0710.5180 \[astro-ph\]](#).
 - [20] D. Gorbunov, A. Khmelnitsky, and V. Rubakov, Constraining sterile neutrino dark matter by phase-space density observations, *JCAP* **10**, 041, [arXiv:0808.3910 \[hep-ph\]](#).
 - [21] S. Shao, L. Gao, T. Theuns, and C. S. Frenk, The phase space density of fermionic dark matter haloes, *Mon. Not. Roy. Astron. Soc.* **430**, 2346 (2013), [arXiv:1209.5563 \[astro-ph.CO\]](#).
 - [22] J. Alvey, N. Sabti, V. Tiki, D. Blas, K. Bondarenko, A. Boyarsky, M. Escudero, M. Fairbairn, M. Orkney, and J. I. Read, New constraints on the mass of fermionic dark matter from dwarf spheroidal galaxies, *Mon. Not. Roy. Astron. Soc.* **501**, 1188 (2021), [arXiv:2010.03572 \[hep-ph\]](#).
 - [23] V. Domcke and A. Urbano, Dwarf spheroidal galaxies as degenerate gas of free fermions, *JCAP* **01**, 002, [arXiv:1409.3167 \[hep-ph\]](#).
 - [24] L. Randall, J. Scholtz, and J. Unwin, Cores in Dwarf Galaxies from Fermi Repulsion, *Mon. Not. Roy. Astron. Soc.* **467**, 1515 (2017), [arXiv:1611.04590 \[astro-ph.GA\]](#).
 - [25] C. Di Paolo, F. Nesti, and F. L. Villante, Phase space mass bound for fermionic dark matter from dwarf spheroidal galaxies, *Mon. Not. Roy. Astron. Soc.* **475**, 5385 (2018), [arXiv:1704.06644 \[astro-ph.GA\]](#).
 - [26] B. G. Giraud and R. Pechanski, Profile of a Galactic Spherical Cloud of Self-Gravitating Fermions, *Phys. Scripta* **94**, 085003 (2019), [arXiv:1806.07283 \[hep-th\]](#).
 - [27] D. Savchenko and A. Rudakovskiy, New mass bound on fermionic dark matter from a combined analysis

- of classical dSphs, *Mon. Not. Roy. Astron. Soc.* **487**, 5711 (2019), [arXiv:1903.01862 \[astro-ph.CO\]](#).
- [28] R. D. Peccei and H. R. Quinn, CP Conservation in the Presence of Instantons, *Phys. Rev. Lett.* **38**, 1440 (1977).
 - [29] S. Weinberg, A New Light Boson?, *Phys. Rev. Lett.* **40**, 223 (1978).
 - [30] F. Wilczek, Problem of Strong P and T Invariance in the Presence of Instantons, *Phys. Rev. Lett.* **40**, 279 (1978).
 - [31] J. Preskill, M. B. Wise, and F. Wilczek, Cosmology of the Invisible Axion, *Phys. Lett. B* **120**, 127 (1983).
 - [32] L. F. Abbott and P. Sikivie, A Cosmological Bound on the Invisible Axion, *Phys. Lett. B* **120**, 133 (1983).
 - [33] M. Dine and W. Fischler, The Not So Harmless Axion, *Phys. Lett. B* **120**, 137 (1983).
 - [34] L. D. Duffy and K. van Bibber, Axions as Dark Matter Particles, *New J. Phys.* **11**, 105008 (2009), [arXiv:0904.3346 \[hep-ph\]](#).
 - [35] J. E. Kim, Weak Interaction Singlet and Strong CP Invariance, *Phys. Rev. Lett.* **43**, 103 (1979).
 - [36] M. A. Shifman, A. I. Vainshtein, and V. I. Zakharov, Can Confinement Ensure Natural CP Invariance of Strong Interactions?, *Nucl. Phys. B* **166**, 493 (1980).
 - [37] A. R. Zhitnitsky, On Possible Suppression of the Axion Hadron Interactions. (In Russian), *Sov. J. Nucl. Phys.* **31**, 260 (1980).
 - [38] M. Dine, W. Fischler, and M. Srednicki, A Simple Solution to the Strong CP Problem with a Harmless Axion, *Phys. Lett. B* **104**, 199 (1981).
 - [39] C. Beasley, J. J. Heckman, and C. Vafa, GUTs and Exceptional Branes in F-theory - I, *JHEP* **01**, 058, [arXiv:0802.3391 \[hep-th\]](#).
 - [40] S. A. Abel, M. D. Goodsell, J. Jaeckel, V. V. Khoze, and A. Ringwald, Kinetic Mixing of the Photon with Hidden U(1)s in String Phenomenology, *JHEP* **07**, 124, [arXiv:0803.1449 \[hep-ph\]](#).
 - [41] R. Donagi and M. Wijnholt, Breaking GUT Groups in F-Theory, *Adv. Theor. Math. Phys.* **15**, 1523 (2011), [arXiv:0808.2223 \[hep-th\]](#).
 - [42] R. Blumenhagen, V. Braun, T. W. Grimm, and T. Weigand, GUTs in Type IIB Orientifold Compactifications, *Nucl. Phys. B* **815**, 1 (2009), [arXiv:0811.2936 \[hep-th\]](#).
 - [43] A. Arvanitaki, S. Dimopoulos, S. Dubovsky, N. Kaloper, and J. March-Russell, String Axiverse, *Phys. Rev. D* **81**, 123530 (2010), [arXiv:0905.4720 \[hep-th\]](#).
 - [44] R. Blumenhagen, J. P. Conlon, S. Krippendorff, S. Moster, and F. Quevedo, SUSY Breaking in Local String/F-Theory Models, *JHEP* **09**, 007, [arXiv:0906.3297 \[hep-th\]](#).
 - [45] M. Goodsell, J. Jaeckel, J. Redondo, and A. Ringwald, Naturally Light Hidden Photons in LARGE Volume String Compactifications, *JHEP* **11**, 027, [arXiv:0909.0515 \[hep-ph\]](#).
 - [46] M. Bullimore, J. P. Conlon, and L. T. Witkowski, Kinetic mixing of U(1)s for local string models, *JHEP* **11**, 142, [arXiv:1009.2380 \[hep-th\]](#).
 - [47] A. Caputo, A. J. Millar, C. A. J. O'Hare, and E. Vitagliano, Dark photon limits: A handbook, *Phys. Rev. D* **104**, 095029 (2021), [arXiv:2105.04565 \[hep-ph\]](#).
 - [48] W. E. East and J. Huang, Dark photon vortex formation and dynamics, *JHEP* **12**, 089, [arXiv:2206.12432 \[hep-ph\]](#).
 - [49] H. B. Nielsen and P. Olesen, Vortex Line Models for Dual Strings, *Nucl. Phys. B* **61**, 45 (1973).
 - [50] P. W. Graham, J. Mardon, and S. Rajendran, Vector Dark Matter from Inflationary Fluctuations, *Phys. Rev. D* **93**, 103520 (2016), [arXiv:1504.02102 \[hep-ph\]](#).
 - [51] P. Adshead, K. D. Lozanov, and Z. J. Weiner, Dark photon dark matter from an oscillating dilaton, *Phys. Rev. D* **107**, 083519 (2023), [arXiv:2301.07718 \[hep-ph\]](#).
 - [52] D. Cyncynates and Z. J. Weiner, Detectable and Defect-Free Dark Photon Dark Matter, *Phys. Rev. Lett.* **134**, 211002 (2025), [arXiv:2310.18397 \[hep-ph\]](#).
 - [53] H. Ruegg and M. Ruiz-Altaba, The Stueckelberg field, *Int. J. Mod. Phys. A* **19**, 3265 (2004), [arXiv:hep-th/0304245](#).
 - [54] M. Reece, Photon Masses in the Landscape and the Swampland, *JHEP* **07**, 181, [arXiv:1808.09966 \[hep-th\]](#).
 - [55] T. Damour and A. M. Polyakov, The String dilaton and a least coupling principle, *Nucl. Phys. B* **423**, 532 (1994), [arXiv:hep-th/9401069](#).
 - [56] P. Agrawal, N. Kitajima, M. Reece, T. Sekiguchi, and F. Takahashi, Relic Abundance of Dark Photon Dark Matter, *Phys. Lett. B* **801**, 135136 (2020), [arXiv:1810.07188 \[hep-ph\]](#).

- [57] M. Hindmarsh and A. Rajantie, Defect formation and local gauge invariance, *Phys. Rev. Lett.* **85**, 4660 (2000), [arXiv:cond-mat/0007361](#).
- [58] N. Aghanim *et al.* (Planck), Planck 2018 results. VI. Cosmological parameters, *Astron. Astrophys.* **641**, A6 (2020), [Erratum: *Astron. Astrophys.* 652, C4 (2021)], [arXiv:1807.06209 \[astro-ph.CO\]](#).
- [59] B. Holdom, Two U(1)'s and Epsilon Charge Shifts, *Phys. Lett. B* **166**, 196 (1986).
- [60] G. F. Giudice and M. McCullough, A Clockwork Theory, *JHEP* **02**, 036, [arXiv:1610.07962 \[hep-ph\]](#).
- [61] J. Redondo, Helioscope Bounds on Hidden Sector Photons, *JCAP* **07**, 008, [arXiv:0801.1527 \[hep-ph\]](#).
- [62] H.-S. Zechlin, D. Horns, and J. Redondo, New Constraints on Hidden Photons using Very High Energy Gamma-Rays from the Crab Nebula, *AIP Conf. Proc.* **1085**, 727 (2009), [arXiv:0810.5501 \[astro-ph\]](#).
- [63] S.-P. Li and X.-J. Xu, Production rates of dark photons and Z' in the Sun and stellar cooling bounds, *JCAP* **09**, 009, [arXiv:2304.12907 \[hep-ph\]](#).
- [64] S. Dubovsky and G. Hernández-Chifflet, Heating up the Galaxy with Hidden Photons, *JCAP* **12**, 054, [arXiv:1509.00039 \[hep-ph\]](#).
- [65] N. Vinyoles, A. Serenelli, F. L. Villante, S. Basu, J. Redondo, and J. Isern, New axion and hidden photon constraints from a solar data global fit, *JCAP* **10**, 015, [arXiv:1501.01639 \[astro-ph.SR\]](#).
- [66] M. Baryakhtar, R. Lasenby, and M. Teo, Black Hole Superradiance Signatures of Ultralight Vectors, *Phys. Rev. D* **96**, 035019 (2017), [arXiv:1704.05081 \[hep-ph\]](#).
- [67] D. Wadekar and G. R. Farrar, Gas-rich dwarf galaxies as a new probe of dark matter interactions with ordinary matter, *Phys. Rev. D* **103**, 123028 (2021), [arXiv:1903.12190 \[hep-ph\]](#).
- [68] T. Linden, T. T. Q. Nguyen, and T. M. P. Tait, X-Ray Constraints on Dark Photon Tridents, [arXiv:2406.19445 \[hep-ph\]](#) (2024).
- [69] D. K. Hong, C. S. Shin, and S. Yun, Cooling of young neutron stars and dark gauge bosons, *Phys. Rev. D* **103**, 123031 (2021), [arXiv:2012.05427 \[hep-ph\]](#).
- [70] X.-J. Bi, Y. Gao, J. Guo, N. Houston, T. Li, F. Xu, and X. Zhang, Axion and dark photon limits from Crab Nebula high energy gamma-rays, *Phys. Rev. D* **103**, 043018 (2021), [arXiv:2002.01796 \[astro-ph.HE\]](#).
- [71] M. A. Fedderke, P. W. Graham, D. F. J. Kimball, and S. Kalia, Earth as a transducer for dark-photon dark-matter detection, *Phys. Rev. D* **104**, 075023 (2021), [arXiv:2106.00022 \[hep-ph\]](#).
- [72] P. Arias, D. Cadamuro, M. Goodsell, J. Jaeckel, J. Redondo, and A. Ringwald, WISPy Cold Dark Matter, *JCAP* **06**, 013, [arXiv:1201.5902 \[hep-ph\]](#).
- [73] S. D. McDermott and S. J. Witte, Cosmological evolution of light dark photon dark matter, *Phys. Rev. D* **101**, 063030 (2020), [arXiv:1911.05086 \[hep-ph\]](#).
- [74] A. Caputo, H. Liu, S. Mishra-Sharma, and J. T. Ruderman, Modeling Dark Photon Oscillations in Our Inhomogeneous Universe, *Phys. Rev. D* **102**, 103533 (2020), [arXiv:2004.06733 \[astro-ph.CO\]](#).
- [75] A. Caputo, H. Liu, S. Mishra-Sharma, and J. T. Ruderman, Dark Photon Oscillations in Our Inhomogeneous Universe, *Phys. Rev. Lett.* **125**, 221303 (2020), [arXiv:2002.05165 \[astro-ph.CO\]](#).
- [76] S. J. Witte, S. Rosauro-Alcaraz, S. D. McDermott, and V. Poulin, Dark photon dark matter in the presence of inhomogeneous structure, *JHEP* **06**, 132, [arXiv:2003.13698 \[astro-ph.CO\]](#).
- [77] J. Chluba, B. Cyr, and M. C. Johnson, Revisiting dark photon constraints from CMB spectral distortions, *Mon. Not. Roy. Astron. Soc.* **535**, 1874 (2024), [arXiv:2409.12115 \[astro-ph.CO\]](#).
- [78] G. Arsenadze, A. Caputo, X. Gan, H. Liu, and J. T. Ruderman, Shaping dark photon spectral distortions, *JHEP* **03**, 018, [arXiv:2409.12940 \[astro-ph.CO\]](#).
- [79] J. Suzuki, T. Horie, Y. Inoue, and M. Minowa, Experimental Search for Hidden Photon CDM in the eV mass range with a Dish Antenna, *JCAP* **09**, 042, [arXiv:1504.00118 \[hep-ex\]](#).
- [80] S. Knirck, T. Yamazaki, Y. Okesaku, S. Asai, T. Idehara, and T. Inada, First results from a hidden photon dark matter search in the meV sector using a plane-parabolic mirror system, *JCAP* **11**, 031, [arXiv:1806.05120 \[hep-ex\]](#).
- [81] P. Brun, L. Chevalier, and C. Flouzat, Direct Searches for Hidden-Photon Dark Matter with the SHUKET Experiment, *Phys. Rev. Lett.* **122**, 201801 (2019), [arXiv:1905.05579 \[hep-ex\]](#).
- [82] Y. Hochberg, I. Chiriac, S.-W. Nam, V. Verma, M. Colangelo, and K. K. Berggren, Detecting Sub-GeV Dark Matter with Superconducting Nanowires, *Phys. Rev. Lett.* **123**, 151802 (2019), [arXiv:1903.05101 \[hep-ph\]](#).
- [83] L. H. Nguyen, A. Lobanov, and D. Horns, First results from the WISPDMMX radio frequency cavity searches for hidden photon dark matter, *JCAP* **10**, 014, [arXiv:1907.12449 \[hep-ex\]](#).
- [84] A. Phipps *et al.*, Exclusion Limits on Hidden-Photon Dark Matter near 2 neV from a Fixed-Frequency

- Superconducting Lumped-Element Resonator, *Springer Proc. Phys.* **245**, 139 (2020), [arXiv:1906.08814 \[astro-ph.CO\]](#).
- [85] T. Aralis *et al.* (SuperCDMS), Constraints on dark photons and axionlike particles from the SuperCDMS Soudan experiment, *Phys. Rev. D* **101**, 052008 (2020), [Erratum: *Phys.Rev.D* 103, 039901 (2021)], [arXiv:1911.11905 \[hep-ex\]](#).
 - [86] E. Aprile *et al.* (XENON), Light Dark Matter Search with Ionization Signals in XENON1T, *Phys. Rev. Lett.* **123**, 251801 (2019), [arXiv:1907.11485 \[hep-ex\]](#).
 - [87] A. Aguilar-Arevalo *et al.* (DAMIC), Constraints on Light Dark Matter Particles Interacting with Electrons from DAMIC at SNOLAB, *Phys. Rev. Lett.* **123**, 181802 (2019), [arXiv:1907.12628 \[astro-ph.CO\]](#).
 - [88] H. An, M. Pospelov, J. Pradler, and A. Ritz, New limits on dark photons from solar emission and keV scale dark matter, *Phys. Rev. D* **102**, 115022 (2020), [arXiv:2006.13929 \[hep-ph\]](#).
 - [89] A. V. Dixit, S. Chakram, K. He, A. Agrawal, R. K. Naik, D. I. Schuster, and A. Chou, Searching for Dark Matter with a Superconducting Qubit, *Phys. Rev. Lett.* **126**, 141302 (2021), [arXiv:2008.12231 \[hep-ex\]](#).
 - [90] A. Andrianavalomahefa *et al.* (FUNK Experiment), Limits from the Funk Experiment on the Mixing Strength of Hidden-Photon Dark Matter in the Visible and Near-Ultraviolet Wavelength Range, *Phys. Rev. D* **102**, 042001 (2020), [arXiv:2003.13144 \[astro-ph.CO\]](#).
 - [91] L. Barak *et al.* (SENSEI), SENSEI: Direct-Detection Results on sub-GeV Dark Matter from a New Skipper-CCD, *Phys. Rev. Lett.* **125**, 171802 (2020), [arXiv:2004.11378 \[astro-ph.CO\]](#).
 - [92] N. Tomita, S. Oguri, Y. Inoue, M. Minowa, T. Nagasaki, J. Suzuki, and O. Tajima, Search for hidden-photon cold dark matter using a K-band cryogenic receiver, *JCAP* **09**, 012, [arXiv:2006.02828 \[hep-ex\]](#).
 - [93] E. Aprile *et al.* (XENON), Excess electronic recoil events in XENON1T, *Phys. Rev. D* **102**, 072004 (2020), [arXiv:2006.09721 \[hep-ex\]](#).
 - [94] J. Chiles *et al.*, New Constraints on Dark Photon Dark Matter with Superconducting Nanowire Detectors in an Optical Haloscope, *Phys. Rev. Lett.* **128**, 231802 (2022), [arXiv:2110.01582 \[hep-ex\]](#).
 - [95] M. A. Fedderke, P. W. Graham, D. F. Jackson Kimball, and S. Kalia, Search for dark-photon dark matter in the SuperMAG geomagnetic field dataset, *Phys. Rev. D* **104**, 095032 (2021), [arXiv:2108.08852 \[hep-ph\]](#).
 - [96] L. Manenti *et al.*, Search for dark photons using a multilayer dielectric haloscope equipped with a single-photon avalanche diode, *Phys. Rev. D* **105**, 052010 (2022), [arXiv:2110.10497 \[hep-ex\]](#).
 - [97] E. Aprile *et al.* (XENON), Emission of single and few electrons in XENON1T and limits on light dark matter, *Phys. Rev. D* **106**, 022001 (2022), [Erratum: *Phys.Rev.D* 110, 109903 (2024)], [arXiv:2112.12116 \[hep-ex\]](#).
 - [98] E. Aprile *et al.* (XENON), Search for New Physics in Electronic Recoil Data from XENONnT, *Phys. Rev. Lett.* **129**, 161805 (2022), [arXiv:2207.11330 \[hep-ex\]](#).
 - [99] H. An, S. Ge, W.-Q. Guo, X. Huang, J. Liu, and Z. Lu, Direct Detection of Dark Photon Dark Matter Using Radio Telescopes, *Phys. Rev. Lett.* **130**, 181001 (2023), [arXiv:2207.05767 \[hep-ph\]](#).
 - [100] R. Cervantes *et al.*, Search for 70 μeV Dark Photon Dark Matter with a Dielectrically Loaded Multiwavelength Microwave Cavity, *Phys. Rev. Lett.* **129**, 201301 (2022), [arXiv:2204.03818 \[hep-ex\]](#).
 - [101] P. Agnes *et al.* (DarkSide), Search for Dark Matter Particle Interactions with Electron Final States with DarkSide-50, *Phys. Rev. Lett.* **130**, 101002 (2023), [arXiv:2207.11968 \[hep-ex\]](#).
 - [102] S. Kotaka *et al.* (DOSUE-RR), Search for Dark Photon Dark Matter in the Mass Range 74–110 μeV with a Cryogenic Millimeter-Wave Receiver, *Phys. Rev. Lett.* **130**, 071805 (2023), [arXiv:2205.03679 \[hep-ex\]](#).
 - [103] X. Fan, G. Gabrielse, P. W. Graham, R. Harnik, T. G. Myers, H. Ramani, B. A. D. Sukra, S. S. Y. Wong, and Y. Xiao, One-Electron Quantum Cyclotron as a Milli-eV Dark-Photon Detector, *Phys. Rev. Lett.* **129**, 261801 (2022), [arXiv:2208.06519 \[hep-ex\]](#).
 - [104] K. Ramanathan, N. Klimovich, R. Basu Thakur, B. H. Eom, H. G. LeDuc, S. Shu, A. D. Beyer, and P. K. Day, Wideband Direct Detection Constraints on Hidden Photon Dark Matter with the QUALIPHIDE Experiment, *Phys. Rev. Lett.* **130**, 231001 (2023), [arXiv:2209.03419 \[astro-ph.CO\]](#).
 - [105] F. Bajjali *et al.*, First results from BRASS-p broadband searches for hidden photon dark matter, *JCAP* **08**, 077, [arXiv:2306.05934 \[hep-ex\]](#).
 - [106] H. An, X. Chen, S. Ge, J. Liu, and Y. Luo, Searching for ultralight dark matter conversion in solar

- corona using Low Frequency Array data, *Nature Commun.* **15**, 915 (2024), [arXiv:2301.03622 \[hep-ph\]](#).
- [107] S. Knirck *et al.* (BREAD), First Results from a Broadband Search for Dark Photon Dark Matter in the 44 to 52 μeV Range with a Coaxial Dish Antenna, *Phys. Rev. Lett.* **132**, 131004 (2024), [arXiv:2310.13891 \[hep-ex\]](#).
 - [108] H. An, S. Ge, J. Liu, and M. Liu, In Situ Measurements of Dark Photon Dark Matter Using Parker Solar Probe: Going beyond the Radio Window, *Phys. Rev. Lett.* **134**, 171001 (2025), [arXiv:2405.12285 \[hep-ph\]](#).
 - [109] J. Levine, B. Godfrey, J. A. Tyson, S. M. Tripathi, D. Polin, A. Aminaei, B. H. Kolner, and P. Stucky, New limit on dark photon kinetic mixing in the 0.2–1.2 μeV mass range from the Dark E-field Radio experiment, *Phys. Rev. D* **110**, 032010 (2024), [arXiv:2405.20444 \[hep-ex\]](#).
 - [110] L. Brouwer *et al.* (DMRadio), Projected sensitivity of DMRadio-m3: A search for the QCD axion below 1 μeV , *Phys. Rev. D* **106**, 103008 (2022), [arXiv:2204.13781 \[hep-ex\]](#).
 - [111] B. Godfrey *et al.*, Search for dark photon dark matter: Dark E field radio pilot experiment, *Phys. Rev. D* **104**, 012013 (2021), [arXiv:2101.02805 \[physics.ins-det\]](#).
 - [112] A. J. Millar *et al.* (ALPHA), Searching for dark matter with plasma haloscopes, *Phys. Rev. D* **107**, 055013 (2023), [arXiv:2210.00017 \[hep-ph\]](#).
 - [113] G. B. Gelmini, A. J. Millar, V. Takhistov, and E. Vitagliano, Probing dark photons with plasma haloscopes, *Phys. Rev. D* **102**, 043003 (2020), [arXiv:2006.06836 \[hep-ph\]](#).
 - [114] J. Liu *et al.* (BREAD), Broadband Solenoidal Haloscope for Terahertz Axion Detection, *Phys. Rev. Lett.* **128**, 131801 (2022), [arXiv:2111.12103 \[physics.ins-det\]](#).
 - [115] X. Fan, G. Gabrielse, P. W. Graham, H. Ramani, S. S. Y. Wong, and Y. Xiao, Highly excited electron cyclotron for QCD axion and dark-photon detection, *Phys. Rev. D* **111**, 075022 (2025), [arXiv:2410.05549 \[hep-ph\]](#).
 - [116] M. Baryakhtar, J. Huang, and R. Lasenby, Axion and hidden photon dark matter detection with multilayer optical haloscopes, *Phys. Rev. D* **98**, 035006 (2018), [arXiv:1803.11455 \[hep-ph\]](#).
 - [117] I. M. Bloch, R. Essig, K. Tobioka, T. Volansky, and T.-T. Yu, Searching for Dark Absorption with Direct Detection Experiments, *JHEP* **06**, 087, [arXiv:1608.02123 \[hep-ph\]](#).
 - [118] D. S. Akerib *et al.* (LZ), Projected sensitivities of the LUX-ZEPLIN experiment to new physics via low-energy electron recoils, *Phys. Rev. D* **104**, 092009 (2021), [arXiv:2102.11740 \[hep-ex\]](#).
 - [119] E. W. Kolb and A. J. Long, Cosmological gravitational particle production and its implications for cosmological relics, *Rev. Mod. Phys.* **96**, 045005 (2024), [arXiv:2312.09042 \[astro-ph.CO\]](#).
 - [120] P. A. R. Ade *et al.* (BICEP, Keck), Improved Constraints on Primordial Gravitational Waves using Planck, WMAP, and BICEP/Keck Observations through the 2018 Observing Season, *Phys. Rev. Lett.* **127**, 151301 (2021), [arXiv:2110.00483 \[astro-ph.CO\]](#).
 - [121] R. Basu, A. H. Guth, and A. Vilenkin, Quantum creation of topological defects during inflation, *Phys. Rev. D* **44**, 340 (1991).
 - [122] M. Redi and A. Tesi, Dark photon Dark Matter without Stueckelberg mass, *JHEP* **10**, 167, [arXiv:2204.14274 \[hep-ph\]](#).
 - [123] T. Sato, F. Takahashi, and M. Yamada, Gravitational production of dark photon dark matter with mass generated by the Higgs mechanism, *JCAP* **08** (08), 022, [arXiv:2204.11896 \[hep-ph\]](#).
 - [124] Y. Ema, K. Nakayama, and Y. Tang, Production of purely gravitational dark matter: the case of fermion and vector boson, *JHEP* **07**, 060, [arXiv:1903.10973 \[hep-ph\]](#).
 - [125] E. W. Kolb and A. J. Long, Completely dark photons from gravitational particle production during the inflationary era, *JHEP* **03**, 283, [arXiv:2009.03828 \[astro-ph.CO\]](#).
 - [126] A. Ahmed, B. Grzadkowski, and A. Socha, Gravitational production of vector dark matter, *JHEP* **08**, 059, [arXiv:2005.01766 \[hep-ph\]](#).
 - [127] G. F. Giudice, E. W. Kolb, and A. Riotto, Largest temperature of the radiation era and its cosmological implications, *Phys. Rev. D* **64**, 023508 (2001), [arXiv:hep-ph/0005123](#).
 - [128] M. Kawasaki, K. Kohri, and N. Sugiyama, MeV scale reheating temperature and thermalization of neutrino background, *Phys. Rev. D* **62**, 023506 (2000), [arXiv:astro-ph/0002127](#).
 - [129] M. Kawasaki, K. Kohri, and T. Moroi, Big-Bang nucleosynthesis and hadronic decay of long-lived massive particles, *Phys. Rev. D* **71**, 083502 (2005), [arXiv:astro-ph/0408426](#).
 - [130] S. Hannestad, What is the lowest possible reheating temperature?, *Phys. Rev. D* **70**, 043506 (2004), [arXiv:astro-ph/0403291](#).
 - [131] K. Ichikawa, M. Kawasaki, and F. Takahashi, The Oscillation effects on thermalization of the neutrinos in

- the Universe with low reheating temperature, *Phys. Rev. D* **72**, 043522 (2005), [arXiv:astro-ph/0505395](#).
- [132] P. F. de Salas, M. Lattanzi, G. Mangano, G. Miele, S. Pastor, and O. Pisanti, Bounds on very low reheating scenarios after Planck, *Phys. Rev. D* **92**, 123534 (2015), [arXiv:1511.00672 \[astro-ph.CO\]](#).
 - [133] T. Hasegawa, N. Hiroshima, K. Kohri, R. S. L. Hansen, T. Tram, and S. Hannestad, MeV-scale reheating temperature and thermalization of oscillating neutrinos by radiative and hadronic decays of massive particles, *JCAP* **12**, 012, [arXiv:1908.10189 \[hep-ph\]](#).
 - [134] J. A. R. Cembranos, L. J. Garay, A. Parra-López, and J. M. Sánchez Velázquez, Vector dark matter production during inflation and reheating, *JCAP* **02**, 013, [arXiv:2310.07515 \[gr-qc\]](#).
 - [135] O. Özsoy and G. Tasinato, Vector dark matter, inflation, and non-minimal couplings with gravity, *JCAP* **06**, 003, [arXiv:2310.03862 \[astro-ph.CO\]](#).
 - [136] B. Himmetoglu, C. R. Contaldi, and M. Peloso, Instability of anisotropic cosmological solutions supported by vector fields, *Phys. Rev. Lett.* **102**, 111301 (2009), [arXiv:0809.2779 \[astro-ph\]](#).
 - [137] B. Himmetoglu, C. R. Contaldi, and M. Peloso, Ghost instabilities of cosmological models with vector fields nonminimally coupled to the curvature, *Phys. Rev. D* **80**, 123530 (2009), [arXiv:0909.3524 \[astro-ph.CO\]](#).
 - [138] M. Karčiauskas and D. H. Lyth, On the health of a vector field with $(R A^2)/6$ coupling to gravity, *JCAP* **11**, 023, [arXiv:1007.1426 \[astro-ph.CO\]](#).
 - [139] C. Capanelli, L. Jenks, E. W. Kolb, and E. McDonough, Runaway Gravitational Production of Dark Photons, *Phys. Rev. Lett.* **133**, 061602 (2024), [arXiv:2403.15536 \[hep-th\]](#).
 - [140] C. Capanelli, L. Jenks, E. W. Kolb, and E. McDonough, Gravitational production of completely dark photons with nonminimal couplings to gravity, *JHEP* **09**, 071, [arXiv:2405.19390 \[hep-th\]](#).
 - [141] M. Bastero-Gil, J. Santiago, L. Ubaldi, and R. Vega-Morales, Vector dark matter production at the end of inflation, *JCAP* **04**, 015, [arXiv:1810.07208 \[hep-ph\]](#).
 - [142] B. Salehian, M. A. Gorji, H. Firouzjahi, and S. Mukohyama, Vector dark matter production from inflation with symmetry breaking, *Phys. Rev. D* **103**, 063526 (2021), [arXiv:2010.04491 \[hep-ph\]](#).
 - [143] H. Firouzjahi, M. A. Gorji, S. Mukohyama, and B. Salehian, Dark photon dark matter from charged inflaton, *JHEP* **06**, 050, [arXiv:2011.06324 \[hep-ph\]](#).
 - [144] Y. Nakai, R. Namba, and Z. Wang, Light Dark Photon Dark Matter from Inflation, *JHEP* **12**, 170, [arXiv:2004.10743 \[hep-ph\]](#).
 - [145] M. Bastero-Gil, J. Santiago, R. Vega-Morales, and L. Ubaldi, Dark photon dark matter from a rolling inflaton, *JCAP* **02** (02), 015, [arXiv:2103.12145 \[hep-ph\]](#).
 - [146] Y. Nakai, R. Namba, and I. Obata, Peak production of light dark photon dark matter, *JCAP* **08**, 032, [arXiv:2212.11516 \[hep-ph\]](#).
 - [147] N. D. Barrie, Resonant Vector Dark Matter Production during Inflation, [arXiv:2211.03902 \[hep-ph\]](#) (2022).
 - [148] J. T. Deskins, J. T. Giblin, and R. R. Caldwell, Gauge Field Preheating at the End of Inflation, *Phys. Rev. D* **88**, 063530 (2013), [arXiv:1305.7226 \[astro-ph.CO\]](#).
 - [149] P. Adshead, J. T. Giblin, T. R. Scully, and E. I. Sfakianakis, Gauge-preheating and the end of axion inflation, *JCAP* **12**, 034, [arXiv:1502.06506 \[astro-ph.CO\]](#).
 - [150] P. Adshead, J. T. Giblin, T. R. Scully, and E. I. Sfakianakis, Magnetogenesis from axion inflation, *JCAP* **10**, 039, [arXiv:1606.08474 \[astro-ph.CO\]](#).
 - [151] P. Adshead, J. T. Giblin, and Z. J. Weiner, Non-Abelian gauge preheating, *Phys. Rev. D* **96**, 123512 (2017), [arXiv:1708.02944 \[hep-ph\]](#).
 - [152] P. Adshead, J. T. Giblin, and Z. J. Weiner, Gravitational waves from gauge preheating, *Phys. Rev. D* **98**, 043525 (2018), [arXiv:1805.04550 \[astro-ph.CO\]](#).
 - [153] J. R. C. Cuissa and D. G. Figueroa, Lattice formulation of axion inflation. Application to preheating, *JCAP* **06**, 002, [arXiv:1812.03132 \[astro-ph.CO\]](#).
 - [154] K. D. Lozanov and M. A. Amin, GFIRE—Gauge Field integrator for Reheating, *JCAP* **04**, 058, [arXiv:1911.06827 \[astro-ph.CO\]](#).
 - [155] P. Adshead, J. T. Giblin, M. Pieroni, and Z. J. Weiner, Constraining axion inflation with gravitational waves from preheating, *Phys. Rev. D* **101**, 083534 (2020), [arXiv:1909.12842 \[astro-ph.CO\]](#).
 - [156] P. Adshead, J. T. Giblin, M. Pieroni, and Z. J. Weiner, Constraining Axion Inflation with Gravitational Waves across 29 Decades in Frequency, *Phys. Rev. Lett.* **124**, 171301 (2020), [arXiv:1909.12843 \[astro-ph.CO\]](#).
 - [157] P. Adshead, J. T. Giblin, R. Grutkoski, and Z. J. Weiner, Gauge preheating with full general relativity,

- JCAP **03**, 017, [arXiv:2311.01504 \[astro-ph.CO\]](#).
- [158] T. W. B. Kibble, Topology of Cosmic Domains and Strings, *J. Phys. A* **9**, 1387 (1976).
 - [159] J. I. Kapusta, *Finite Temperature Field Theory*, Cambridge Monographs on Mathematical Physics (Cambridge University Press, Cambridge, 1989).
 - [160] R. T. Co, A. Pierce, Z. Zhang, and Y. Zhao, Dark Photon Dark Matter Produced by Axion Oscillations, *Phys. Rev. D* **99**, 075002 (2019), [arXiv:1810.07196 \[hep-ph\]](#).
 - [161] R. T. Co, K. Harigaya, and A. Pierce, Gravitational waves and dark photon dark matter from axion rotations, *JHEP* **12**, 099, [arXiv:2104.02077 \[hep-ph\]](#).
 - [162] N. Kitajima and F. Takahashi, Resonant production of dark photons from axions without a large coupling, *Phys. Rev. D* **107**, 123518 (2023), [arXiv:2303.05492 \[hep-ph\]](#).
 - [163] J. A. Dror, K. Harigaya, and V. Narayan, Parametric Resonance Production of Ultralight Vector Dark Matter, *Phys. Rev. D* **99**, 035036 (2019), [arXiv:1810.07195 \[hep-ph\]](#).
 - [164] P. Agrawal, J. Fan, and M. Reece, Clockwork Axions in Cosmology: Is Chromonatural Inflation Chrononatural?, *JHEP* **10**, 193, [arXiv:1806.09621 \[hep-th\]](#).
 - [165] P. Agrawal, J. Fan, M. Reece, and L.-T. Wang, Experimental Targets for Photon Couplings of the QCD Axion, *JHEP* **02**, 006, [arXiv:1709.06085 \[hep-ph\]](#).
 - [166] A. E. Nelson and J. Scholtz, Dark Light, Dark Matter and the Misalignment Mechanism, *Phys. Rev. D* **84**, 103501 (2011), [arXiv:1105.2812 \[hep-ph\]](#).
 - [167] T. G. Rizzo, Kinetic Mixing and Portal Matter Phenomenology, *Phys. Rev. D* **99**, 115024 (2019), [arXiv:1810.07531 \[hep-ph\]](#).
 - [168] N. Craig and I. Garcia Garcia, Rescuing Massive Photons from the Swampland, *JHEP* **11**, 067, [arXiv:1810.05647 \[hep-th\]](#).
 - [169] B. Heidenreich, J. McNamara, and M. Reece, Non-standard axion electrodynamics and the dual Witten effect, *JHEP* **01**, 120, [arXiv:2309.07951 \[hep-ph\]](#).
 - [170] A. Ringwald, Axion dark matter (theory & experiment), *PoS TAUP2023*, 015 (2024), [arXiv:2311.11660 \[hep-ph\]](#).
 - [171] A. Arvanitaki, S. Dimopoulos, M. Galanis, L. Lehner, J. O. Thompson, and K. Van Tilburg, Large-misalignment mechanism for the formation of compact axion structures: Signatures from the QCD axion to fuzzy dark matter, *Phys. Rev. D* **101**, 083014 (2020), [arXiv:1909.11665 \[astro-ph.CO\]](#).
 - [172] J. Huang, A. Madden, D. Racco, and M. Reig, Maximal axion misalignment from a minimal model, *JHEP* **10**, 143, [arXiv:2006.07379 \[hep-ph\]](#).
 - [173] D. Cyncynates, T. Giurgica-Tiron, O. Simon, and J. O. Thompson, Resonant nonlinear pairs in the axiverse and their late-time direct and astrophysical signatures, *Phys. Rev. D* **105**, 055005 (2022), [arXiv:2109.09755 \[hep-ph\]](#).
 - [174] D. Cyncynates, O. Simon, J. O. Thompson, and Z. J. Weiner, Nonperturbative structure in coupled axion sectors and implications for direct detection, *Phys. Rev. D* **106**, 083503 (2022), [arXiv:2208.05501 \[hep-ph\]](#).
 - [175] J. Fan, Ultralight Repulsive Dark Matter and BEC, *Phys. Dark Univ.* **14**, 84 (2016), [arXiv:1603.06580 \[hep-ph\]](#).
 - [176] N. Gendler, D. J. E. Marsh, L. McAllister, and J. Moritz, Glimmers from the axiverse, *JCAP* **09**, 071, [arXiv:2309.13145 \[hep-th\]](#).
 - [177] D. G. Figueroa and M. Shaposhnikov, Lattice implementation of Abelian gauge theories with Chern–Simons number and an axion field, *Nucl. Phys. B* **926**, 544 (2018), [arXiv:1705.09629 \[hep-lat\]](#).
 - [178] A. V. Sokolov and A. Ringwald, Magnetic anomaly coefficients for QCD axion couplings, *PoS EPS-HEP2021*, 178 (2022), [arXiv:2109.08503 \[hep-ph\]](#).
 - [179] E. Witten, Dyons of Charge $e\theta/2\pi$, *Phys. Lett. B* **86**, 283 (1979).
 - [180] I. K. Affleck, O. Alvarez, and N. S. Manton, Pair Production at Strong Coupling in Weak External Fields, *Nucl. Phys. B* **197**, 509 (1982).
 - [181] D. L. J. Ho and A. Rajantie, Instanton solution for Schwinger production of 't Hooft-Polyakov monopoles, *Phys. Rev. D* **103**, 115033 (2021), [arXiv:2103.12799 \[hep-th\]](#).
 - [182] M. Reece, private communication (2024).
 - [183] M. Baryakhtar, O. Simon, and Z. J. Weiner, Cosmology with varying fundamental constants from hyperlight, coupled scalars, *Phys. Rev. D* **110**, 083505 (2024), [arXiv:2405.10358 \[astro-ph.CO\]](#).
 - [184] D. Cyncynates and O. Simon, Minimal targets for dilaton direct detection, [arXiv:2408.16816 \[hep-ph\]](#) (2024).

- [185] S. Schlamminger, K. Y. Choi, T. A. Wagner, J. H. Gundlach, and E. G. Adelberger, Test of the equivalence principle using a rotating torsion balance, *Phys. Rev. Lett.* **100**, 041101 (2008), [arXiv:0712.0607 \[gr-qc\]](#).
- [186] T. A. Wagner, S. Schlamminger, J. H. Gundlach, and E. G. Adelberger, Torsion-balance tests of the weak equivalence principle, *Class. Quant. Grav.* **29**, 184002 (2012), [arXiv:1207.2442 \[gr-qc\]](#).
- [187] P. Touboul *et al.*, Result of the MICROSCOPE weak equivalence principle test, *Class. Quant. Grav.* **39**, 204009 (2022), [arXiv:2209.15488 \[gr-qc\]](#).
- [188] L. Dolan and R. Jackiw, Symmetry Behavior at Finite Temperature, *Phys. Rev. D* **9**, 3320 (1974).
- [189] S. Weinberg, Gauge and Global Symmetries at High Temperature, *Phys. Rev. D* **9**, 3357 (1974).
- [190] C. Brans and R. H. Dicke, Mach's principle and a relativistic theory of gravitation, *Phys. Rev.* **124**, 925 (1961).
- [191] A. L. Erickcek, N. Barnaby, C. Burrage, and Z. Huang, Chameleons in the Early Universe: Kicks, Rebounds, and Particle Production, *Phys. Rev. D* **89**, 084074 (2014), [arXiv:1310.5149 \[astro-ph.CO\]](#).
- [192] K. N. Abazajian *et al.* (CMB-S4), CMB-S4 Science Book, First Edition, [arXiv:1610.02743 \[astro-ph.CO\]](#) (2016).
- [193] K. Abazajian *et al.* (CMB-S4), CMB-S4: Forecasting Constraints on Primordial Gravitational Waves, *Astrophys. J.* **926**, 54 (2022), [arXiv:2008.12619 \[astro-ph.CO\]](#).
- [194] P. Ade *et al.* (Simons Observatory), The Simons Observatory: Science goals and forecasts, *JCAP* **02**, 056, [arXiv:1808.07445 \[astro-ph.CO\]](#).
- [195] J. Bergé, P. Brax, G. Métris, M. Pernot-Borràs, P. Touboul, and J.-P. Uzan, MICROSCOPE Mission: First Constraints on the Violation of the Weak Equivalence Principle by a Light Scalar Dilaton, *Phys. Rev. Lett.* **120**, 141101 (2018), [arXiv:1712.00483 \[gr-qc\]](#).
- [196] F. Apers, J. P. Conlon, M. Mosny, and F. Revello, Kination, meet Kasner: on the asymptotic cosmology of string compactifications, *JHEP* **08**, 156, [arXiv:2212.10293 \[hep-th\]](#).
- [197] F. Revello, Attractive (s)axions: cosmological trackers at the boundary of moduli space, *JHEP* **05**, 037, [arXiv:2311.12429 \[hep-th\]](#).
- [198] F. Apers, J. P. Conlon, E. J. Copeland, M. Mosny, and F. Revello, String theory and the first half of the universe, *JCAP* **08**, 018, [arXiv:2401.04064 \[hep-th\]](#).
- [199] M.-S. Seo, Asymptotic Behavior of Saxion–Axion System in Stringy Quintessence Model, *Fortsch. Phys.* **72**, 2400112 (2024), [arXiv:2403.07307 \[hep-th\]](#).
- [200] M. Garny, Quantum corrections in quintessence models, *Phys. Rev. D* **74**, 043009 (2006), [arXiv:hep-ph/0606120](#).
- [201] E. J. Copeland, A. R. Liddle, and D. Wands, Exponential potentials and cosmological scaling solutions, *Phys. Rev. D* **57**, 4686 (1998), [arXiv:gr-qc/9711068](#).
- [202] P. J. Steinhardt, L.-M. Wang, and I. Zlatev, Cosmological tracking solutions, *Phys. Rev. D* **59**, 123504 (1999), [arXiv:astro-ph/9812313](#).
- [203] E. J. Copeland, M. Sami, and S. Tsujikawa, Dynamics of dark energy, *Int. J. Mod. Phys. D* **15**, 1753 (2006), [arXiv:hep-th/0603057](#).
- [204] N. Arkani-Hamed, L. Motl, A. Nicolis, and C. Vafa, The String landscape, black holes and gravity as the weakest force, *JHEP* **06**, 060, [arXiv:hep-th/0601001](#).
- [205] B. Heidenreich, M. Reece, and T. Rudelius, Evidence for a sublattice weak gravity conjecture, *JHEP* **08**, 025, [arXiv:1606.08437 \[hep-th\]](#).
- [206] B. Heidenreich, M. Reece, and T. Rudelius, The Weak Gravity Conjecture and Emergence from an Ultraviolet Cutoff, *Eur. Phys. J. C* **78**, 337 (2018), [arXiv:1712.01868 \[hep-th\]](#).
- [207] M. Tegmark and M. Zaldarriaga, Separating the early universe from the late universe: Cosmological parameter estimation beyond the black box, *Phys. Rev. D* **66**, 103508 (2002), [arXiv:astro-ph/0207047](#).
- [208] N. Aghanim *et al.* (Planck), Planck 2018 results. I. Overview and the cosmological legacy of Planck, *Astron. Astrophys.* **641**, A1 (2020), [arXiv:1807.06205 \[astro-ph.CO\]](#).
- [209] S. Chabanier, M. Millea, and N. Palanque-Delabrouille, Matter power spectrum: from Ly α forest to CMB scales, *Mon. Not. Roy. Astron. Soc.* **489**, 2247 (2019), [arXiv:1905.08103 \[astro-ph.CO\]](#).
- [210] J. de Kruijf, E. Vanzan, K. K. Boddy, A. Raccanelli, and N. Bartolo, Searching for blue-tilted power spectra in the dark ages, *Phys. Rev. D* **111**, 063507 (2025), [arXiv:2408.04991 \[astro-ph.CO\]](#).
- [211] W. H. Press and P. Schechter, Formation of galaxies and clusters of galaxies by selfsimilar gravitational condensation, *Astrophys. J.* **187**, 425 (1974).
- [212] J. M. Bardeen, J. R. Bond, N. Kaiser, and A. S. Szalay, The Statistics of Peaks of Gaussian Random

- Fields, *Astrophys. J.* **304**, 15 (1986).
- [213] K. Van Tilburg, A.-M. Taki, and N. Weiner, Halometry from Astrometry, *JCAP* **07**, 041, [arXiv:1804.01991 \[astro-ph.CO\]](#).
 - [214] N. Blinov, M. J. Dolan, P. Draper, and J. Shelton, Dark Matter Microhalos From Simplified Models, *Phys. Rev. D* **103**, 103514 (2021), [arXiv:2102.05070 \[astro-ph.CO\]](#).
 - [215] L. Dai and J. Miralda-Escudé, Gravitational Lensing Signatures of Axion Dark Matter Minihalos in Highly Magnified Stars, *Astron. J.* **159**, 49 (2020), [arXiv:1908.01773 \[astro-ph.CO\]](#).
 - [216] A. L. Erickcek and N. M. Law, Astrometric Microlensing by Local Dark Matter Subhalos, *Astrophys. J.* **729**, 49 (2011), [arXiv:1007.4228 \[astro-ph.CO\]](#).
 - [217] A. G. A. Brown *et al.* (Gaia), Gaia Data Release 2: Summary of the contents and survey properties, *Astron. Astrophys.* **616**, A1 (2018), [arXiv:1804.09365 \[astro-ph.GA\]](#).
 - [218] A. Bellini, J. Anderson, R. Van der Marel, L. Watkins, I. King, P. Bianchini, J. Chaname, R. Chandar, A. Cool, F. R. Ferraro, *et al.*, Hubble space telescope proper motion (hstpromo) catalogs of galactic globular clusters. i. sample selection, data reduction, and ngc 7078 results, *The Astrophysical Journal* **797**, 115 (2014).
 - [219] C. Boehm *et al.* (Theia), Theia: Faint objects in motion or the new astrometry frontier, [arXiv:1707.01348 \[astro-ph.IM\]](#) (2017).
 - [220] WFIRST Astrometry Working Group, R. E. Sanderson, A. Bellini, S. Casertano, J. R. Lu, P. Melchior, M. Libralato, D. Bennett, M. Shao, J. Rhodes, S. T. Sohn, S. Malhotra, S. Gaudi, S. M. Fall, E. Nelan, P. Guhathakurta, J. Anderson, and S. Ho, Astrometry with the Wide-Field Infrared Space Telescope, *Journal of Astronomical Telescopes, Instruments, and Systems* **5**, 044005 (2019), [arXiv:1712.05420 \[astro-ph.IM\]](#).
 - [221] E. Fomalont and M. Reid, Microarcsecond astrometry using the ska, *New Astronomy Reviews* **48**, 1473 (2004), science with the Square Kilometre Array.
 - [222] W. Skidmore and T. I. S. D. T. . T. S. A. Committee, Thirty meter telescope detailed science case: 2015*, *Research in Astronomy and Astrophysics* **15**, 1945 (2015).
 - [223] O. F. Ramadan, T. Karwal, and J. Sakstein, Attractive proposal for resolving the Hubble tension: Dynamical attractors that unify early and late dark energy, *Phys. Rev. D* **109**, 063525 (2024), [arXiv:2309.08082 \[astro-ph.CO\]](#).
 - [224] E. J. Copeland, A. Moss, S. Sevilano Muñoz, and J. M. M. White, Scaling solutions as Early Dark Energy resolutions to the Hubble tension, *JCAP* **05**, 078, [arXiv:2309.15295 \[astro-ph.CO\]](#).
 - [225] A. G. Riess *et al.*, A Comprehensive Measurement of the Local Value of the Hubble Constant with $1 \text{ km s}^{-1} \text{ Mpc}^{-1}$ Uncertainty from the Hubble Space Telescope and the SH0ES Team, *Astrophys. J. Lett.* **934**, L7 (2022), [arXiv:2112.04510 \[astro-ph.CO\]](#).
 - [226] G. W. Anderson and S. M. Carroll, Dark matter with time dependent mass, in *1st International Conference on Particle Physics and the Early Universe* (1997) pp. 227–229, [arXiv:astro-ph/9711288](#).
 - [227] M. Archidiacono, E. Castorina, D. Redigolo, and E. Salvioni, Unveiling dark fifth forces with linear cosmology, *JCAP* **10**, 074, [arXiv:2204.08484 \[astro-ph.CO\]](#).
 - [228] J. T. Giblin, G. Kane, E. Nesbit, S. Watson, and Y. Zhao, Was the Universe Actually Radiation Dominated Prior to Nucleosynthesis?, *Phys. Rev. D* **96**, 043525 (2017), [arXiv:1706.08536 \[hep-th\]](#).
 - [229] B. Battelier *et al.*, Exploring the foundations of the physical universe with space tests of the equivalence principle, *Exper. Astron.* **51**, 1695 (2021), [arXiv:1908.11785 \[physics.space-ph\]](#).
 - [230] A. V. Sokolov and A. Ringwald, Electromagnetic Couplings of Axions, [arXiv:2205.02605 \[hep-ph\]](#) (2022).
 - [231] I. A. Sulai *et al.*, Hunt for magnetic signatures of hidden-photon and axion dark matter in the wilderness, *Phys. Rev. D* **108**, 096026 (2023), [arXiv:2306.11575 \[hep-ph\]](#).
 - [232] M. Jiang *et al.*, Search for dark photons with synchronized quantum sensor network, *Nature Commun.* **15**, 3331 (2024), [arXiv:2305.00890 \[quant-ph\]](#).
 - [233] P. Adshead and K. D. Lozanov, Self-gravitating Vector Dark Matter, *Phys. Rev. D* **103**, 103501 (2021), [arXiv:2101.07265 \[gr-qc\]](#).
 - [234] H.-Y. Zhang, M. Jain, and M. A. Amin, Polarized vector oscillons, *Phys. Rev. D* **105**, 096037 (2022), [arXiv:2111.08700 \[astro-ph.CO\]](#).
 - [235] M. Jain and M. A. Amin, Polarized solitons in higher-spin wave dark matter, *Phys. Rev. D* **105**, 056019 (2022), [arXiv:2109.04892 \[hep-th\]](#).
 - [236] M. Gorghetto, E. Hardy, J. March-Russell, N. Song, and S. M. West, Dark photon stars: formation

- and role as dark matter substructure, *JCAP* **08** (08), 018, [arXiv:2203.10100 \[hep-ph\]](#).
- [237] M. A. Amin, M. Jain, R. Karur, and P. Mocz, Small-scale structure in vector dark matter, *JCAP* **08** (08), 014, [arXiv:2203.11935 \[astro-ph.CO\]](#).
 - [238] M. A. Amin and M. Mirbabayi, A Lower Bound on Dark Matter Mass, *Phys. Rev. Lett.* **132**, 221004 (2024), [arXiv:2211.09775 \[hep-ph\]](#).
 - [239] M. Jain, M. A. Amin, J. Thomas, and W. Wanichwecharungruang, Kinetic relaxation and Bose-star formation in multicomponent dark matter, *Phys. Rev. D* **108**, 043535 (2023), [arXiv:2304.01985 \[astro-ph.CO\]](#).
 - [240] M. Jain, W. Wanichwecharungruang, and J. Thomas, Kinetic relaxation and nucleation of Bose stars in self-interacting wave dark matter, *Phys. Rev. D* **109**, 016002 (2024), [arXiv:2310.00058 \[astro-ph.CO\]](#).
 - [241] H.-Y. Zhang, Unified view of scalar and vector dark matter solitons, *JHEP* **04**, 174, [arXiv:2406.05031 \[hep-ph\]](#).
 - [242] R. Liu, W. Hu, and H. Xiao, Warm and fuzzy dark matter: Free streaming of wave dark matter, *Phys. Rev. D* **111**, 023535 (2025), [arXiv:2406.12970 \[hep-ph\]](#).
 - [243] S. Ling and M. A. Amin, Free streaming in warm wave dark matter, *JCAP* **02**, 025, [arXiv:2408.05591 \[astro-ph.CO\]](#).
 - [244] H. An, T. Li, J. Shu, X. Wang, X. Xue, and Y. Zhao, Dark Photon Dark Matter and Low-frequency Gravitational-wave Detection with Gaia-like Astrometry, *Astrophys. J.* **976**, 247 (2024), [arXiv:2407.16488 \[hep-ph\]](#).
 - [245] C. O'Hare, [cajohare/axionlimits: Axionlimits](#), <https://cajohare.github.io/AxionLimits/> (2020).
 - [246] S. Weinberg, *The Quantum theory of fields. Vol. 1: Foundations* (Cambridge University Press, 2005).
 - [247] I. S. Gerstein, R. Jackiw, S. Weinberg, and B. W. Lee, Chiral loops, *Phys. Rev. D* **3**, 2486 (1971).
 - [248] D. Seery, One-loop corrections to a scalar field during inflation, *JCAP* **11**, 025, [arXiv:0707.3377 \[astro-ph\]](#).
 - [249] P. Adshead, R. Easther, and E. A. Lim, Cosmology With Many Light Scalar Fields: Stochastic Inflation and Loop Corrections, *Phys. Rev. D* **79**, 063504 (2009), [arXiv:0809.4008 \[hep-th\]](#).
 - [250] R. Jackiw, Functional evaluation of the effective potential, *Phys. Rev. D* **9**, 1686 (1974).
 - [251] M. M. Anber and L. Sorbo, Naturally inflating on steep potentials through electromagnetic dissipation, *Phys. Rev. D* **81**, 043534 (2010), [arXiv:0908.4089 \[hep-th\]](#).
 - [252] L. D. Landau and E. M. Lifshitz, *Course of theoretical physics* (Elsevier, 2013).
 - [253] N. N. Bogoliubov and Y. A. Mitropolsky, *Asymptotic methods in the theory of non-linear oscillations*, Vol. 1 (Gordon and Breach New York, 1961).
 - [254] J. Fajans and L. Friedland, Autoresonant (nonstationary) excitation of pendulums, platinos, plasmas, and other nonlinear oscillators, *American Journal of Physics* **69**, 1096 (2001).
 - [255] S. Rajasekar and M. A. Sanjuan, Autoresonance, *Nonlinear Resonances*, 293 (2016).
 - [256] S. G. Glebov, O. M. Kiselev, and N. N. Tarkhanov, *Oscillations and Resonances* (Walter de Gruyter GmbH & Co KG, 2017).
 - [257] C. Grayson, C. T. Yang, M. Formanek, and J. Rafelski, Electron–positron plasma in BBN: Damped-dynamic screening, *Annals Phys.* **458**, 169453 (2023), [arXiv:2307.11264 \[astro-ph.CO\]](#).
 - [258] S. Weinberg, *Cosmology* (2008).